

รายงานวิจัยแบบสมบูรณ์
เรื่อง

การพัฒนาเครื่องมือ Phase Doppler Anemometer สำหรับวัดความเร็ว
และการกระจายขนาดของวัสดุอนุภาค

DEVELOPMENT OF PHASE DOPPLER ANEMOMETER FOR MEASURING VELOCITY
AND SIZE DISTRIBUTION OF PARTICULATE MATERIALS

โดย

ศาสตราจารย์ ดร. วิวัฒน์ ตัณฑะพานิชกุล และคณะฯ
จุฬาลงกรณ์มหาวิทยาลัย

รายงานวิจัยนี้ได้รับเงินทุนสนับสนุนจากโครงการวิจัยร่วมภาครัฐ-เอกชน
ประจำปีงบประมาณ 2547

จุฬาลงกรณ์มหาวิทยาลัย

รายงานวิจัยฉบับสมบูรณ์

โครงการ

การพัฒนาเครื่องมือ Phase Doppler Anemometer สำหรับวัด ความเร็วและการกระจายขนาดของวัสดุอนุภาค

คณะผู้วิจัย

1. ศ.ดร.วิวัฒน์ ตัณฑะพานิชกุล
2. ผศ.ดร.หทัยชนก วานิชศรี
3. รศ.ดร.ธวัชชัย ชรินพานิชกุล
4. Dr.Gerard Grehan
5. นายธนณัฐชัย บุญนะทิ

หัวหน้าโครงการ

หัวหน้าโครงการวิจัยย่อย

รองหัวหน้าโครง

ที่ปรึกษาโครงการ

ผู้ช่วยวิจัย

สังกัด

จุฬาลงกรณ์มหาวิทยาลัย

จุฬาลงกรณ์มหาวิทยาลัย

จุฬาลงกรณ์มหาวิทยาลัย

INSA University Rouen, France

จุฬาลงกรณ์มหาวิทยาลัย

ศูนย์วิทยทรัพยากร
จุฬาลงกรณ์มหาวิทยาลัย

Abstract

Particle size analysis is an essential analytical task in a large variety of processes of industrial and laboratorial relevance. Phase Doppler anemometer (PDA) is one of well-established techniques allowing simultaneous measurement of velocity and size of particles, droplets, or bubbles in two-phase flows including spray atomization. The method is based upon the principle of light scattering interferometry. When a particle passes through the probe volume defined by the intersection of two laser beams, the phase of the light scattered by the particle carries information about the particle size, whereas its frequency provides the information of particle velocity.

This research work has been devoted to the development of a one-dimensional PDA instrument by using He-Ne laser with wavelength of 632.8 nm and two detectors for measuring velocity and size distribution of water droplets generated by binary and ultrasonic nozzles. The calibration of the developed PDA with the transparent glass spheres of precisely known size was conducted before investigating the reliability and accuracy of the developed system by comparing the measurement results obtained from the developed with that of the commercial PDA instruments. It was found that the relative difference of the droplet mean velocity and diameter measured by the developed system were less than 15 % and 25 %, respectively. These results demonstrate the potential of the PDA instrument developed in this work.

ศูนย์วิทยทรัพยากร
จุฬาลงกรณ์มหาวิทยาลัย

เลขหมู่

เลขทะเบียน 013588

วัน, เดือน, ปี 16 พ.ค. 51

บทคัดย่อ

การวิเคราะห์ขนาดของละอองน้ำที่ได้จากการพ่นละอองถือว่าเป็นงานการวิเคราะห์ลักษณะสมบัติอนุภาคที่จำเป็นอย่างยิ่ง ไม่ว่าจะเป็นทางอุตสาหกรรมและห้องปฏิบัติการ เฟสคอปเปอเรอร์อิมมิเตอร์เป็นอีกเทคนิคหนึ่งที่กำลังได้รับความนิยมเพราะสามารถวัดความเร็วและขนาดของอนุภาค ไม่ว่าจะเป็นอนุภาค หยดของของเหลว หรือฟองอากาศในระบบการไหลแบบ 2 วัฏภาค ได้ในเวลาเดียวกัน เทคนิคนี้อาศัยหลักการการกระเจิงของแสง เมื่ออนุภาควิ่งผ่านปริมาตรที่จะทำการวัด ซึ่งเกิดขึ้นบริเวณที่ลำแสง 2 ลำแสงตัดกัน โดยข้อมูลเกี่ยวกับขนาดจะคำนวณได้จากการเปลี่ยนแปลงเฟสของการกระเจิงแสง และความเร็วของอนุภาคคำนวณได้จากค่าความถี่ในการกระเจิงแสง

งานวิจัยนี้มีจุดประสงค์เพื่อพัฒนาเครื่องมือเฟสคอปเปอเรอร์อิมมิเตอร์ ชนิดหนึ่งมิติ โดยใช้แสงเลเซอร์ฮีเลียม-นีออน ที่มีความยาวคลื่น 632.8 นาโนเมตร และตัวรับสัญญาณ 2 ตัว เพื่อวัดความเร็วและการกระจายขนาดของหยดน้ำที่ถูกพ่นออกจากหัวฉีดแบบไบนารีและหัวฉีดคลื่นเหนือเสียง โดยทำการปรับเทียบมาตรฐานของเครื่องมือที่พัฒนาขึ้นด้วยอนุภาคทรงกลมที่รู้ขนาดแน่นอน จากนั้นทำการศึกษาผลของความน่าเชื่อถือและความแม่นยำของเครื่องมือที่พัฒนาขึ้นโดยเปรียบเทียบผลการวัดความเร็วและการกระจายขนาดของอนุภาคหยดน้ำกับเครื่องมือที่มีขายในท้องตลาด ผลการเปรียบเทียบพบว่าค่าความคลาดเคลื่อนเฉลี่ยของความเร็ว และขนาดของอนุภาคมีค่าน้อยกว่า 15 % และ 25 % ตามลำดับ ซึ่งผลการศึกษานี้แสดงให้เห็นถึงศักยภาพของเครื่องมือที่พัฒนาขึ้น

ศูนย์วิทยทรัพยากร
จุฬาลงกรณ์มหาวิทยาลัย

ACKNOWLEDGEMENTS

The author wishes to express his gratitude to his advisor, Associate Professor Tawatchai Charinpanitkul, and co-advisor, Assistant Professor Hathaichanok Vanisri for their encouraging guidance, advice and helpful suggestions throughout this study. Their comments and suggestions not merely provide valuable knowledge but broaden his perspective in practical applications as well. The author also wishes to express his gratitude to his oversea co-advisor, Dr. Gerard GREHAN (Director of LESP Laboratory INSA University de Rouen, France) for his on-the-job training, inspiring guidance, advice, and helpful suggestions. It has been a great experience learning a lot of things from him.

The author would like to express gratitude to Professor Wiwut Tanthapanichakoon, Associate Professor Suttichai Assabumrungrat and Dr. Pумыos Vallikul for their stimulating comments and participation as the thesis committee.

The author is very grateful to University-Industry Research Project Fund of Center of Excellence in Particle Technology, Chulalongkorn University, and the Laboratoire d'Energetique des Systemes et Procedes, Institut National des Sciences Appliques de Rouen, France for providing partial financial support to the author. The author is also grateful to the Department of Chemical Engineering, Chulalongkorn University for allowing to set-up the experimental apparatus and using the accessories.

Moreover, special thanks to senior student, Miss Sawitree Saengkaew as talented research assistant for her patience, generosity, useful suggestions and very helpful skills in this research field.

Furthermore, thank you very much to all members of the Particle Technology and Material Processing Laboratory for their warm collaborations, kindness and assistance.

Finally, the author is beholden to his parents and family for their encouragement, understanding, inspiration and very useful help.

CONTENTS

	Page
ABSTRACT IN THAI.....	iv
ABSTRACT IN ENGLISH.....	v
ACKNOWLEDGEMENTS.....	vi
CONTENTS.....	vii
LIST OF TABLES.....	xi
LIST OF FIGURES.....	xii
NOMENCLATURE.....	xviii
CHAPTER	
1. INTRODUCTION.....	1
1.1 Purpose and Description.....	1
1.2 Objectives of Present Study.....	4
1.3 Scope of Study.....	4
1.4 Obtained Benefit.....	5
1.5 Description.....	5
2. SURVEY OF APPLICATIONS.....	7
2.1 Categorization of Measuring Techniques.....	7
2.2 Applications on PDA Techniques.....	11
2.2.1 Two-Component LDA/PDA System.....	14
2.2.2 Applications to Spray Atomization.....	16
3. BASIC OPTICS AND LASER.....	20
3.1 Light as Electromagnetic Radiation.....	20
3.2 Geometrical Optics.....	22
3.3 Interference.....	23

CONTENTS (CONTINUED)

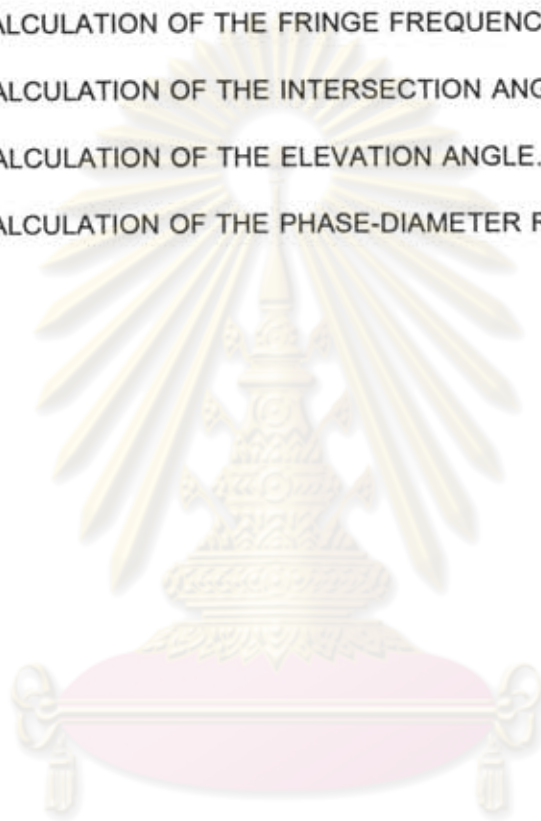
	Page
3.4 Diffraction.....	26
3.5 Gaussian Beam Optics.....	27
3.6 Polarization of Light Waves.....	29
3.7 Laser.....	32
3.7.1 General Laser Properties.....	32
3.7.2 Laser Types.....	33
3.8 Light Detectors PDA.....	37
4. BASIC PRINCIPLE OF LASER DOPPLER ANEMOMETER (LDA) AND PHASE DOPPLER ANEMOMETER (PDA) TECHNIQUES.....	39
4.1 The Doppler Shift.....	39
4.2 Model of LDA and PDA Techniques.....	40
4.2.1 The Doppler Model.....	40
4.2.2 The Fringe Model.....	45
4.3 Probe Volume.....	48
4.4 Laser Doppler Anemometer.....	50
4.5 Phase-Diameter Relations.....	52
4.6 Phase Doppler Anemometer.....	59
5. DESIGN AND SET-UP OF THE PDA SYSTEM.....	61
5.1 LDA System Components.....	62
5.1.1 Transmitting Parts.....	62
5.1.2 Receiving Parts.....	78
5.2 PDA System Components.....	89

CONTENTS (CONTINUED)

	Page
5.3 Signals and Signal Processing.....	94
5.3.1 Signal Capture.....	94
5.3.2 Signal Processing.....	96
5.3.3 Display of Results.....	117
5.4 Experimental Set-up.....	119
5.4.1 Default Settings.....	120
5.4.2 General Experimental Procedures.....	121
6. RESULTS AND DISCUSSION	124
6.1 Experiments for Verifying Reliability of Signal Processing System	124
6.1.1 Verification with the Signal Generator.....	124
6.1.2 Verification by Comparison with Commercial PDA System.....	126
6.2 Verification of the Developed PDA System using Stationary Object.....	132
6.3 Verification of the Developed PDA System using Liquid Spray.....	138
6.3.1 Velocity Verification.....	140
6.3.2 Diameter Verification.....	144
6.4 Sources of Discrepancies in the Experiments.....	149
7. CONCLUSIONS AND RECOMMENDATIONS.....	154
7.1 Concluding Remarks.....	155
7.2 Recommendations.....	156
REFERENCES.....	158

CONTENTS (CONTINUED)

	Page
APPENDICES.....	161
APPENDIX A THE FAST FOURIER TRANSFORM (FFT).....	162
APPENDIX B CALCULATION OF THE FRINGE FREQUENCY.....	167
APPENDIX C CALCULATION OF THE INTERSECTION ANGLE.....	171
APPENDIX D CALCULATION OF THE ELEVATION ANGLE.....	173
APPENDIX E CALCULATION OF THE PHASE-DIAMETER RELATIONS.....	175



ศูนย์วิทยทรัพยากร
จุฬาลงกรณ์มหาวิทยาลัย

LIST OF TABLES

	Page
Table 1.1 Application of particle sizing technology.....	2
Table 2.2 Categorization of measurement techniques with respect to the measurable properties of a two-phase system.....	11
Table 2.3 A list of the advantages and disadvantages of the phase Doppler technique.....	14
Table 5.1 The set-up procedure for adjusting the laser.....	65
Table 5.2 The set-up procedure for adjusting the circular concentric diffraction array.....	70
Table 5.3 The set-up procedures for adjusting the plano-convex glass lens.....	76
Table 5.4 The set-up procedures for adjusting the plano-convex glass lens.....	81
Table 5.5 The set-up procedures for adjusting the spatial filter.....	83
Table 5.6 The set-up procedures for adjusting the symmetric-convex glass lens...	85
Table 5.7 The set-up procedures for adjusting the plano-convex glass lens.....	87
Table 5.8 The measurable size range of the PDA system for the different masks.	91
Table 6.1 The experimental results of mean velocity obtained by the commercial PDA and developed PDA software.....	130
Table 6.2 Diameter of glass sphere No. 1 measured with the developed PDA.....	134
Table 6.3 Diameter of glass sphere No. 2 measured with the developed PDA.....	135
Table 6.4 Diameter of glass sphere No. 3 measured with the developed PDA.....	136
Table 6.5 The specification of the PDA system.....	138

LIST OF TABLES (CONTINUED)

	Page
Table 6.6 The experimental results of mean velocity and their standard deviations obtained by the commercial PDA and developed PDA instrument.....	141
Table 6.7 The experimental results of mean diameter and their standard deviations obtained by the commercial PDA and developed PDA instrument.....	145
Table 7.1 The particle size range of the PDA instrument developed in this work...	155



ศูนย์วิทยทรัพยากร
จุฬาลงกรณ์มหาวิทยาลัย

LIST OF FIGURES

	Page
Figure 2.1 Categorization of measurement techniques for analysis of two-phase systems.....	9
Figure 3.1 The electromagnetic spectrum.....	21
Figure 3.2 Reflection and refraction of light at a plane surface.....	23
Figure 3.3 The formation of interference fringes by parallel light beams crossing at an angle α	25
Figure 3.4 Diagram showing the relation of interference fringes to the wave fronts of intersecting beams.....	26
Figure 3.5 Characterization of a Gaussian beam.....	29
Figure 3.6 Schematic diagram of an electromagnetic wave propagating in the x direction.....	30
Figure 3.7 (a) An unpolarized light beam viewed along the direction of propagation (perpendicular to the page) (b) A linearly polarized light beam with the electric field vector vibrating in the vertical direction.....	32
Figure 3.8 Schematic of a continuously gas laser.....	34
Figure 3.9 Schematic of a solid-state laser.....	35
Figure 3.10 Schematic of a pulsed dye laser.....	35
Figure 3.11 Schematic of a semiconductor laser.....	36
Figure 3.12 Diagram of photomultiplier detector.....	38
Figure 4.1 Doppler shift of scattered light from a moving particle.....	41

LIST OF FIGURES (CONTINUED)

	Page
Figure 4.2 Configuration of reference beam LDA system.....	43
Figure 4.3 Configuration of the Doppler difference frequency method (dual beam LDA system).....	45
Figure 4.4 Schematic of two interfering beams at measurement volume.....	46
Figure 4.5 Dimensions of LDA probe volume.....	50
Figure 4.6 Typical optical setup of LDA instrument.....	52
Figure 4.7 Fringe model for phase Doppler principle for the case of refraction.....	53
Figure 4.8 Phase difference of a light ray refracted at a spherical particle.....	56
Figure 4.9 Determinations of phase shift from two Doppler signals.....	58
Figure 4.10 Representative response functions for a PDA system using three detectors.....	59
Figure 4.11 Typical optical set-up of PDA instrument.....	60
Figure 5.1 Optical configuration of a one detectors PDA system.....	63
Figure 5.2 The optical rail.....	64
Figure 5.3 A 17 mW cylindrical Helium Neon laser and power supply.....	65
Figure 5.4 A spherical laser focusing lens with 100 mm focal length and 20 mm in diameter	67
Figure 5.5 A circular concentric diffraction array.....	68
Figure 5.6 A Plano-convex glass lens for emitting parts.....	72
Figure 5.7 Two circular apertures mask for (a) track 1 (b) track 2 (c) track 3.....	74
Figure 5.8 Optical configuration of the receiving parts at the off-axis angle in 30 degree.....	79

LIST OF FIGURES (CONTINUED)

	Page
Figure 5.9 A 300 mm focal length and 95 mm in diameter plano-convex glass lens for the receiving parts.....	80
Figure 5.10 A 200 μm spherical aperture special filter.....	82
Figure 5.11 A symmetric-convex lens with 100 mm focal length and 50 mm in diameter.....	84
Figure 5.12 A plano-convex glass lens with 40 mm focal length and 10 mm in diameter.....	86
Figure 5.13 A Photomultiplier.....	88
Figure 5.14 Optical configuration of a two detectors PDA system.....	90
Figure 5.15 Two rectangular slits mask.....	91
Figure 5.16 The complete set-up of a PDA instrument.....	93
Figure 5.17 Anatomy of a typical LDA/PDA signal burst generated when a particle passes through the measurement volume.....	95
Figure 5.18 The experimental set-up program interface.....	97
Figure 5.19 Data acquisition program interface.....	102
Figure 5.20 Scattering signals with (a) single channel mode and (b) dual channel mode.....	103
Figure 5.21 The effect of the input range.....	104
Figure 5.22 The effect of low input range in a signal.....	105
Figure 5.23 The effect of trigger level.....	106
Figure 5.24 The effect of trigger level result in a signal.....	107
Figure 5.25 Low sampling rate result in a signal.....	108

LIST OF FIGURES (CONTINUED)

	Page
Figure 5.26 Example trigger depths.....	109
Figure 5.27 The computable signal from particles crossing a measurement volume.....	111
Figure 5.28 The data processing window.....	112
Figure 5.29 (a) Frequency cut mode; (b) Draw figure diagram; (c) Information on modified signal.....	113
Figure 5.30 The signal processing.....	114
Figure 5.31 The spline interpolation.....	115
Figure 5.32 Flow diagram of developed PDA system	116
Figure 5.33 LDA window after taking a measurement.....	118
Figure 5.34 LDA/PDA window after taking a measurement.....	119
Figure 5.35 The image of the spray nozzle indicating the measuring position.....	123
Figure 6.1 Tektronix AFG310 signal generator.....	125
Figure 6.2 A typical example of signal at 10 kHz.....	125
Figure 6.3 Comparison of generated signal and input signal.....	126
Figure 6.4 (a) The Commercial PDA instrument (Dantec Dynamics Co.,Ltd.) (b) The transmitting part (c) The receiving part.....	128
Figure 6.5 (a) Schematic of an ultrasonic nozzle (b) Image of spray profile.....	129
Figure 6.6 Comparison of mean velocities obtained by the commercial and developed software.....	130

LIST OF FIGURES (CONTINUED)

	Page
Figure 6.7 The comparison of the velocity distributions obtained by the commercial PDA instrument and the developed PDA instrument by using water flow rate (a) $16 \text{ mm}^3/\text{sec}$ (b) $33 \text{ mm}^3/\text{sec}$ (c) $66 \text{ mm}^3/\text{sec}$	131
Figure 6.8 The photograph of the glass sphere attached to thin pin at the measurement volume.....	132
Figure 6.9 Microscopic image of glass spheres of different size.....	133
Figure 6.10 The image of the recorded signal from the actual measurement volume.....	137
Figure 6.11 (a) Schematic of a binary nozzle, (b) Image of spray profile.....	139
Figure 6.12 Comparison of mean velocity obtained by the developed PDA instrument and the commercial PDA instrument.....	142
Figure 6.13 The comparison of the velocity distributions obtained by the developed PDA instrument and the commercial PDA instrument by using air pressure 0.05 N/mm^2 and water flow rate (a) $250 \text{ mm}^3/\text{sec}$ (b) $416 \text{ mm}^3/\text{sec}$ (c) $500 \text{ mm}^3/\text{sec}$	143
Figure 6.14 The comparison of the velocity distributions obtained by the developed PDA instrument and the commercial PDA instrument by using air pressure 0.10 N/mm^2 and water flow rate $500 \text{ mm}^3/\text{sec}$...	144

LIST OF FIGURES (CONTINUED)

	Page
Figure 6.15 Comparison of mean diameter obtained by the PDA instrument under development and the commercial PDA instrument.....	146
Figure 6.16 The comparison of the size distributions obtained by the developed PDA instrument and the commercial PDA instrument by using air pressure 0.05 N/mm^2 and water flow rate $250 \text{ mm}^3/\text{sec}$ (b) $416 \text{ mm}^3/\text{sec}$ (c) $500 \text{ mm}^3/\text{sec}$	147
Figure 6.17 The comparison of the size distributions obtained by the developed PDA instrument and the commercial PDA instrument by using air pressure 0.10 N/mm^2 and water flow rate $500 \text{ mm}^3/\text{sec}$...	148
Figure 6.18 The comparison result of the diameter measurement for the unparallel fringe and the parallel fringe.....	150
Figure 6.19 The phase/diameter response for each track of the circular concentric diffraction array: (a) track 1, (b) track 2 and (c) track 3.....	153

ศูนย์วิทยทรัพยากร
จุฬาลงกรณ์มหาวิทยาลัย

NOMENCLATURE

C_0	=	speed of light in vacuum (m/s)
D	=	the particle diameter (μ m)
E	=	the electric field vector (-)
e	=	a mathematical constant which is base of the natural logarithm (-)
f_D	=	Doppler frequency (Hz)
f_e	=	the frequency of the laser source (emitter) (Hz)
f_r	=	the frequency of the scattered light (Hz)
\bar{k}	=	unit vector (-)
\bar{l}	=	unit vector (-)
N_f	=	the number of fringes (-)
n	=	refractive index of substance (-)
P	=	the type of scattering
T	=	the time of one cycle of the signal
X	=	dimensionless x-coordinate (-)
Y	=	dimensionless y-coordinate (-)
Z	=	dimensionless z-coordinate (-)
z	=	the distance along the beam from the cross-section of minimum diameter (mm)

Greek symbols

θ_1	=	angle between the incident ray and a perpendicular line to the surface (degree)
θ_2	=	angle between the reflected ray and a perpendicular line to the surface (degree)

NOMENCLATURE (CONTINUED)

α	=	crossing angle of two parallel beams (degree)
λ	=	the light wavelength (μm)
r_0	=	the radius at the waist (mm)
ϕ	=	the angle of divergence or convergence (degree)
ϕ	=	the scattering angle (degree)
v	=	the velocity of the moving particle (m/s)
γ	=	the particle velocity angle (degree)
δ	=	the fringe spacing (μm)
ψ	=	the elevation angle (degree)
Φ	=	the Doppler difference (degree)
τ	=	the angles between the incident ray and the surface tangent (degree)
τ'	=	the angles between the refracted ray and the surface tangent (degree)

Subscripts

D	=	Doppler
e	=	laser source
f	=	fringe
p	=	particle
r	=	scattering light
x	=	x-direction
y	=	y-direction
z	=	z-direction

CHAPTER 1

INTRODUCTION

1.1 Purpose and Description

Since particle size and its distribution is crucial characteristics of every particulate material, particle size analysis (PSA) is an important task for researchers, scientists and engineers involving with either the research or the development of industrial works within a broad range of disciplines. Examples of those representative processes, which make use of PSA, include the combustion of pulverized coal and liquid fuels, the analysis and control of particulate emissions, the manufacture of metallic powders, the powder and liquid paint production and the production of pharmaceutical products. Table 1.1 describes some of applications in which particle size analysis is essential and lists some of the primary use of particle sizing methods in these areas. It is thus necessary to understand the techniques capable of measuring particle size together with its benefits and limitations of each. In response to different situations encountered in sizing particles, many techniques have been proposed and developed to measure the size of particles accurately.

Nowadays, use of the laser, based on light scattering, has become increasingly popular optical techniques in particle sizing applications, since the laser is distinctive properties, which are, for instance, of nearly planar waves, monochromatic nature, coherence, and high spectral power, make it an extremely useful tool for particle sizing.

Instruments incorporating these techniques can provide the real-time measurements of the process stream. Since this measurement technique is based on the analysis of light scattering by airborne particle, it could avoid the sample handling problems encountered by mechanical technique such as sedimentation, sieving and impactor which must collect particle sample for analysis. Consequently, the technique, based on light scattering, is a field of current interest.

Table 1.1 Application of particle sizing technology [1]

Uses of particle size analysis	Applications in area
Combustion	Size and velocity measurements
Sprays	Characterizations and descriptions of nozzles
Medicine/Pharmaceuticals	Control of manufacturing processes
Paints	Control of pigment size distribution
Metallic powders	Control of manufacturing processes
Agriculture	Control of pesticide application
Pollution control	Monitoring and analysis of emissions
Foods and consumer products	Control of taste and texture

Laser optical techniques are often preferred owing to their ability to perform above mentions. Phase Doppler Anemometer (PDA) is one of these well-established measurement techniques. It is the laser based techniques that is now one of the most popular and most powerful techniques allowing simultaneous measurement of the velocity and the size of homogeneous spherical particles, drops, or bubbles in two-phase flows, with

high resolution in time and space, without being intrusive. The method is based upon the principles of light scattering interferometry. The intersection of the two beams creates a fringe pattern within the probe volume. As a particle passes through the probe volume, it scatters light from the beams and projects the fringe pattern. A receiving lens strategically located at an off-axis collection angle project a portion of this fringe pattern onto several detectors. Each detector produces a Doppler burst signal with a frequency proportional to the particle velocity. The phase shift between the Doppler burst signals from two different detectors is proportional to the size of the spherical particle.

The PDA technique requires no calibration because the particle size and velocity are dependent only on the laser wavelength and optical configuration. However, the verification of the PDA system is still required in order to confirm the accuracy of the instrument. The PDA measurements are not based upon the scattered light intensity and consequently they are not subject to errors from beam attenuation or deflection, which occur in dense particle and combustion environments. However, its use is restricted to spherical particles. This occurs because light scattered by refraction and reflection is used to determine the phase shift in the light scattering signal that is a measure of the local radius of curvature of the particle. Since for non-spherical particles the local radius of curvature can result in large errors in the particle size.

Regarding the success of the PDA technique for optical particle sizing of spherical homogeneous particles and the non-intrusiveness and the insensitivity of the size measurement to signal amplitude are attractive features, the approach developed in this

work is essentially based on this technique. Furthermore, the present work is a part of the research collaborative program with the Institut National des Science Appliquees de Rouen (INSA de Rouen, France) where is the most excellence over 20 years in the optical techniques. The objective of this program is to transfer research information and technology for developing a PDA instrument at Particle Technology & Material Processing Laboratory, Department of Chemical Engineering, Faculty of Engineering, Chulalongkorn University.

1.2 Objectives of Present Study

To develop a one-dimensional Phase Doppler Anemometer (PDA) instrument using a 17 mW Helium Neon laser which produces light of wavelength 632.8 nm for measuring velocity and size distribution of water droplets.

1.3 Scope of Study

1.3.1 Assemble a PDA instrument for measuring velocity and size distribution of water droplets; generated by an atomizing nozzle, moving through the region of interference of two crossing laser beams. Following assumptions would be employed:

- Spherical shape and smooth surface particles;
- Constant refractive index due to its homogeneous composition.

1.3.2 Conduct experiments to measure the velocity and size distribution of water droplets and compare the results with that of the standard PDA instrument.

1.4 Obtained Benefit

1.4.1 Obtaining a Phase Doppler Anemometer instrument for measuring velocity and size distribution of particulate material.

1.4.2 Making a good relationship between INSA University, France and Chulalongkorn University, in order to transfer knowledge and new technology.

1.4.3 Better understanding in optical technique for particle size analysis especially a technique use for Phase Doppler Anemometer.

1.5 Description

A subject of considerable interest is the development of Phase Doppler Anemometer for measuring velocity and size distribution of water droplets. The organization of the book is as follows:

Chapter 1 is an introduction to the book. The general aim of developing the PDA is presented.

Chapter 2 provided a survey of applications of measuring techniques especially on PDA system used in the both the industrial and research and development on two-phase flow communities.

Chapter 3 has been devoted to summarizing basic optical concepts and geometric concerns relating to the instrument together with a discussion of the properties of lasers.

Readers familiar with optics may omit this chapter referring back to it for special results and formulae when necessary.

Chapter 4 describes the basic principles of LDA and PDA techniques by using an extended receiving optical system of LDA with two or more photodetectors, the velocity and size of individual particles are simultaneously measured. These include the theories relating to LDA and PDA techniques such as the Doppler shift, two models for explaining the physical principle of LDA and PDA techniques, probe volume and phase-diameter relations.

Chapter 5 deals with the developed PDA instrument. The design and set-up of the PDA system and for operating the PDA software have been explained for whoever wishing to employ it to serve their objective. By reading this chapter, the reader would have the better understanding how the LDA and PDA work. Next, the descriptions of the signals and signal processing to obtain the information from PDA experiments and the general PDA experimental set-up to conduct the experiment are also presented.

Chapter 6 discusses the experiments for verifying reliability of signal processing system and the developed PDA instrument. The instrument reliability experiments were conducted by taking the measurement results from the developed PDA instrument to compare with those of the commercial PDA instrument. The sources of discrepancies in the experiments are also discussed in the end of chapter.

Chapter 7 presents the conclusions and recommendation of the PDA instrument under development.

CHAPTER 2

SURVEY OF APPLICATIONS

Applicability of the techniques discussed in this work to industrial needs and problems is important if the phase Doppler technique is to find wide acceptance in both the industrial and research environments. Eventually, research into new techniques and theories should result in some instruments and techniques that have applications in some practical environment. To accomplish this goal, both fundamental researches into new approaches as well as development of instrumentation is needed. For the development to continue, a demand for the developed products needs to exist.

This chapter is devoted to the application of the phase Doppler technique in both the industrial and research and development communities but before that the categorization of several broad methods of particle size analysis has been first considered.

2.1 Categorization of measuring techniques

Numerous measuring techniques are available for such experimental studies on particle size analysis. These measuring techniques are categorized in certain groups according to their capabilities [2] as shown in Figure 2.1, although the list is not all-inclusive. Due to the large number of techniques available for sizing particles in many different fields, the information in this book has been restricted to techniques applied in two-

phase flow processes. The first classification is based on the way the information is extracted from the two-phase system. Sampling methods are still quite frequently applied in the process industry and powder technology industries to provide a detailed characterization of bulk solids at the different stages of the process for quality and process control (e.g., during milling or classification processes). Using mechanical sampling equipment, a number of characteristic samples of the bulk solids are collected and analyzed. The analysis of the samples may be performed using a microscope, mechanical methods such as sieving, fluid classification or sedimentation. Optical methods such as light scattering or light attenuation may also be applied. The result of these analyses could be, for example, characteristic dimensions of the particles, particle shape factors, equivalent particle diameters or particle surface area.

On-line measuring techniques are those methods which can be directly applied within the process or in a bypass line to analyze the properties. Moreover, on-line measuring techniques are widely used in research programs to characterize the development and the properties of a two-phase flow system. A further classification of on-line measurement techniques may be based on the spatial resolution of the measurement. Integral methods provide time-resolved, spatially-averaged properties of two-phase systems over an entire cross-section of the flow or along a light beam passing through the flow, depending on the method applied.

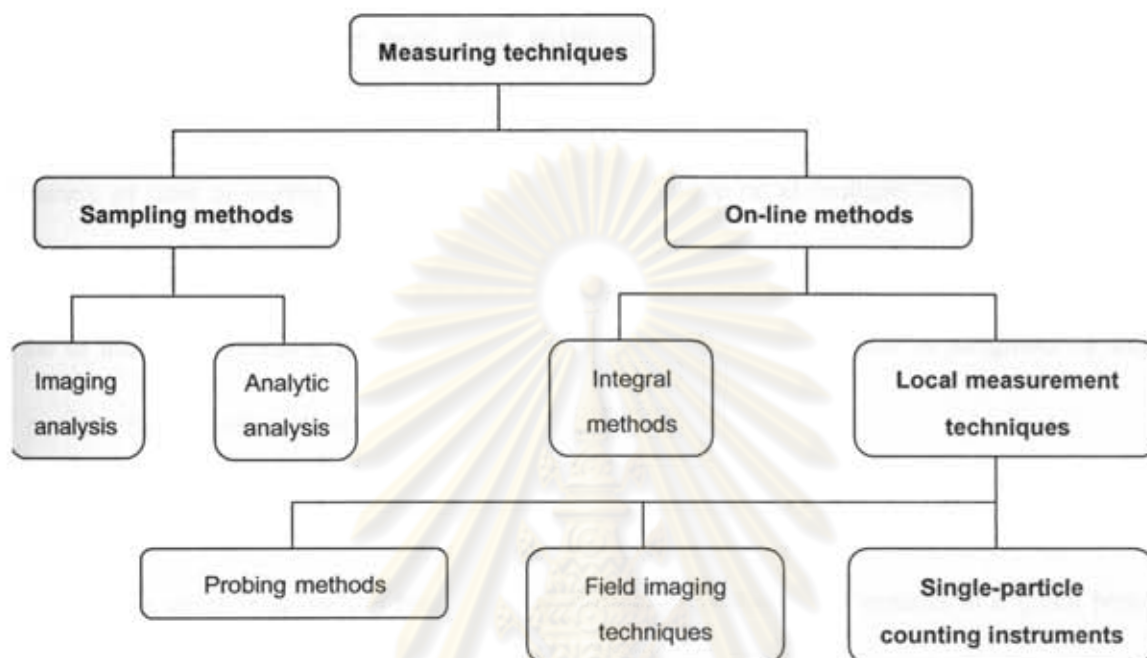


Figure 2.1 Categorization of measurement techniques for analysis of two-phase systems.

On the other hand, local measurement techniques allow the determination of local properties in a two-phase system with a spatial resolution which depends on the measurement technique applied. Those techniques which allow the determination of the properties of a two-phase system with a high spatial resolution (i.e., probe volume dimensions of the order of $100 \mu\text{m}$) are mainly based on optical methods. Such optical methods provide information either about the particle properties at a given instant of time or during a time sequence within a finite but relatively large probe volume (e.g., field imaging

techniques, such as particle image velocimetry or holography), or are based on measuring the properties of the particles moving through a small finite probe volume within a certain measurement time interval (e.g., light scattering or laser Doppler and phase Doppler anemometer). Methods of the first kind are based on visualizing the particles at a given instant of time or during a relatively short time sequence or at multiple times. Distribution functions of particle phase properties are therefore obtained for all particles that happen to be in the probe volume at a given instant of time. Hence the result is weighted by the particle number concentration.

Instrument based on the second method are also called single particle counting techniques since they require that only one particle be in the probe volume at a given time. Therefore, the size of the probe volume quite often needs to be very small in order to fulfill this requirement, depending on the particle concentration. Since the particle phase properties and the respective distribution functions are obtained for all particles that pass through the probe volume during the measurement time, the results obtained by such methods is weighted by the particle number flux.

A summary of the various measurement techniques and the dispersed phase properties, which can be obtained by the above described measurement techniques is given in Table 2.2. In the following sections, several of the most common measurement techniques and their capabilities are introduced and the limitations of their applications are summarized.

Table 2.2 Categorization of measurement techniques with respect to the measurable properties of a two-phase system [2].

Particle phase property	Sampling methods	On-line methods	
		Integral methods	Local measurement techniques
Size	Sieving	Laser diffraction	Light scattering
	Sedimentation		Phase Doppler Anemometer
Concentration	Isokinetic sampling	Laser diffraction	Isokinetic sampling
		Light absorption	Light scattering Phase Doppler Anemometer
Velocity	Direct velocity measurements are not possible	Correlation technique	Laser Doppler Anemometer Phase Doppler Anemometer Particle image velocimetry

2.2 Applications on PDA techniques

The phase Doppler technique has quickly found numerous applications. It is principally of value in studies of fluid flow. The principal advantages are its high spatial resolution and the fact that the light beams do not disturb the flow. Nothing but light is needed to be transmitted to the point of interest and light from a laser can be focused into a very small volume where the velocity is required. The consequent resolution, typically 20–100 μm exceeds that obtainable by any other methods [3]. The technique is not a

general replacement for other methods such as hot wires or pitot tubes since optical access is not always available.

PDA has the advantage of linearity and can cover a wide range of droplet size and flow velocities normally about 5 to 300 μm and millimeters per second to supersonic for size and velocity range, respectively [4]. The calibration can be calculated from optical geometry. In liquids and seeded gas flows, continuous signals can be obtained and the response of PDA is essentially instantaneous and fast fluctuations from turbulence can be followed. The technique therefore cannot be better in this application.

Also, with the phase Doppler technique there are methods available that enable the direction as well as the magnitude of a velocity to be determined. This is not possible with most other techniques of size and velocity measurement and is an invaluable feature in studying complex flows.

It should be remembered that this is a high-resolution fast response technique and thus it is in the field of turbulence that its potentialities are fully realized. Some measurements are not well suited to the technique. Measurement of total flow down a tube, for example, would have to be obtained by integration over the cross section, rather tedious for general application.

Very frequency velocity and turbulence profiles are required for design studies in wind tunnels and in flow situations, actual or modeled. It is here that the PDA technique is most useful and enables much detailed flow information to be rapidly obtained. The

absence of material probes enables measurements to be made in hostile environments such as corrosive liquids or flames. The measurements are not affected by temperature unless unusually long light paths through hot gases are involved. It should be recommended that in a hot temperature environment the temperature of the droplets would increase then their refractive index must change and the PDA measurement be wrongly interpreted.

The chief limitation of the phase Doppler technique is that it depends on the presence of particles in the flow. Insufficient particles may be present naturally, resulting in poor signal to noise ratios and the need for expensive processing equipment and/or long measurement times. The addition of particles may not always be possible or desirable. Fluids studied by PDA must of course be transparent. There is usually no difficulty here except for liquid metals of course or if long light paths through turbid water are required. Optical access to the fluid flow area must usually be provided by a transparent tube or window that does not necessarily need to be of very high optical quality.

A list of the advantages and disadvantages of the phase Doppler technique is given in Table 2.3

ศูนย์วิจัยทรัพยากร
จุฬาลงกรณ์มหาวิทยาลัย

Table 2.3 A list of the advantages and disadvantages of the phase Doppler technique [3].

Advantages	Disadvantages
<ul style="list-style-type: none"> - Does not disturb flow - High spatial resolution - Fast response - Response linear and easily calibrated - Directional discrimination possible - Operation not usually seriously affected by temperature 	<ul style="list-style-type: none"> - Medium must be transparent - Needs scattering particles: artificial seeding may be necessary - Optical access is required: windows may have to be installed - Expensive signal processing equipment may be required in difficult situations where the signal to noise ratio is poor - Not well suited for measurements of total flow as this requires a tedious integration over a cross section

2.2.1 Two-Component LDA/ PDA System

In the LDA or PDA system which has only one form of fringes called one-component LDA or PDA system, it is not possible to select different components of velocity by positioning the detector, since the Doppler beat frequency is the same in all directions. Some other method of distinguishing channels corresponding to different velocity components is required.

To measure two components of velocity in the same probe volume, it is necessary to form two superimposed sets of fringes which called two-component LDA or PDA system. They may be discriminated by polarization or more satisfactorily by color, and this is the method most widely used.

Grant, G. R. and Orloff, K. L., 1973 [5] studied the experimental construction on this principle by using blue and green colors obtained simultaneously from an argon ion laser operating in an 'all-lines' mode, i.e. with a simple mirror cavity without a prism wavelength selector. The strongest lines are normally of wavelengths 488.0 and 514.5 nm. A simpler arrangement using a color selective beam splitter was chosen to separate the different colors from the laser output. In this case three parallel beams are formed, one containing both colors. The scattered light received is divided into two channels by a beam splitter that preferably is color discrimination and reject light from the minor lines of the spectrum of the argon laser. It is important that the fringes of the two colors are accurately aligned, particularly when Doppler signals are intermittent. Unless the two components of velocity are recorded simultaneously for each particle, the utility of the system is much reduced.

Orloff, K. L. and Logan, S. E., 1973 [6] described that the measurement of the 'in-line' component of velocity can present a problem in the Doppler techniques since the components measured directly are those perpendicular to the bisector of the illuminating beams. It is not easy to make this sufficiently different from the viewing

direction since there are practical limitations on the directions from which it is possible to provide illuminating beams.

2.2.2 Applications to Spray Atomization

Spray atomization is widely employed within industrial and agricultural processes. A knowledge of the precise droplet distribution generated by an atomization nozzle and variation factors which have to achieve a satisfactory emissions performance in order to meet current and future legislation standards.

Quite clearly, in view of the greater emphasis placed today on the use of clean technology, engineers need to have a better appreciation of the capabilities and performance of individual spray nozzles. Advances in optical instrumentation, based on diffraction, visibility and phase techniques, to provide precise details of the diameter and velocity of droplets generated by individual sprays has been rapid over the past two decades. The phase technique has proved to be suitable for any kind of spherical particles, including droplets in gas streams.

This part presents some of the literature reviews of the PDA applications achieved on the spray atomization.

Brena de la Rosa, A., Sankar, S. V., Wang, G. and Bachalo, W. D., 1993 [7]
studied the PDA technique on turbulence properties in a confined swirling spray completed

that illustrates the capabilities of this technique to measure turbulence parameters in complex flow configurations.

McDonell, V. G., Samuelsen, G. S., Wang, M. R., Hong, C. H. and Lai, W. H., 1994 [8] studied PDA technique is particularly suited to spray measurements and is a valuable tool in nozzle characterization and conducted an interlaboratory comparison of spray measurements taken with several different instruments to establish a 'standard' spray for the evaluation of instruments and operator performance.

G. Wigley, J. Heath, G. Pitcher and A. Whybrew., 1999 [9] studied the systematic approach adopted to establish the LDA/PDA experimental technique that would allow measurements to be made over a wide droplet size range with confidence. The analysis considers the sprays generated by different gasoline direct injection systems injecting into air under atmospheric conditions. The work concludes that the applied LDA/PDA measurement technique is robust. It can discriminate between partially and fully atomized sprays, can accurately measure droplet sizes larger than the measurement volume with a high probability as long as the PDA system parameters match the measurement task and give a realistic indication of sizes for non-spherical droplets.

Fabrice Onofri, Damien Blondel, Gerard Grehan, Gerard Gouesbet., 1996 [10] investigated the extension of generalized Lorenz-Mie theory to the case of multilayered spheres, results connected with PDA system are considered, showing the influence of Gaussian beam intensity profiles on the light scattering properties of these particles.

Particular emphasis is placed on the case of water-coated carbon core particles, for which the possibility of obtaining simultaneous size measurements of the core and outer diameters is discussed. The sensitivity of the technique to particles with a refractive index profile is also considered, showing that this technique is more sensitive to changes in the average refractive index of the particles than to refractive index profile, such as produced by high pressure and temperature stresses, at least for the studied geometry.

H. Mignon, G. Grehan, G. Gouesbet, T. H. Xu, and C. Tropea., 1996 [11] studied the feasibility of one measuring the diameter of cylindrical particles by using PDA system. Two important characteristics of the measurement system have been identified, quantified, and to some extent verified. For certain particle orientations the scattered light no longer falls onto the detector apertures and no measurement is possible. The detected phase difference also changes with particle orientation, leading to an error in the size measurement. On the other hand, the optical and geometric parameters of the system can be chosen so that the instrument ceases measurement for orientations that would lead to errors exceeding a given limit. This is most easily realized through the choice of focal length and detector aperture size.

N. Gauchet, T. Girasole, K.F. Ren, G. Grehan and G. Gouesbet., 1997 [12] studied the generalized Lorenz-Mie theory for applying to cylindrical particle. It describes the interaction between an infinite cylinder and an illuminating arbitrarily shaped beam. In the study the applicability of this theory to the evaluation of phase-Doppler instruments for

cylindrical particle characterization is demonstrated, exemplifying the particular case when the cylinder is perpendicular to the impinging laser beams.



ศูนย์วิทยทรัพยากร
จุฬาลงกรณ์มหาวิทยาลัย

CHAPTER 3

BASIC OPTICS AND LASER

In this chapter the fundamental principles of optics are recalled and the basic *properties of lasers described paying special attention to the aspects relevant to the practical use of the phase Doppler technique.* For a detailed and rigorous discussion, the reader is referred to standard optical textbooks, but the treatment given here should enable a reader with some general knowledge of optics to appreciate the design and limitations of PDA instruments.

3.1 Light as Electromagnetic Radiation

Light is a special case of the general type of radiation arising from the interaction of electric and magnetic fields. The spectrum of electromagnetic waves extends from long radio waves to the γ -rays of nuclear physics and all these waves travel with the same velocity, i.e. $C_0 = 2.99776 \times 10^8 \text{ m s}^{-1}$. The range of wavelengths or frequencies is conventionally divided into regions depending on the common methods of production and detection. The main divisions are shown in Figure 3.1. Visible radiation has wavelengths in the range approximately $0.40 - 0.70 \mu\text{m}$, depending on color.

The technique of velocity and size measurement by means of the Doppler shift is applied to the whole range of electromagnetic waves but the practical methods discussed in this work apply principally to wavelengths of around the visible region. The neighboring

ultra-violet and infrared regions may also be included and these waves may be loosely referred to as light.

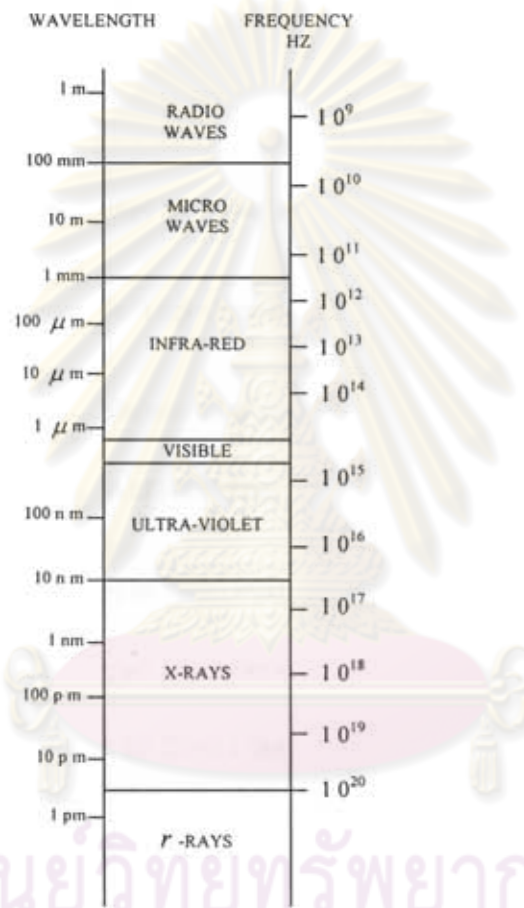


Figure 3.1 *The electromagnetic spectrum.*

The propagation of light, as of all electromagnetic waves, is determined by equations first derived by Maxwell and these are fundamental to the complete understanding of optics. Approximations valid for distances of propagation large compared

with the wavelength will be used. For many purposes, the use of simple geometrical optics is adequate.

3.2 Geometrical Optics

In many situations, the use of elementary geometrical optics is all that is needed to determine the propagation of light beams and much of the design of PDA systems is based on these principles. In this approximation the laws are as follows:

- (1) in a uniform medium light travels in straight lines along rays;
- (2) when rays are reflected at a smooth surface, the angle of incidence is equal to the angle of reflection;
- (3) when passing from one medium to another, light is deviated or refracted, the angles of incidence and refraction θ_1 and θ_2 (see Figure 3.2) being related by Snell's law:

$$\frac{\sin \theta_1}{\sin \theta_2} = \frac{n_2}{n_1} \quad (3.1)$$

where n_1 and n_2 are the refractive indices of the media (usually referred to vacuum).

Refraction from a dense to a less dense medium ($n_2 < n_1$) is not possible if $\theta_1 > \sin^{-1}(n_2/n_1)$. In this case the incident light is totally reflected. Total internal reflection inside prisms is often used for beam deflection.

The most familiar optical devices using the principle of refraction are lenses. They have many uses in PDA system for expanding and focusing laser beams, image formation, and concentrating light onto detectors. The lens performance required is usually less demanding than in most optical instruments or in photography, and for most PDA applications simple one-component lenses are adequate. This is because of the small diameters of laser beams and monochromatic nature of the light.

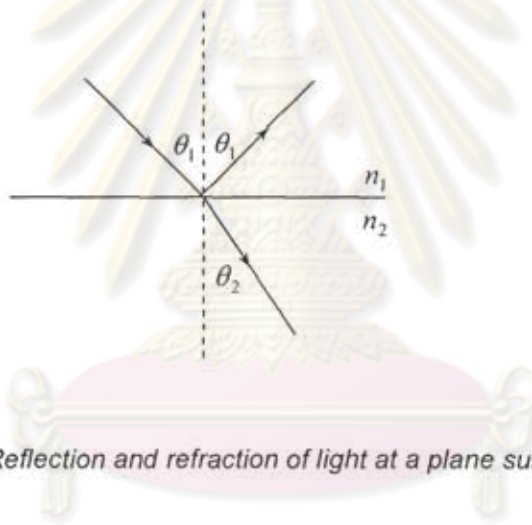


Figure 3.2 Reflection and refraction of light at a plane surface.

3.3 Interference

The wave nature of light is very evident in the phenomenon of interference, which occurs when two beams are superimposed. If the light beams have a sufficiently well defined frequency and consistent phase relation, light and dark bands, interference fringes, can be observed. A simple situation of this type, often applied in PDA work, is the crossing of two parallel beams at an angle α . This may be produced for example by splitting a

plane wave with a small angle prism (Fresnel biprism), as shown in Figure 3.3. Points in the crossover region are subject to the alternating electric fields of both beams. Where these alternations are in phase, the resultant electric field amplitude is the sum of the amplitudes from the two beams, and an increase in light intensity is obtained. Where the alternations are out of phase, the resultant is the difference of the amplitudes, and the light intensity is reduced.

The phases of the electric field alternations produced by the beams at a point P in Figure 3.3 are determined by the distances x_1 and x_2 measured along the beams from reference planes. Constructive interference occurs for

$$x_1 - x_2 = n\lambda + \phi \quad (3.2)$$

where λ is the light wavelength, n is an integer and ϕ is a phase constant. Points satisfying this condition lie on planes bisecting the angle between the two beams and separated by a distance s given by

$$s = \frac{\lambda}{2 \sin(\alpha/2)} \quad (3.3)$$

ศูนย์วิจัยทรัพยากร
จุฬาลงกรณ์มหาวิทยาลัย

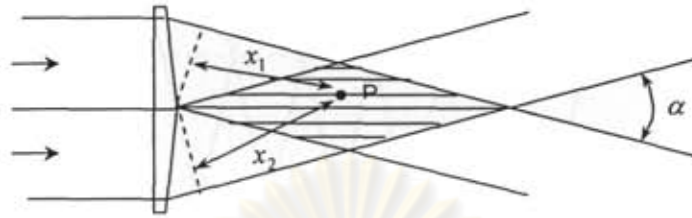


Figure 3.3 *The formation of interference fringes by parallel light beams crossing at an angle α .*

Each plane corresponds to a different value of n . This formula may easily be derived by mathematical analysis or by the geometrical construction shown in Figure 3.4. Planes of equal phase, wave fronts, separated by one wavelength are drawn for each beam. These are denoted by $A_1, A_2, \dots, B_1, B_2, \dots$, etc. and could be interpreted as wave crests at a particular instant. The points where the waves reinforce lie on the planes C_1, C_2 , etc. The separation of these bright fringes is denoted by s . Consideration of the right-angled triangle XYZ formed by the construction shown immediately yields formula (3.3)

ศูนย์วิจัยทรัพยากร
จุฬาลงกรณ์มหาวิทยาลัย

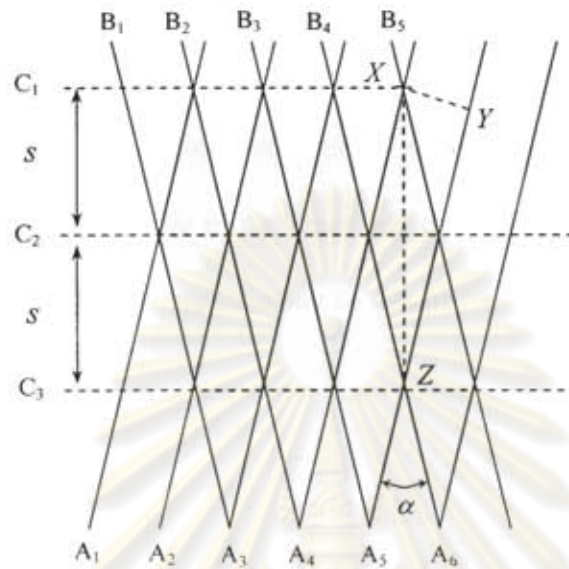


Figure 3.4 Diagram showing the relation of interference fringes to the wave fronts of intersecting beams.

3.4 Diffraction

A consequence of the wave nature of light is the derivation from the strict straight-line law of propagation assumed in geometrical optics. A beam only travels in a straight line if its diameter is very large compared with the wavelength λ . The divergence of a beam of diameter d is given approximately by λ/d . Diffraction sets a limit to the definition and resolution obtainable in an optical system. Optical systems giving as good a definition as is theoretically possible are termed diffraction limited.

Most problems in the diffraction of light may be solved by the application of Huygens's principle, an old idea but still a valid approach. It may be derived as an approximation from electromagnetic theory. This principle enables the optical field to be derived from a given wave front by treating infinitesimal elements of the wave front as point sources having amplitude proportional to the amplitude of the incident light at that point. The total amplitude at any given point is obtained by integrating the contribution from every point on the wave front.

3.5 Gaussian Beam Optics

In most laser applications it is necessary to focus, modify, or shape the laser beam by using lenses and other optical elements. In general, laser-beam propagation can be approximated by assuming that the laser beam has an ideal Gaussian intensity profile, corresponding to the theoretical TEM_{00} mode. Coherent Gaussian beams have peculiar transformation properties that require special consideration. In order to select the best optics for a particular laser application, it is important to understand the basic properties of Gaussian beams.

In PDA, we are more often concerned with Gaussian intensity distribution. The intensity distribution across the beam is Gaussian in all cross-sections. In general, a 'Gaussian' beam has the shape shown in Figure 3.5 [3]. The radius r_2 of the beam of $1/e^2$ intensity points at a typical cross-section is given by

$$r_z^2 = \frac{\lambda^2 z^2}{\pi^2 r_0^2} + r_0^2 \quad (3.4)$$

where e is a mathematical constant which is base of the natural logarithm, z is the distance along the beam from the cross-section of minimum diameter or 'waist' and r_0 is the radius at the waist (the distance from the center where the intensity is reduced to $1/e^2$ of its maximum value) in the focal plane. At the waist we have an equiphase plane but elsewhere the beam is converging or diverging. The angle of divergence or convergence (ϕ) at distance z is

$$\phi = \frac{2 dr_z}{dz} = \frac{2\lambda^2 z}{\pi^2 r_0^2 r_z} = \frac{2\lambda}{\pi r_0} \left/ \left(1 + \frac{\pi^2 r_0^4}{\lambda^2 z^2} \right)^{1/2} \right. \quad (3.5)$$

These relations may be used to calculate the propagation of Gaussian beams where diffraction effects are important. For example, we see that a plane wave (which corresponds to the waist position in Figure 3.5) spreads out by diffraction to a limiting divergence angle ϕ_∞ at infinity of

$$\phi_\infty = \frac{2\lambda}{\pi r_0} \quad (3.6)$$

It is interesting to note that when a parallel Gaussian beam is focused by a lens, the minimum beam diameter does not occur exactly at the focal plane but slightly nearer the lens. The difference is sometimes significant for narrow beams and long focal lengths. Supposing that the light is traveling from right to left in Figure 3.5, it may be considered the converging beam at the plane z to be formed from a parallel beam by a lens in that plane.

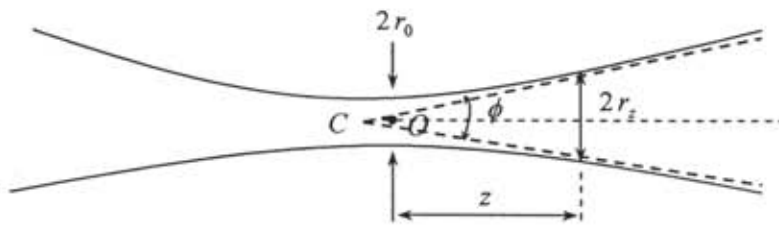


Figure 3.5 Characterization of a Gaussian beam.

The distance of the center of the waist from the point of convergence C may be calculated from equations (3.4) and (3.5) in terms of the focal length F and the radius of the beam at the lens R_0 we have:

$$OC = F - z = F / \left(1 + \frac{\pi^2 R_0^4}{\lambda^2 F^2} \right) \quad (3.7)$$

or approximately

$$F \left(\frac{F\lambda}{\pi R_0^2} \right) \quad (3.8)$$

when $R_0^2 \gg F\lambda$

3.6 Polarization of Light Waves

In electromagnetic radiation, the oscillating field is transverse to the direction of propagation. This allows a degree of freedom for the orientation of the field or different states of polarization. The plane containing the electric field and the direction of

propagation will be called the 'plane of polarization', but the convention on this is not universal.

Figure 3.6 shows that the electric and magnetic vectors associated with an electromagnetic wave are at right angles to each other and also to the direction of wave propagation is firm evidence of the transverse nature of electromagnetic waves.

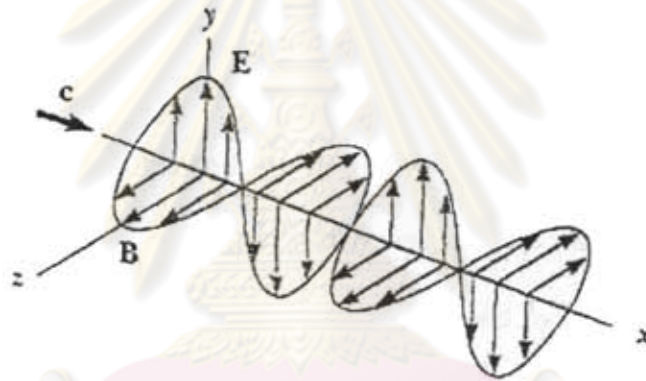


Figure 3.6 Schematic diagram of an electromagnetic wave propagating in the x direction.

The electric field vector E vibrates in the xy plane, and the magnetic field vector B vibrates

in the xz plane.

An ordinary beam of light consists of a large number of waves emitted by the atoms or molecules of the light source. Each atom produces a wave with its own orientation of E , as in Figure 3.6, corresponding to the direction of atomic vibration. The direction of

polarization of the electromagnetic wave is defined to be the direction in which E is vibrating. However, because all directions of vibration are possible, the resultant electromagnetic wave is a superposition of waves produced by the individual atomic sources. The result is an unpolarized light waves, described in Figure 3.7 (a). The direction of wave propagation in this figure is perpendicular to the page. Note that all directions of the electric field vector, lying in a plane perpendicular to the direction of propagation, are equally probable. At any given point and at some instant of time, there is only one resultant electric field.

A wave is said to be linearly polarized if E vibrates in the same direction at all times at a particular point, as in Figure 3.7 (b). The wave described in Figure 3.6 is an example of a wave linearly polarized in the y direction. As the wave propagates in the x direction, E is always in the y direction. The plane formed by E and the direction of propagation is called the plane of polarization of the wave.

In Figure 3.6 the plane of polarization is the xy plane. It is possible to obtain a linearly polarized beam from an unpolarized beam by removing all waves from the beam except those whose electric field vectors oscillate in a single plane.

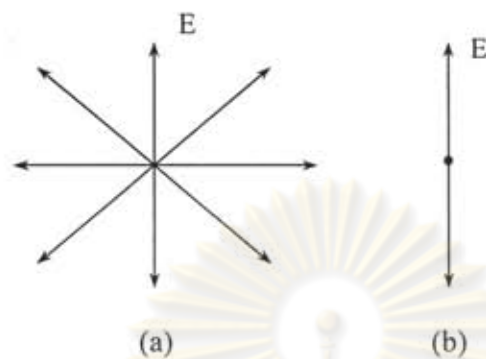


Figure 3.7 (a) An unpolarized light beam viewed along the direction of propagation (perpendicular to the page). The transverse electric field vector can vibrate in any direction with equal probability. (b) A linearly polarized light beam with the electric field vector vibrating in the vertical direction.

3.7 Laser

3.7.1 General Laser Properties

The term 'laser' is an acronym for light amplification by stimulated emission of radiation. All lasers produce intense beams of light that are monochromatic, coherent, and highly collimated. The wavelength of the laser light is extremely pure (monochromatic) when compared to other sources of light, and all of the photons (energy) that make up the laser beam have a fixed phase relationship (coherence) with respect to one another. This causes the light to form a beam with a very low rate of expansion (low divergence) that can travel over great distances, or can be focused to a very small spot with a brightness that

can approximate that of the sun. Because of these properties, lasers are used in a wide variety of applications in all walks of life.

All lasers consist of at least three components as follows:

- i) a gain medium that can amplify light that passes through it;
- ii) an energy pump source to create a population inversion in the gain medium;
- iii) two mirrors that form a resonator cavity.

The gain medium can be solid, liquid, or gas and the pump source can be an electrical discharge, a flashlamp, or another laser. The specific components of a laser vary depending on the gain medium and whether the laser is operated continuously or pulsed. The following headings describe specific laser designs.

3.7.2 Laser Types

- Gas Lasers

Gas lasers are typically excited by an electrical discharge. The most commonly used gas lasers are helium and helium-neon, which have a primary output of visible red light. The schematic of a continuously gas laser is shown in Figure 3.8.

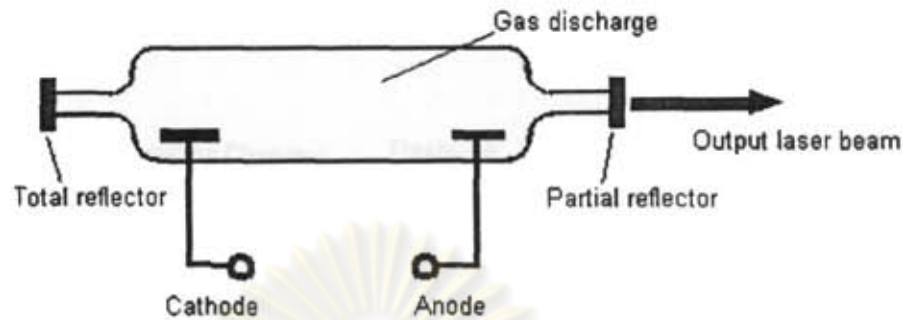


Figure 3.8 Schematic of a continuously gas laser.

- Solid-State Lasers

The gain medium in a solid-state laser is an impurity center in a crystal or glass. Solid-state lasers made from semiconductors are described below. The first laser was a ruby crystal (Cr^{3+} in Al_2O_3) that lased at 694 nm when pumped by a flashlamp. The most commonly used solid-state laser is one with Nd^{3+} in a $\text{Y}_3\text{Al}_5\text{O}_8$ (YAG) or YLiF_4 (YLF) crystal or in a glass. These Nd^{3+} lasers operate either pulsed or continuously and lased at approximately 1064 nm. The schematic of a solid-state laser shown in Figure 3.9

- Dye Lasers

The gain medium in a dye laser is an organic dye molecule that is dissolved in a solvent. The dye and solvent are circulated through a cell or a jet, and the dye molecules are excited by flashlamps or other lasers. Pulsed dye lasers use a cell and continuously dye lasers typically use a jet. The organic dye molecules have broad fluorescence bands and dye lasers are typically tunable over 30 to 80 nm. Dyes exist to

cover the near-ultraviolet to near-infrared spectral region: 330-1020 nm. The schematic of a pulsed dye laser shown in Figure 3.10.

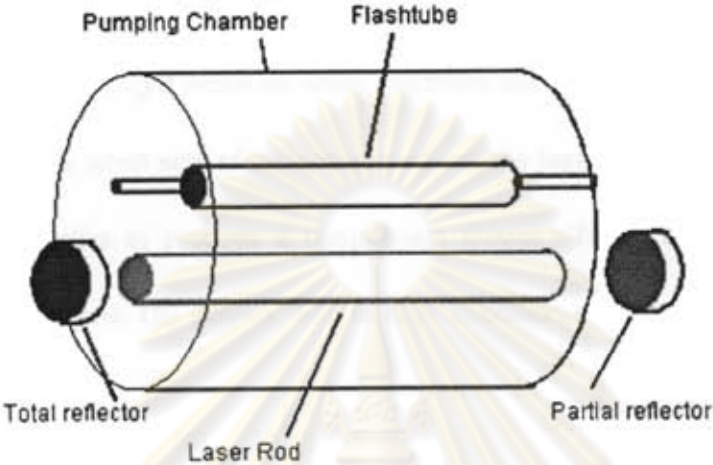


Figure 3.9 Schematic of a solid-state laser.

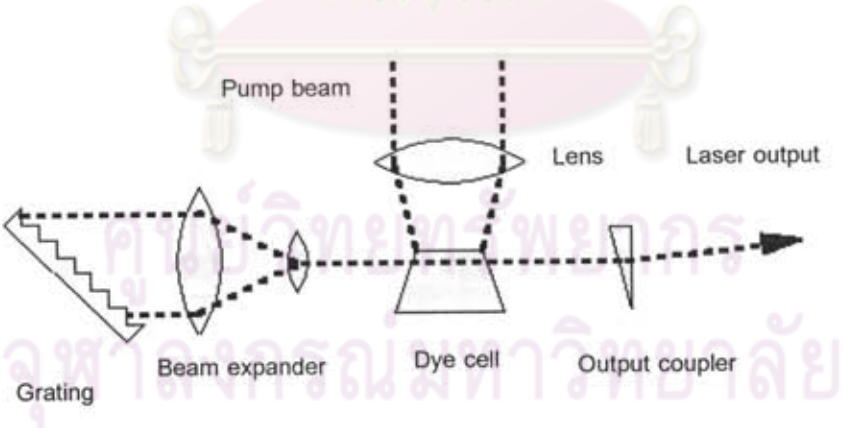


Figure 3.10 Schematic of a pulsed dye laser.

- Semiconductor Lasers

Semiconductor lasers are light-emitting diodes within a resonator cavity that is formed either on the surfaces of the diode or externally. An electric current passing through the diode produces light emission when electrons and holes recombine at the p-n junction. Because of the small size of the active medium, the laser output is very divergent and requires special optics to produce a good beam shape. These lasers are used in optical fiber communications, CD players, and in high-resolution molecular spectroscopy in the near-infrared. Diode laser arrays can replace flashlamps to efficiently pump solid-state lasers. Diode lasers are tunable over a narrow range and different semiconductor materials are used to make lasers at 680, 800, 1300, and 1500 nm. The schematic of a semiconductor laser shown in Figure 3.11

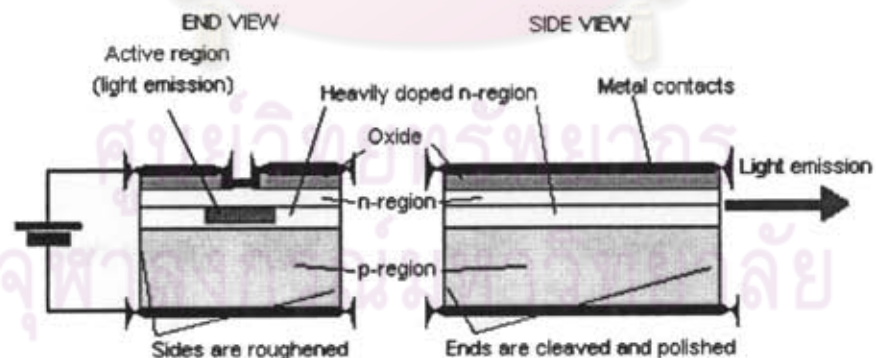


Figure 3.11 Schematic of a semiconductor laser.

3.8 Light Detectors for PDA

An essential element in any phase Doppler equipment is the light detector. This converts changes in light intensity into electrical signals, which are required for most methods of analysis. High sensitivity and fast response are desirable. There is basically one type of detector available, namely photomultipliers.

Photomultipliers are vacuum tubes in which electrons are released by light falling on a special photoemissive surface. These electrons may be collected by a positive electrode to produce a measurable current. The most effective emitters are intermetallic compounds containing alkali metals and these forms the basis of most photosensitive surfaces. With this type of detector, it is usual to arrange for the amplification of the photocurrent by the secondary emission at intermediate electrodes or dynodes at successively higher voltages with respect to the photoemissive cathode. This is illustrated in Figure 3.12. The voltages for the dynodes are usually derived from a common high voltage source via a chain of resistors. Current amplification factors of several tens of thousands are usual in a chain of dynodes. This feature gives photomultipliers an important practical advantage.

Current through the final anode may be directly measured or an output voltage produced across a resistor R . A high value of R will give high voltage output but may reduce the possible high frequency response owing to the parallel capacity of the anode and leads to the amplifier. The ultimate high frequency response is limited by the variation of transit time of electrons from the cathode to the anode. This may be reduced by good

design and the use of high acceleration potentials. Typical transit times are 20 – 100 ns. The spread of these times and the consequent rise times in response to a pulse of light are generally in the range 2 – 20 ns giving frequency response up to 10 – 100 MHz.

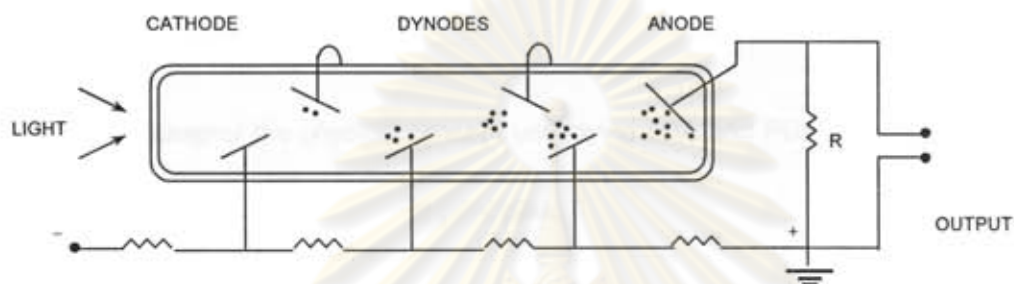


Figure 3.12 *Diagram of photomultiplier detector.*

Most photomultipliers have their highest sensitivity in the blue and green regions of the spectrum, sensitivity to red light being poor unless special cathode emitting materials are used. Where response in the red is important, with helium-neon lasers for example, the multi-alkali cathode Na-K-Cs-Sb (S20) is the type most frequently used and there are photosensitive surfaces available with useful responses in the near infrared to nearly 1.1 μm .

ศูนย์วิทยาศาสตร์
จุฬาลงกรณ์มหาวิทยาลัย

CHAPTER 4

BASIC PRINCIPLES OF LASER DOPPLER ANEMOMETER (LDA) AND PHASE DOPPLER ANEMOMETER (PDA) TECHNIQUES.

In this chapter the physical concept underlying LDA and PDA techniques have been described and followed by their basic principles.

4.1 The Doppler Shift

The technique of using the Doppler shift of laser light to determine the velocities of particles were first demonstrated in 1964 by Yeh and Cummins, who observed the shift of light scattered from particles carried in a water flow. Measurements of size soon followed by three teams independently: Bachalo in USA, Dantec in Denmark and F. Durst in Germany. Lasers produce a very intense monochromatic light very suitable for this type of measurement. There are a number of variations of the technique, which may be broadly described as Phase Doppler Anemometry, commonly abbreviated to "PDA".

In any form of wave propagation, frequency changes can occur owing to movement of the source, receiver, propagating medium, or intervening reflector or scatterer. These shifts are generally called "Doppler" shifts after the Austrian physicist who first considered the phenomenon in 1842. The Doppler shift, familiar in acoustics, is due to the relative

motion of source and receiver and this type of shift is also well known for electromagnetic radiation, including light. The red shift to lower frequencies of light arriving at the earth from distant galaxies is attributed to their movement away from us at extremely high velocities. The shift of γ -rays from a moving radioactive source may be readily demonstrated in the laboratory using extremely well defined resonance adsorption and emission lines that may be obtained in the Mossbauer effect.

4.2 Model of LDA and PDA Techniques

The physical principle of LDA and PDA for velocity measurements can be explained in two models as follows:

4.2.1 The Doppler Model

The Doppler model or Doppler effect which relates the interaction of sound or light waves with a moving observer or the modulation of sound or light waves received by a stationary observer from a moving emitter. In LDA or PDA, this principle is used in such a way that a laser emits plane light waves which are transmitted from a moving emitter, the particle. Hence, the frequency or wavelength of the light received by the particle is already modulated. Since the moving particle scatters the light into space, an additional Doppler shift occurs when the scattered light is received from a stationary observer as shown in Figure 4.1. Hence, the frequency of light received at the photodetector can be determined from [2]

$$f_r = f_c \frac{1 - \frac{\vec{v} \cdot \vec{l}}{c}}{1 - \frac{\vec{v} \cdot \vec{k}}{c}} \quad (4.1)$$

where f_c is the frequency of the laser source (emitter), \vec{v} is the velocity of the moving particle, c is the velocity of the light, and \vec{k}, \vec{l} are unit vectors in the direction as defined in Figure 4.2 The frequency of the scattered light f_r is, however, too high to allow direct detection by a photodetector. Therefore, two different methods, the reference beam and the Doppler frequency difference methods are used in this model.

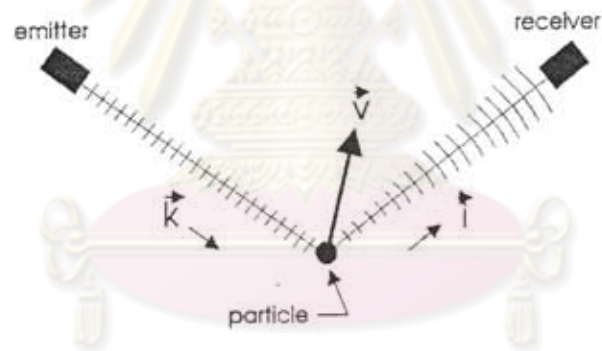


Figure 4.1 Doppler shift of scattered light from a moving particle.

This is achieved in the reference beam method by illuminating the particle with a strong light beam and interfering the resulting scattered light with a weak reference beam from the laser light source at the photodetector as shown in figure 4.2. Subtracting the frequency of the reference beam gives the Doppler frequency, f_D :

$$f_D = f_r - f_e \quad (4.2)$$

Using equation (3.1) and introducing $\vec{v} \cdot \vec{k} = -|\vec{v}| \cos \gamma_1$ and $\vec{v} \cdot \vec{l} = -|\vec{v}| \cos \gamma_2$ gives

$$f_D = f_e \frac{1 + \frac{|\vec{v}|}{c} \cos \gamma_1}{1 + \frac{|\vec{v}|}{c} \cos \gamma_2} \quad (4.3)$$

$$f_D = \frac{1}{\lambda_e} \left(\frac{|\vec{v}| (\cos \gamma_1 - \cos \gamma_2)}{1 + \frac{|\vec{v}|}{c} \cos \gamma_2} \right) \quad (4.4)$$

where γ_1 and γ_2 are the particle velocity angle which coincides with the strong beam and the reference beam, respectively (Figure 4.2) and λ_e is the wavelength of the laser source.

The velocity component perpendicular to the bisector of the two incident beams, v , is

$$v = -|\vec{v}| \sin \left[\frac{\gamma_1 + \gamma_2}{2} \right] \quad (4.5)$$

Using the trigometric relationship

$$\cos \gamma_1 - \cos \gamma_2 = -2 \sin \left[\frac{\gamma_1 + \gamma_2}{2} \right] \sin \left[\frac{\gamma_1 - \gamma_2}{2} \right] \quad (4.6)$$

one obtains

$$f_D = \frac{1}{\lambda_e} \left[\frac{2v \sin \theta}{1 + \frac{v}{c} \sin \theta} \right] \quad (4.7)$$

where $\theta = \frac{1}{2}(\gamma_1 - \gamma_2)$. Since, in general, $v \ll c$, equation (4.7) finally becomes

$$f_D = \frac{2v \sin \theta}{\lambda_e} \quad (4.8)$$

It should be noted that the reference beam mode could be only operated at a fixed observation angle which coincides with the reference beam angle θ . Furthermore, the solid angle for light collection is limited to satisfy coherence requirements, i.e., the amount of scattered light which is collected is restricted.

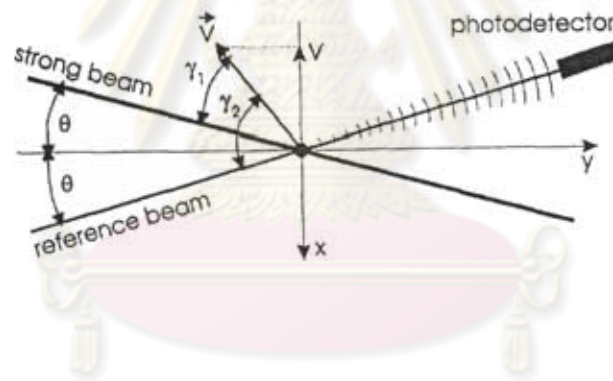


Figure 4.2 Configuration of reference beam LDA system.

More frequently, the Doppler frequency difference method is used for LDA and PDA measurement. Here the moving particle is illuminated by two laser beams from different directions as shown in Figure 4.3. In this case, the frequency of the scattered light is obtained from the difference of the contributions from two incident beams

$$f_D = f_{r1} - f_{r2} \quad (4.9)$$

where f_{r1} and f_{r2} are the frequency of the two laser beam from different directions which are beam 1 and beam 2, respectively.

Using, once again, equation (4.1) and the velocity components in the directions of the two beams, one obtains

$$\begin{aligned}
 f_D &= f_c \left(\frac{1 + (|\vec{v}|/c) \cos \gamma_1}{1 + (|\vec{v}|/c) \cos \gamma_3} - \frac{1 + (|\vec{v}|/c) \cos \gamma_2}{1 + (|\vec{v}|/c) \cos \gamma_3} \right) \\
 &= \frac{|\vec{v}|}{\lambda_c} \left[\frac{(\cos \gamma_1 - \cos \gamma_2)}{1 + (|\vec{v}|/c) \cos \gamma_3} \right]
 \end{aligned} \tag{4.10}$$

For the velocity component perpendicular to the bisector of the two incident beams and with $v \ll c$, equation (4.10) becomes

$$f_D = \frac{2v \sin \theta}{\lambda_c} \tag{4.11}$$

This expression is identical to the one obtained for the reference beam method. However, the observation angle can be arbitrarily selection in the Doppler difference method. This implies that the observation angle and solid angle of scattered light collection may be selected for convenience according to the desired application.

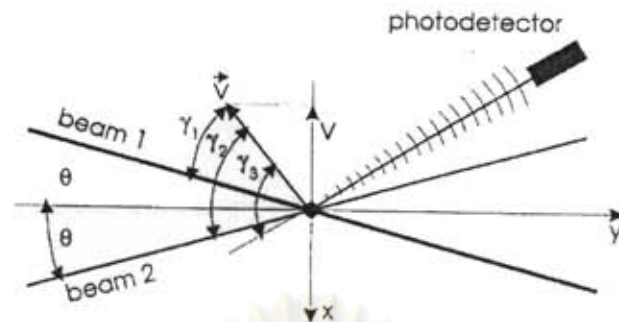


Figure 4.3 Configuration of the Doppler difference frequency method.
(dual beam LDA system).

4.2.2 The Fringe Model

Typical LDA and PDA techniques use two equal intensity laser beams that are split from a single beam. If two beams cross at a known angle 2θ , the interference of the light waves results in a fringe pattern parallel to the bisector plane as shown in Figure 4.4.

Given that the laser light has a wavelength λ_c , we would like to find the spacing d_f of the interference fringes where the combined laser light intensity is zero.

Consider an isosceles triangle bounded by a fringe and two wave fronts, as illustrated by the blue triangle in the schematic above. Recalling basic geometric properties of triangles, we find that the following three triangles (and subtriangles) are geometrically similar

$$\Delta ADB \sim \Delta BEC \sim \Delta CFB$$

Furthermore, let the angle ΔBAC be equal to α , we have the following relationships amongst three of the triangle's angles

$$\Delta ABC = \Delta ACB = \frac{1}{2}(\pi - \alpha) \quad (4.12)$$

$$\Delta ABE = \Delta ACF = \frac{\pi}{2} - 2\theta \quad (4.13)$$

$$\Delta CBE = \Delta BCF = \Delta BAD = \frac{\alpha}{2} \quad (4.14)$$

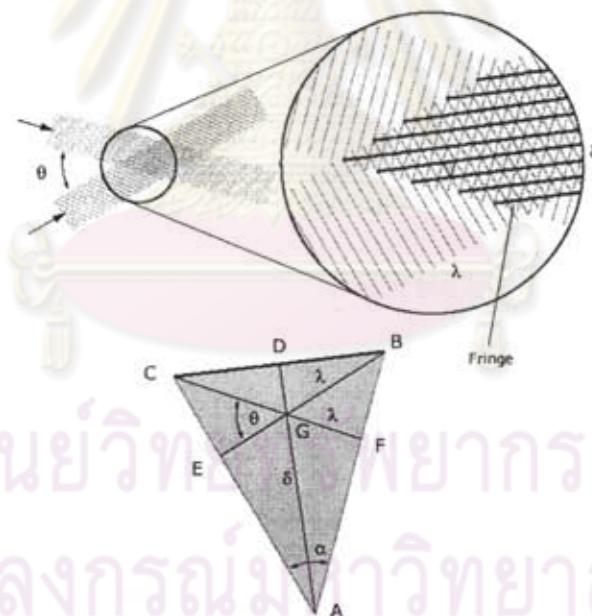


Figure 4.4 Schematic of two interfering beams at measurement volume.

Simplifying the above equations gives

$$\Delta ABC = \Delta ABE + \Delta CBE \quad (4.15)$$

$$\frac{\pi - \alpha}{2} = \frac{\pi}{2} - 2\theta + \frac{\alpha}{2} \quad (4.16)$$

which yields the solution for α :

$$\alpha = 2\theta \quad (4.17)$$

In order to link d_r to λ_e and θ , the base of the triangle ABC is used in the following equations

$$BC = BE \sec \theta = \lambda_e \frac{1}{\cos \theta} \quad (4.18)$$

$$= 2BD = 2AD \tan \theta = 2d_r \frac{\sin \theta}{\cos \theta} \quad (4.19)$$

The fringe spacing δ can now be expressed in terms of the laser properties

$$d_r = \frac{\lambda_e}{2 \sin \theta} \quad (4.20)$$

As the particle passes through the probe volume, the scattering intensity detected by a photodetector is modulated in such a way that the Gaussian-shaped absolute scattering intensity, which results from the Gaussian intensity distribution in the probe volume, is superimposed with an alternating pattern produced by the particles passing through the bright and dark fringe pattern. The fringe spacing d_r is basically the

conversion factor of the determine the particle velocity v from the measured Doppler difference frequency

$$v = f_D d_f \quad (4.21)$$

Since the fringe spacing d_f is a function of the laser wavelength λ_e and crossing angle θ , the velocity of the particle is found to be

$$v = f_D \frac{\lambda_e}{2 \sin \theta} \quad (4.22)$$

4.3 Probe Volume

The region of fringe formed by the crossing of the beams from which signal can be obtained is often called the 'probe volume', 'control volume' or 'scattering volume'. A particle moving in the control volume produces a signal proportional to the modulated component of the intensity distribution or 'fringe amplitude'.

The probe volume is determined by the initial laser beam diameter, the beam crossing angle (determined by the initial beam spacing and focal length of the transmitting lens), the focal length of the receiving lens and the observation angle of the receiving optics. Since the incident focused laser beams have a Gaussian intensity distribution (Figure 4.5), their waist diameter at the focal plane is taken to be that value at which the light intensity (V) has diminished to $1/e^2$ of the maximum value (V_{\max}) at the beam axis. The waist diameter (d'_m) is given by

$$d_m = \frac{4 f_c \lambda_c}{\pi d_0} \quad (4.23)$$

where d_0 is the $1/e^2$ unfocused laser beam diameter, λ_c is the wavelength of the light and f_c is the transmitting lens focal length. The probe volume established by the two crossing beams has an ellipsoidal shape (Figure 4.5). The dimensions of the $1/e^2$ ellipsoid, corresponding to Figure 4.5, are given by

$$\Delta x = \frac{d_m}{\cos \theta} \quad (4.24)$$

$$\Delta y = d_m \quad (4.25)$$

$$\Delta z = \frac{d_m}{\sin \theta} \quad (4.26)$$

where θ is the reference beam angle. The number of fringes (N_f) in the $1/e^2$ measurement volume can be determined from

$$N_f = \frac{8 f_c}{\pi d_0} \tan \theta = \frac{4 \Delta b}{\pi d_0} \quad (4.27)$$

where Δb is the initial spacing of the transmitting beams.

By using an off-axis orientation of the receiving optics, the length of the portion of the measurement volume imaged into the photodetector can be further reduced and the spatial resolution improved. However, due to the angular dependence of the light scattering intensity, any off-axis orientation of the receiving optics results in reduced scattering intensities.

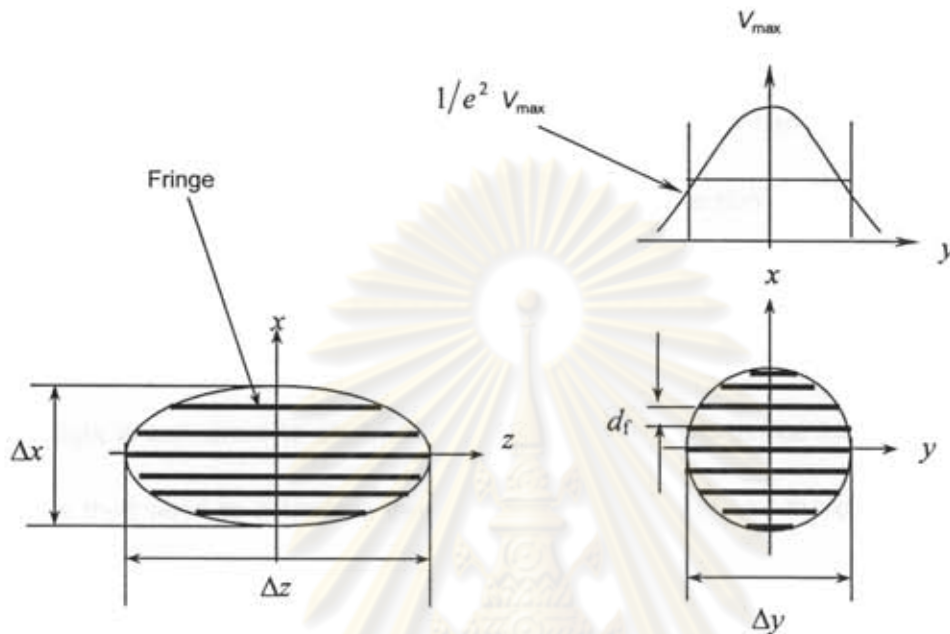


Figure 4.5 Dimensions of LDA probe volume.

It should be noted that the spatial resolution of the velocity measurement depends on the dimensions of the LDA probe volume.

4.4 Laser Doppler Anemometer (LDA)

LDA instrument is the most advanced and accurate non-intrusive measuring technique to obtain velocities of the fluid and particles in a two-phase flow. The system uses a laser beam to emit coherent light (i.e. a beam of light comprised of many amplitude modulated light source waves, all having the same frequency and in phase with each

other). The laser beam is split into two; and these subsequent beams are focused through the transmitting optics and crossed perpendicular to the particle stream. At the point where the beams cross, an interference of the light waves results in a fringe pattern parallel to the bisector plane (i.e., the y - z plane as shown in Figure 4.5), which can be visualized on a screen when a lens of small focal length is placed at the interaction of the beams. As the particle passes through the LDA probe volume (the bright and dark fringe pattern), the beam scattering is then collected by the receiving optics and focused on the photodetector, where the light is converted to electrical energy. An electronic device known as a signal processor is then used to determine the frequency of the signal and therefore the velocity of the flow.

A typical optical setup of an LDA system operated in the forward scattering mode is shown in Figure 4.6. The transmitting optics consist of the laser, a beam splitter and a transmitting lens. The receiving optics consist of an imaging lens with a mask in front of it and a photodetector with a pinhole.

ศูนย์วิทยทรัพยากร
จุฬาลงกรณ์มหาวิทยาลัย

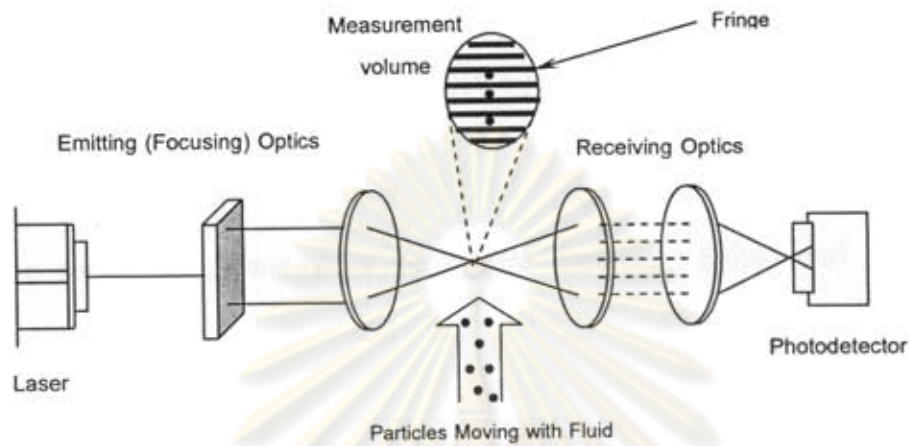


Figure 4.6 Typical optical setup of LDA instrument.

4.5 Phase-Diameter Relations

To size particles, the operational principle of PDA can be explained using the simple fringe type model assuming that the interference fringe in the intersection region of the two incident light beams of the PDA are parallel light rays. A spherical transparent particle placed into this fringe pattern will act as a kind of lens which will project the light rays into space as indicates in Figure 4.7 [2]. The separation of the projected fringe at a distance f_r from the particle (Δs) is given approximately by

$$\Delta s \approx (f_r - f) \frac{d_f}{f} \quad (4.28)$$

where d_f is the fringe spacing in the measurement volume. The focal length of the particle (f) is given by

$$f = \frac{m}{m-1} \left(\frac{D}{4} \right) \quad (4.29)$$

where $m = n_d/n_m$, the ratio of the refractive index of the particle (n_d) to that of the surrounding medium (n_m) and D is the particle diameter. Since small particles are considered and f_r is usually much larger than the particle diameter, one obtains

$$\Delta s \approx f_r \frac{d_f}{f} \quad (4.30)$$

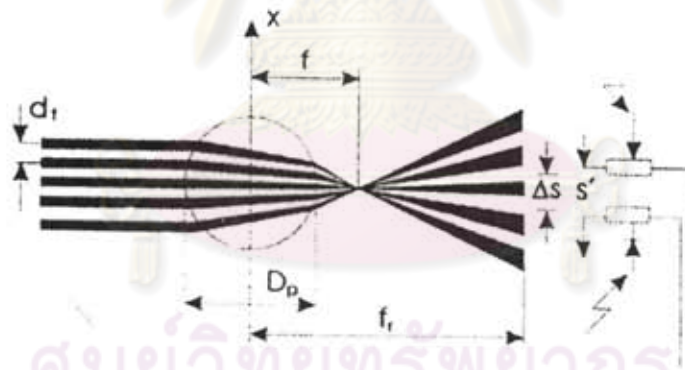


Figure 4.7 Fringe model for phase Doppler principle for the case of refraction.

The separation of the projected fringes is obtained from

$$\Delta s \approx \frac{4f_r d_f}{D} \left(\frac{m-1}{m} \right) \quad (4.31)$$

In general, the particles move through the probe volume and the fringes move as well so it is difficult to measure this spatial separation. However, if two photodetectors are symmetrically placed at f_r with a separation $\Delta s'$, as shown in Figure 4.7, the fringe produced by the moving particle will sweep across the two detectors at the Doppler difference (Φ) given by

$$\Phi = 2\pi \frac{\Delta s'}{\Delta s} = 2\pi \frac{2f_r}{\Delta s} \sin \psi \quad (4.32)$$

or by using equation (4.31)

$$\Delta \Phi = \pi \frac{D}{d_f} \frac{m}{m-1} \sin \psi = \frac{2\pi D}{\lambda} \frac{m}{m-1} \sin \theta \sin \psi \quad (4.33)$$

where ψ is the elevation angle of one photodetector measured from the bisector plane of the two incident beams where the optical axis of the PDA receiver is also located.

It should be emphasized that equation (4.33) is an approximation valid only for small scattering angles ϕ which represents the off-axis angle measured from the forward scattering direction. The equation is very useful, however, to provide a rough estimate of the measurable particle size range for a given system or to perform a preliminary design of the optical configuration for small scattering angles. To determine the particle size from

geometrical optics, which is valid for particles that are large, compared to the wavelength of light. The phase of the scattered light is given by

$$\Phi = \frac{2\pi D n_m}{\lambda} \left(\sin \tau - P \frac{n_d}{n_m} \sin \tau' \right) \quad (4.36)$$

where n_m and n_d are the refractive indices of the medium surrounding the particle and medium of the particle itself.

The parameter P indicates the type of scattering, i.e., $P = 0, 1, 2, \dots$ for reflection, first-order refraction, second-order refraction, and so on. Moreover, τ and τ' are the angles between the incident ray and the surface tangent and the refracted ray and the surface tangent, respectively, as shown in Figure 4.8. For a dual beam PDA system, the phase difference of the light scattered from each of the two beams is given in a similar way

$$\Delta\Phi = \frac{2\pi D n_m}{\lambda} \left[(\sin \tau_1 - \sin \tau_2) - P \frac{n_d}{n_m} (\sin \tau'_1 - \sin \tau'_2) \right] \quad (4.37)$$

where the subscripts 1 and 2 are used to indicate the contributions from both incident beams.

For two photodetectors placed at a certain off-axis angle ϕ and placed symmetrically with respect to the bisector plane at the elevation angles $\pm\psi$, one obtains the phase difference

$$\Delta\Phi = \frac{2\pi D n_m}{\lambda} \varphi \quad (4.38)$$

The parameter φ depends on the scattering mode. For reflection ($P = 0$),

$$\varphi = \sqrt{2} \left[\begin{array}{l} (1 + \sin \theta \sin \psi - \cos \theta \cos \phi \cos \psi)^{1/2} \\ -(1 - \sin \theta \sin \psi - \cos \theta \cos \phi \cos \psi)^{1/2} \end{array} \right] \quad (4.39)$$

and for refraction ($P = 1$),

$$\varphi = 2 \left\{ \begin{array}{l} \left[1 + m^2 - \sqrt{2} m (1 + \sin \theta \sin \psi + \cos \theta \cos \phi \cos \psi)^{1/2} \right]^{1/2} \\ - \left[1 + m^2 - \sqrt{2} m (1 - \sin \theta \sin \psi + \cos \theta \cos \phi \cos \psi)^{1/2} \right]^{1/2} \end{array} \right\} \quad (4.40)$$

where $m = n_d/n_m$ has been used for convenience and 2θ represents the angle between the two incident beams. Since the phase difference is a function of P , one expects a linear relation for the correlation between particle size and phase for only those scattering angles where one scattering mode is dominant (i.e., reflection or refraction).

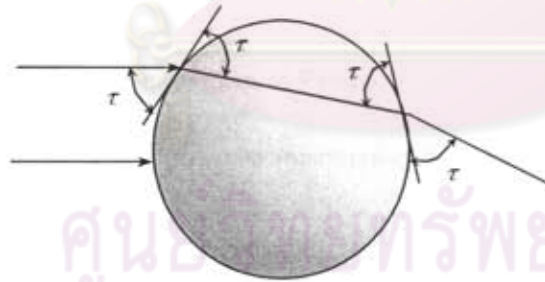


Figure 4.8 Phase difference of a light ray refracted at a spherical particle.

By recording the band-pass filtered Doppler signals from the two photodetectors the phase $\Delta\Phi$ is determined from the time lag between the two signals as indicated in Figure 4.9

$$\Delta\Phi = 2\pi \frac{\Delta t}{T} \quad (4.41)$$

where T is the time of one cycle of the signal. With equation (3.41) it is now possible to determine the particle diameter for a given refractive index n_m and wavelength λ .

$$D = \frac{\lambda}{2\pi n_m \varphi} \Delta\Phi \quad (4.42)$$

From equation (4.41) and Figure 4.9, it is also obvious that only a phase shift between zero and 2π can be distinguished with a two detector PDA system, which limits the measurable particle size range for a given optical configuration. Therefore, three-detector system is also used in which two-phase differences are obtained from detector pairs having different spacing as shown in Figure 4.10. This method enables one to extend the measurable particle size range while maintaining the resolution of the measurement.

For small particles, diffraction represents an especially important contribution to the light scattering that may affect and disturb the phase measurement. Therefore, the more general Mie theory [2] has to also be applied to determine the scattering characteristics for a particle of any given size. However, Mie theory is not used because of the diffraction, but to more accurately take into account complex phenomena as at rainbow or due to the mixing of several kind of interaction ($p = 2,3,\dots$) and for the small size of particle where the

geometrical optics is not good as for the big. The Mie theory relies on the direct solution of Maxwell's equations for the case of the scattering of a plane light wave by a homogeneous spherical particle for arbitrary size and refractive index. In order to calculate the scattered field of a PDA system, it is necessary to add the contributions of the two incident beams and the average over the aperture of the receiving optics configurations. To allow for the influence of the Gaussian beam, the generalized Lorenz-Mie theory (GLMT) [2] has also been recently applied to optimize PDA systems

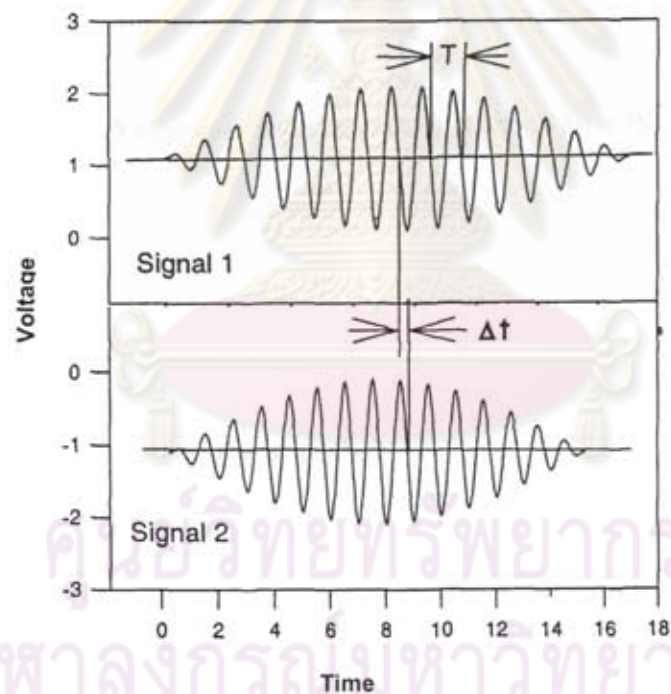


Figure 4.9 Determinations of phase shift from two Doppler signals.

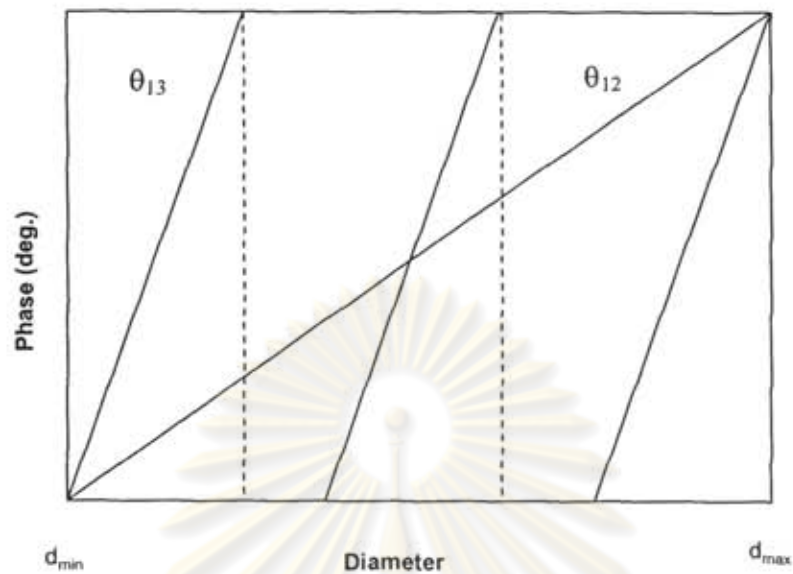


Figure 4.10 Representative response functions for a PDA system using three detectors.

4.6 Phase Doppler Anemometer (PDA)

The principle of PDA technique is based on the Doppler difference method used for conventional LDA technique. By using an extended receiving optical system with two or more photodetectors it is possible to measure particle size and velocity simultaneously. The phase shift of the light scattered which can be explained by the phase-diameter relations by refraction or reflection from the two intersecting laser beams is used to obtain the particle size. A typical optical setup of a two PDA system is shown in Figure 4.11.

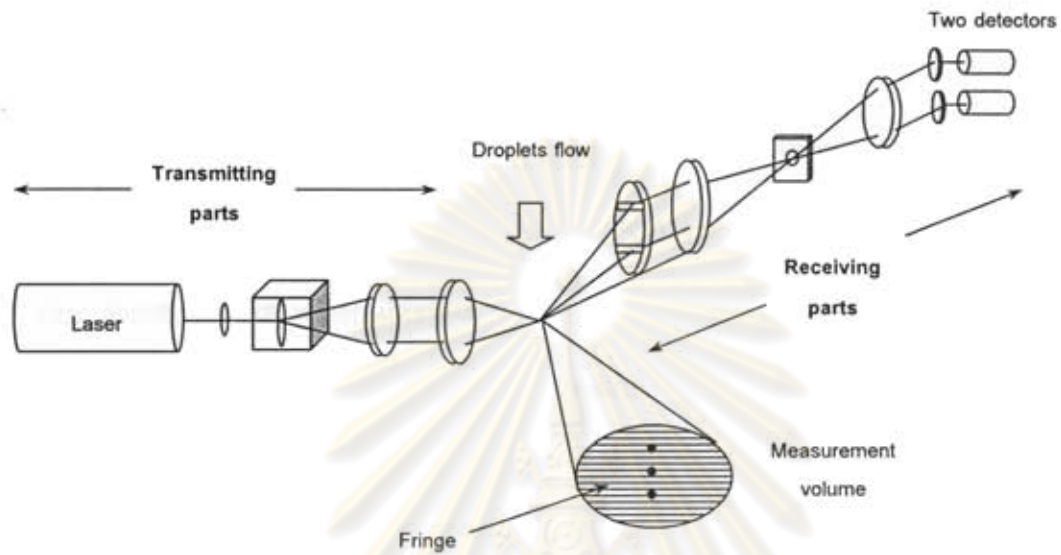


Figure 4.11 Typical optical set-up of PDA instrument.

ศูนย์วิทยทรัพยากร
จุฬาลงกรณ์มหาวิทยาลัย

CHAPTER 5

DESIGN AND SET-UP OF THE PDA SYSTEM

The main motivation for the design and set-up of the PDA system was the need to obtain an inexpensive but reliable and efficient PDA instrument for measuring velocity and size distribution of water droplets. Therefore, this chapter is intended to be a description of the design and set-up of the PDA instrument for whomever wishes to employ it.

The principle of the PDA instrument is based on the Doppler difference method used for LDA instrument. Therefore, the description of system components in the LDA instrument can be divided in two main parts: the transmitting and the receiving parts will be first presented (section 5.1) for making the primary basis of the PDA instrument. It is then followed by the description of the PDA instrument which was developed from the LDA (section 5.2). These descriptions include the explanation of the optical setting in order to confirm that all of the LDA/PDA components are in the perfect alignment. In the set-up it is important to note that the alignment of all LDA/PDA components is critical and highly sensitive to the PDA measurement.

Next, the descriptions of the signals and signal processing to obtain the information from PDA experiments (section 5.3), and the general experimental set-up for operating the PDA system (section 5.4) will be presented.

5.1 LDA System Components

Figure 5.1 shows the set-up scheme of a LDA system. The configuration of this system can be divided into two main parts: the transmitting and the receiving parts. Each part consists of a number of optical parts to create the measurement volume (transmitting parts) and to collect the light scattered (receiving parts) by the particle to the detector. All of them are mounted on the optical rail (Figure 5.2). The optical rail is a solid rod which holds all the optical components in alignment. The details of each component in the set-up are described as follows:

5.1.1 Transmitting Parts

These parts use a laser beam to emit coherent light. The laser beam is splitted into two beams and these subsequent beams are focused by using a lens called the transmitting lens. The lens also changes the direction of the beams causing them to cross at the point where they are focused. The region where the beams intersected is where the measurement is made and is called "the measurement volume". The transmitting parts consist of the following components:

ศูนย์วิทยาศาสตร์
จุฬาลงกรณ์มหาวิทยาลัย

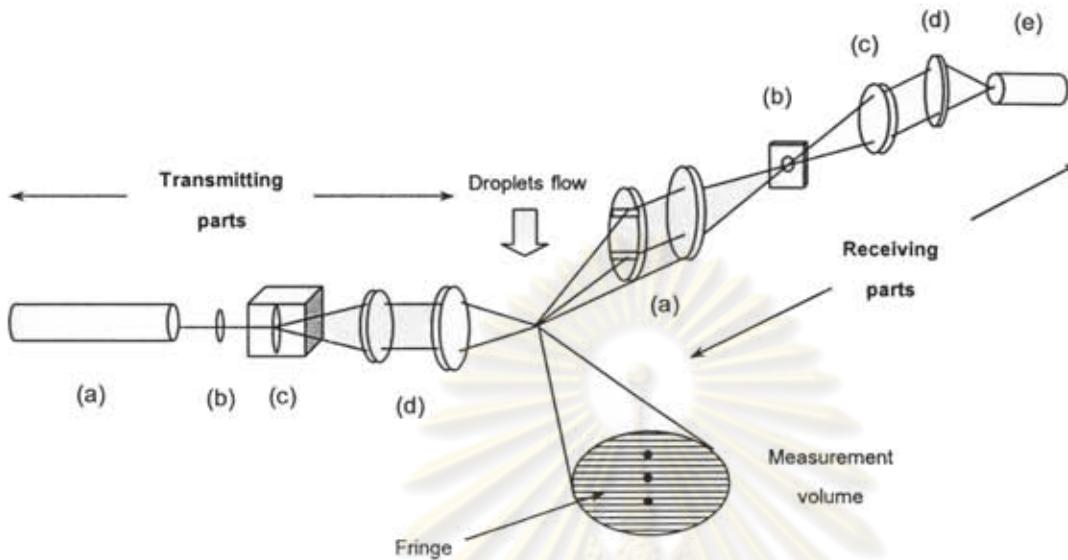


Figure 5.1 Optical configuration of a one detectors LDA system:

Transmitting parts: (a) Helium Neon laser;

(b) Laser focusing lens;

(c) Circular concentric diffraction array;

(d) Two plano-convex glass lenses;

Receiving parts: (a) Two plano-convex glass lenses;

(b) Spatial filter;

(c) Symmetric-convex glass lens;

(d) Plano-convex glass lens;

(e) Photomultiplier.



Figure 5.2 *The optical rail.*

a) Helium Neon laser

A 17 mW cylindrical Helium Neon laser (Melles Griot 25LHP 925, *Figure 5.3*) is used to produce polarized red light of wavelength 632.8 nm and beam diameter of 0.96 mm.

For the ideal LDA system

The laser must be adjusted to be perfectly horizontal and the polarization of the two beams must be perpendicular to the plane of the two beams when creating the measurement volume. Table 5.1 describes the set-up procedures for the success of this adjustment.

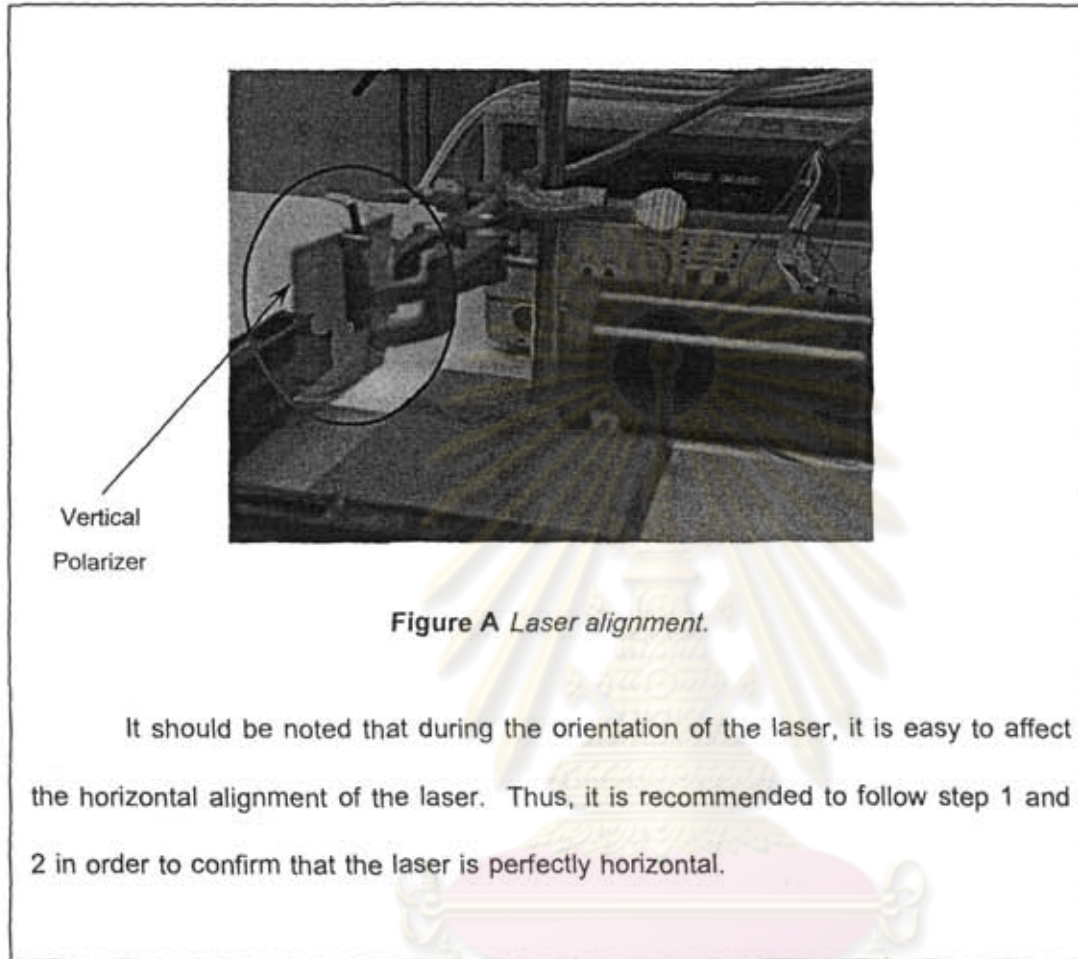


Figure 5.3 A 17 mW cylindrical Helium Neon laser and power supply.

Table 5.1 The set-up procedure for adjusting the laser.

Adjustment:

- 1) Setting the Helium Neon laser on the laser holder which is already mounted on the optical rail.
- 2) Turning on the laser and using the graph paper to find the position of the laser spot in each transmitting axial far from the laser to ensure that the position of laser spot is the same as shown in Figure A.
- 3) Placing a polarizer in front of the light beam incident and orienting the laser until the transmitted light intensity observed in the screen is minimized as much as possible. Note that the direction of the polarization (vertical or horizontal) must be perpendicular to the light plane wave.



b) Laser focusing lens

A spherical lens with 100 mm focal length and 20 mm in diameter (Figure 5.4) is intended to focus the laser beam to the smallest and the most intense spot as possible.



Figure 5.4 A spherical laser focusing lens with 100 mm focal length and 20 mm in diameter.

c) Circular concentric diffraction array

The three tracks circular concentric diffraction array is used (Figure 5.5) to split the incoming beam into two beams and also to produce the frequency shifting.

The additional advantages of the circular concentric diffraction array are as follows:

- the measurement of the particle with very small velocity becomes possible.
- the moving direction of the particle becomes the measurable.

The circular concentric diffraction array is a small glass disk with a circular grating pattern, mounted with the shaft of a small DC motor through the center of the disk. Actually, three different grating patterns are used in different annuli of the disk which allow for a range of beam spacing and frequency shifts.

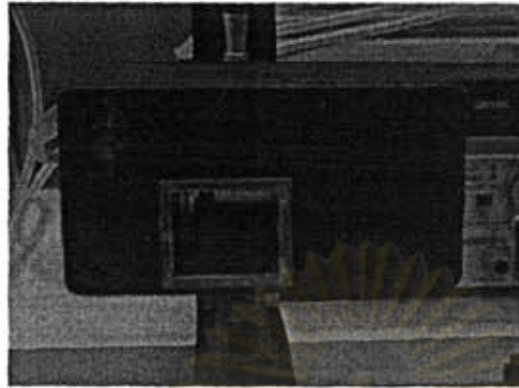


Figure 5.5 *The box containing a circular concentric diffraction array.*

After the light beam passes through this device the light beam is divided in, at least, three beams. The middle beam is going in the same direction as the incident beam, so called the zeroth order beam. The others are relatively symmetrical to the zeroth order beam and so called +1 and -1 order beam. The angle between this +1 and -1 order beam is directly connected with the step of the array.

As the circular concentric diffraction array turns a frequency shift is continuously imposed to the two beams of order +1 and -1; since the LDA system effectively measures the frequency at which a particle crosses a series of equally spaced fringes. By this technique, there are two serious limitations – i) a stationary particle produces no signal and, ii) two particles moving with the same speed but in opposite directions will give rise to indistinguishable signals. Both problems can be solved by using this device and shifting the frequency of one of the laser beams. This causes the fringes in

the measurement volume to move at a constant speed in either U or -U directions depending on the direction of the frequency shift. Stationary particles exposed to these moving fringes now produce signals of constant frequency (remarks that this frequency is the same as the frequency shift). Particles moving with the fringes produce signals with the lower frequency while particles moving against the fringes produce signals of higher frequency. The direction ambiguity is thus removed.

For three tracks of the circular concentric diffraction array the distance between the incident laser beam and the center of the circular array corresponding to each track of this device is changed. Therefore, the angle between the +1/-1 order is also changed (1.99° , 2.85° and 4.85° for track 1, 2 and 3, respectively). This change thus affects the fringe spacing in the measurement volume. This is an efficient way for the PDA system to modify the various sizes of particles under the study.

For the ideal LDA system

The plane of the circular concentric diffraction array could be either horizontal or vertical depending on the direction of the spray nozzle and must be located at the beam waist of the previous lens (laser focusing lens). Table 5.2 describes the set-up procedures for the success of this adjustment.

Table 5.2 The set-up procedure for adjusting the circular concentric diffraction array.

Adjustment:

1) Setting the circular concentric diffraction array on the optical rail and then set the laser focusing lens in front of the circular concentric diffraction array.

2) Adjusting the laser focusing lens with three axes translation (Figure B) and observe the spot passing through the circular concentric diffraction array on the screen. It should be the smooth circular spot with the most intensity of light as possible.



Figure B Laser focusing adjustment.

It should be noted that after adjusting the laser focusing it is recommended to confirm that the laser light is perfectly horizontal again.

3) Turning the circular concentric diffraction array with two axes translation to investigate its plane. It must be confirm that the plane of the circular concentric diffraction array is exactly either horizontal or vertical. As the circular concentric diffraction array turns in different steps, the two beams of order +1 and -1 should also be the most intense spots as possible (Figure C).

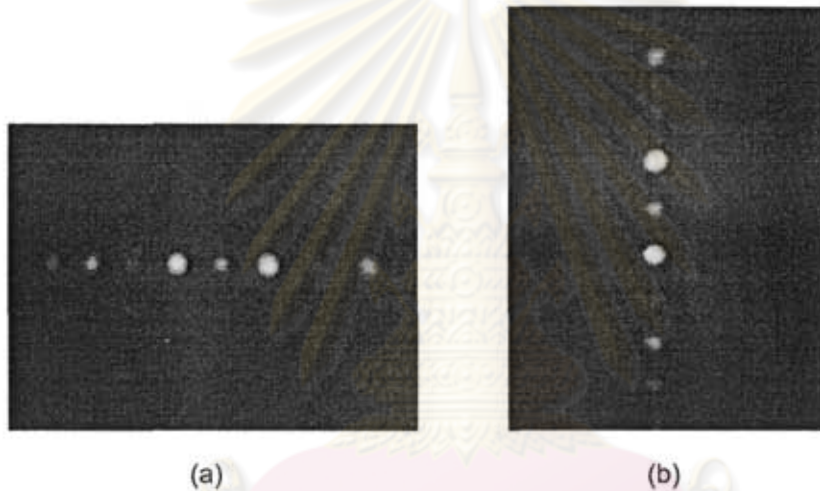
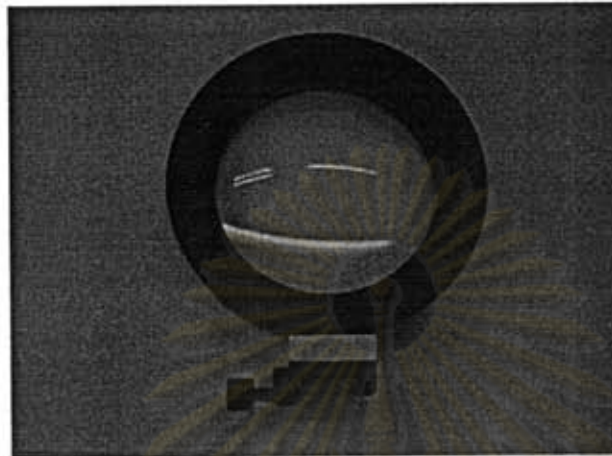


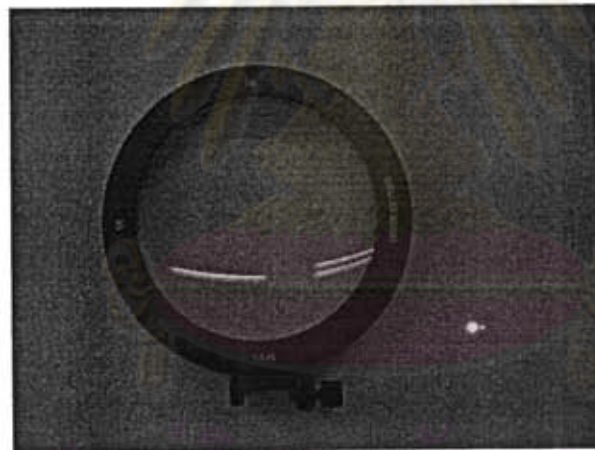
Figure C Laser spots of (a) horizontal diffracted beams;
(b) vertical diffracted beams.

d) Plano-convex glass lens

Two plano-convex glass lenses (Figure 5.6) are used to focus the beams which leave from the circular concentric diffraction array. The direction of two beams is thus diverted and crossed at the focusing point to conform to a measurement volume.



(a)



(b)

Figure 5.6 A Plano-convex glass lens for emitting parts:

(a) a 150 mm focal length and 80 mm in diameter;

(b) a 300 mm focal length and 95 mm in diameter.

The first lens is 150 mm focal length and 80 mm in diameter and the second lens is 300 mm focal length and 95 mm in diameter. It should be noted that it is critical to obtain the perfect parallel beams entering into the second focusing lens in order to make the exact probe diameters and produce a good parallel fringe at the measurement volume. Also, it is important that the mask (Figure 5.7) with two circular apertures must be used to conserve only the beam +1 and -1 from the first lens and reduce unexpected frequency.

This focal length is experimentally determined by setting the beam divergence such that each beam forms a waist at the probe volume. An estimation of the beam waist size or the probe diameter (w) is

$$w = \frac{4\lambda f}{\pi D} \quad (5.1)$$

where λ is the wavelength of light beam, f is a focal length of focus lens and D is the diameter of the light beam. Thus a smaller focal length makes a smaller beam waist.

ศูนย์วิทยทรัพยากร
จุฬาลงกรณ์มหาวิทยาลัย

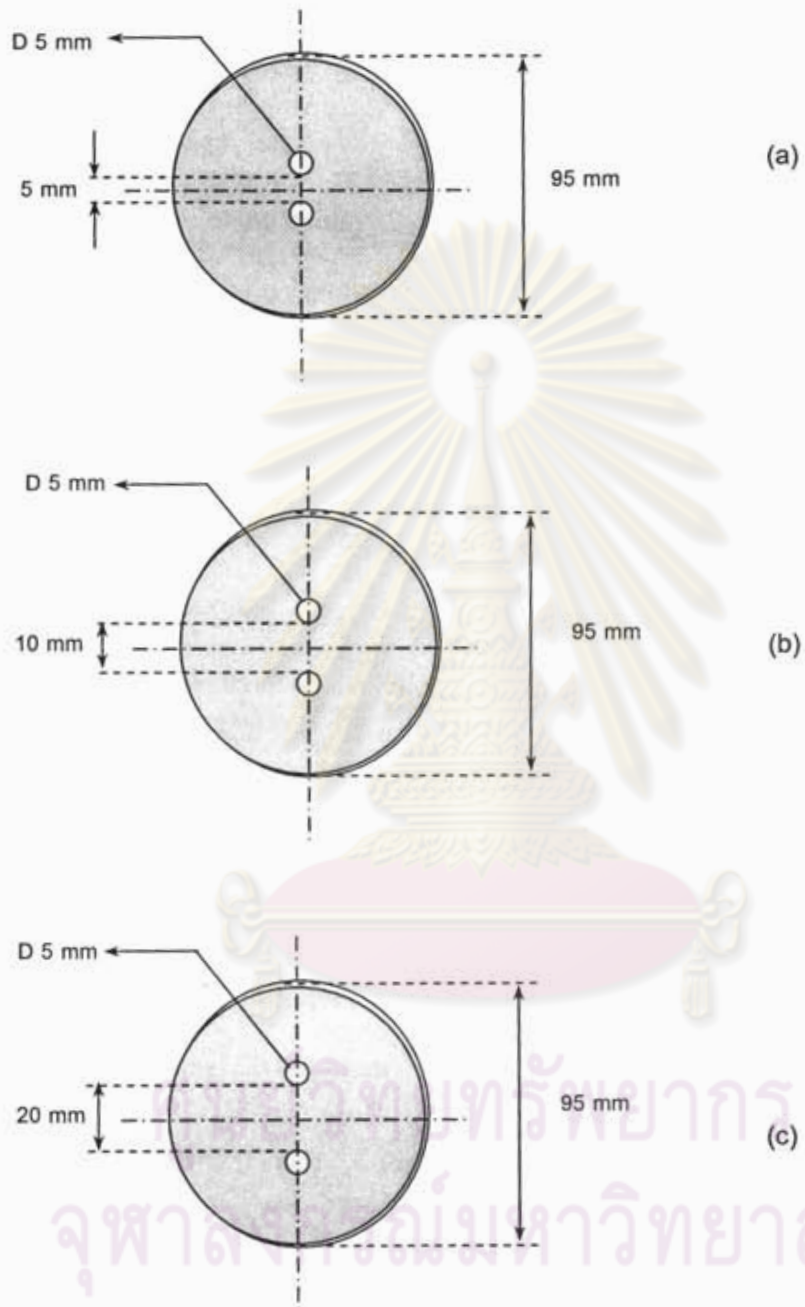


Figure 5.7 Two circular apertures mask for (a) track 1 (b) track 2 (c) track 3.

The following are the nominal optical characteristics of transmitting parts:

- Focal length	300 mm
- Diameter of the beam	0.98 mm
- Measurement volume diameter	0.252 mm
- Fringe spacing	
track 1	18.12 μm
track 2	12.70 μm
track 3	7.46 μm
- Number of fringe in the measurement volume	
track 1	13
track 2	19
track 3	33

For the ideal LDA system

The first lens (Figure 5.6 (a)) must be located in such a way that its object focal plane coincides with the image plane of the laser focusing lens (i.e., with the plane of the circular array). The effects of this lens are as follow:

- i) Creating two perfectly parallel beams;
 - Increasing the size of the diameter of the beam. The beam coming from the laser with a diameter d is increased to a diameter D in the ratio of the focal length of this lens and laser focusing lens.

The second lens (Figure 5.6 (b)) is used to focus the two parallel beams at the measurement point. Its location on the optical rail is not critical but the optical axis must be perfectly adjusted. Then the good parallel fringes should be obtained at the measurement volume.

Table 5.3 describes the set-up procedures for the success this adjustment.

Table 5.3 The set-up procedures for adjusting the plano-convex glass lens.

Adjustment:

- 1) Setting the first plano-convex glass lens on the optical rail and then adjust for the best position of this lens by investigating the creating two parallel beams.
- 2) Using a graph paper to find the position of the two laser spots in transmitting axial direction far from this lens (Figure D). To ensure that the perfectly parallel beams are obtained, it is recommended that two or more positions for investigating the same position of the two laser spots must be done.

It should be noted that the first lens could be adjusted in order to obtain the different distances between the beams (e.g., other characteristic of the optical probe in diameter, number of fringe and fringe spacing).

The second lens (Figure 5.6 (b)) is used to focus the two parallel beams at the measurement point. Its location on the optical rail is not critical but the optical axis must be perfectly adjusted. Then the good parallel fringes should be obtained at the measurement volume.

Table 5.3 describes the set-up procedures for the success this adjustment.

Table 5.3 The set-up procedures for adjusting the plano-convex glass lens.

Adjustment:

1) Setting the first plano-convex glass lens on the optical rail and then adjust for the best position of this lens by investigating the creating two parallel beams.

2) Using a graph paper to find the position of the two laser spots in transmitting axial direction far from this lens (Figure D). To ensure that the perfectly parallel beams are obtained, it is recommended that two or more positions for investigating the same position of the two laser spots must be done.

It should be noted that the first lens could be adjusted in order to obtain the different distances between the beams (e.g., other characteristic of the optical probe in diameter, number of fringe and fringe spacing).

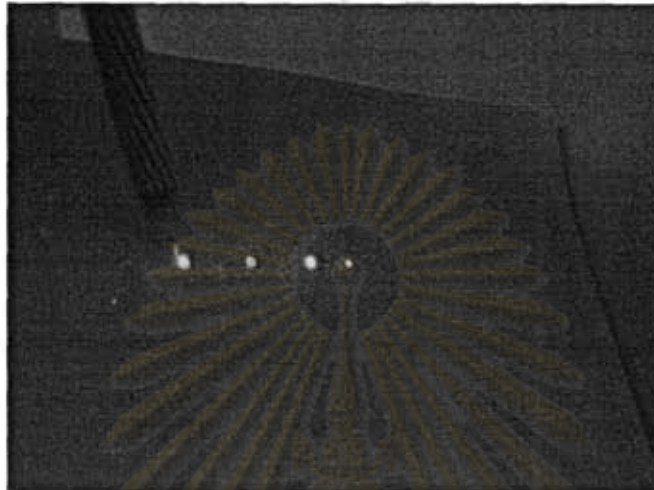
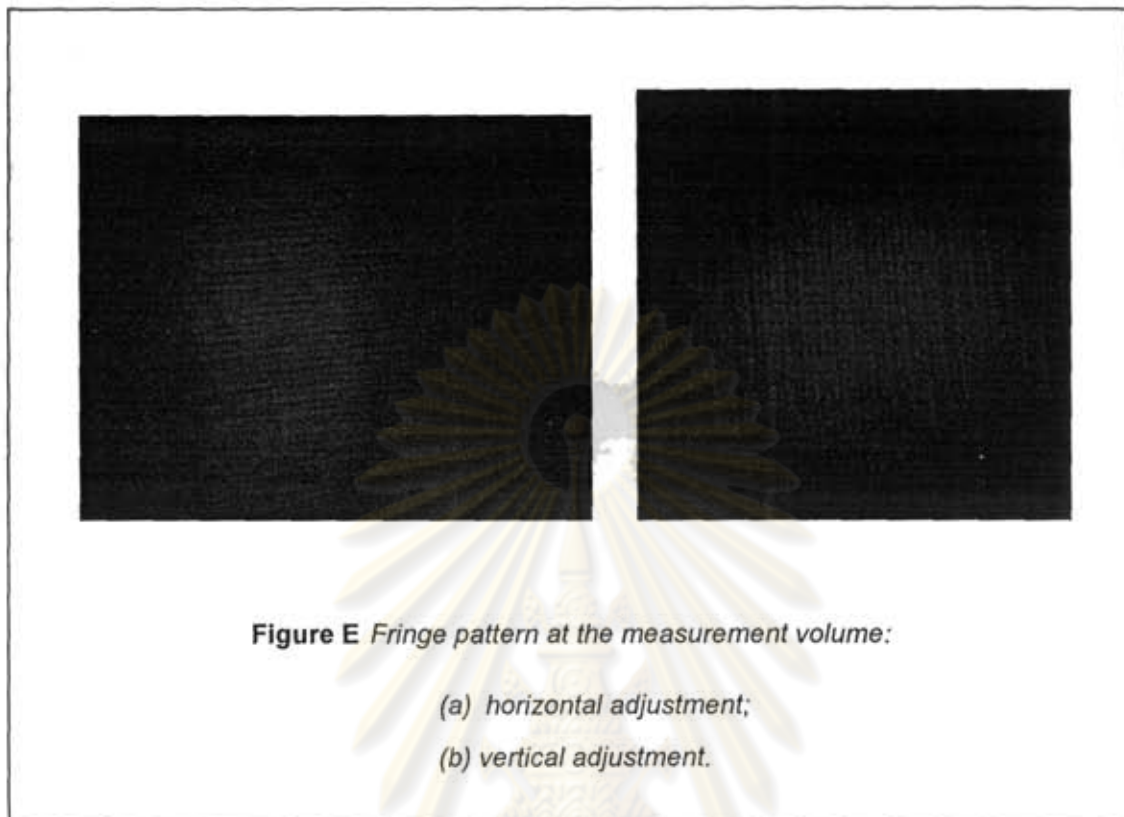
Adjustment:

Figure D *Two parallel beams checking.*

- 3) Setting the second plano-convex glass lens on the optical rail. Its location is not critical but the optical axis must be adjusted perfectly.
- 4) Setting the circular mask in front of the second lens.
- 5) Using the microscope to enlarge the fringe pattern at the measurement volume where the beam crosses and observing the fringe image on the screen. If the fringes are not perfectly parallel, it means that a better alignment is required.

ศูนย์วิจัยทั่วไป
จุฬาลงกรณ์มหาวิทยาลัย



5.1.2 Receiving Parts

As the particle passes through the measurement volume the light scattering is then collected by the receiving optics which is positioned at the off-axis angle. It is then focused on the photodetector which is later converted into an electrical energy. The typical configuration for the receiving optics in the refraction dominated forward scattering region ($25^\circ < \theta < 45^\circ$) is advantageous over side or back scattering due to more light scattering intensity [5].

For obtaining the refraction information and high light scattering intensity the receiving optics in this work are thus positioned at the off-axis angle at 30° from the

forward axis (Figure 5.8). In fact, the off-axis angle can be set at any value between 25° – 45° depending on the proper application that the PDA requires for measuring the size of the particle from the measured phase. The receiving optics consist of the components as follows:

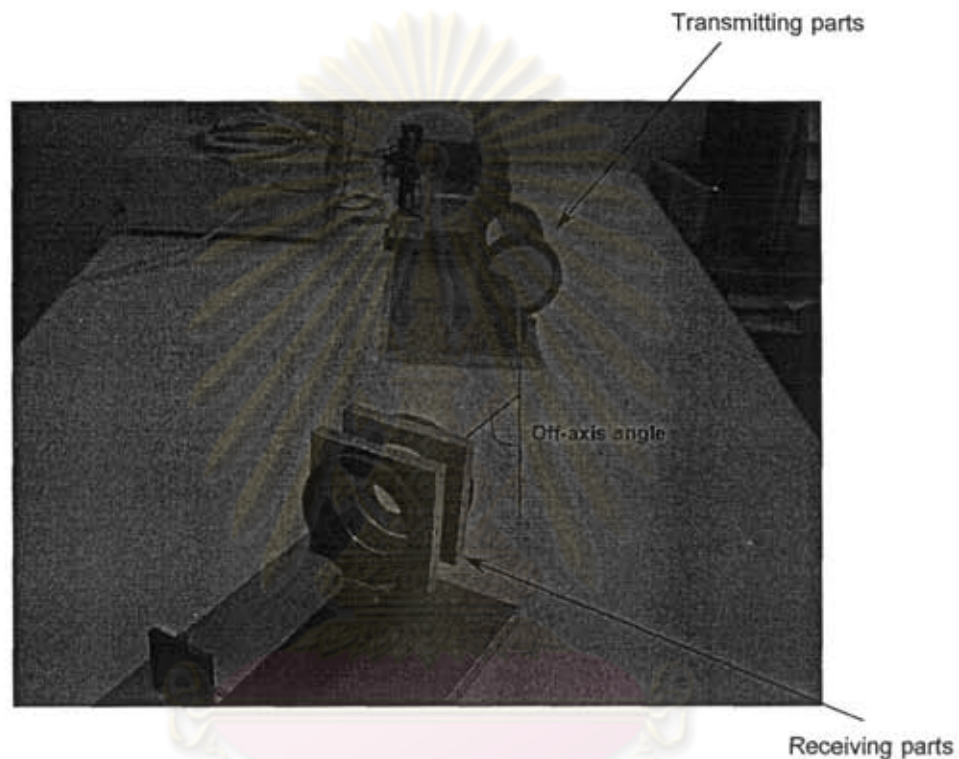


Figure 5.8 Optical configuration of the receiving parts at the off-axis angle in 30° .

a) Plano-convex glass lens

Two 300 mm focal length and 95 mm in diameter plano-convex glass lenses (Figure 5.9) are used to focus the scattered light from particles crossing the measurement volume onto the spatial filter.

For the ideal LDA system

The first lens must be located in the position of its focal length to collect the scattered light occurring by the particle crossing through the measurement volume. The effect of this lens is to collect the light.

The second lens is used to focus the beams coming from the first lens. Its location on the optical rail is not critical, but the optical axis must be perfectly adjusted.

Table 5.4 describes the set-up procedures for successfully making this adjustment.

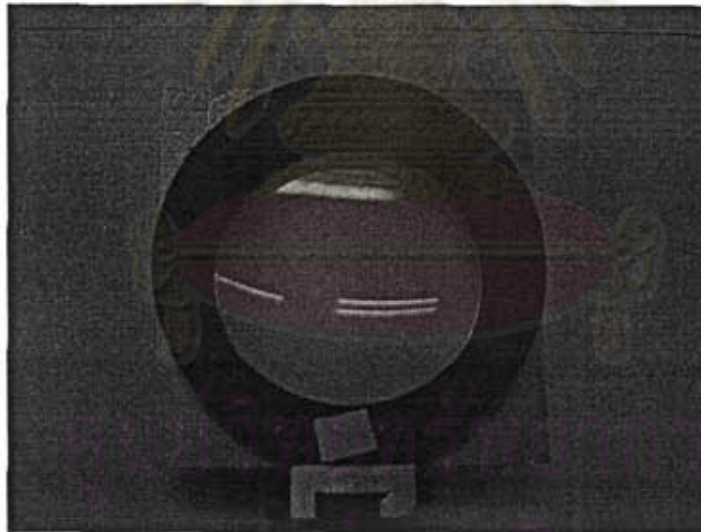


Figure 5.9 A 300 mm focal length and 95 mm in diameter plano-convex glass lens

for the receiving parts.

Table 5.4 The set-up procedures for adjusting the plano-convex glass lens.**Adjustment:**

Before the receiving parts are adjusted the scattered light is required for witnessing the position of the exact measurement volume. To locate the receiving optics at 30° from the forward axis uses a small pin.

1) Setting a pin at the measurement volume by investigating the image of the scattered light on the screen. The image of scattered light should be shown as in Figure F (a) and (b) when only the first beam (+1 order beam) and the second beam (-1 order beam) are allowed to pass through the measurement volume, respectively.



Figure F Pin-scattered light when only (a) the first beam (+1 order beam) and (b) the second beam (-1 order beam) are allowed to pass through the measurement volume.

Adjustment:

- 2) Measuring the angle to offset the receiving part at 30° from the forward axis.
- 3) Setting the first plano-convex glass lens on the optical rail at the position of its focal length.
- 4) Setting the second plano-convex glass lens on the optical rail to focus the scattered light from the previous lens at the focusing point of this lens. However, its position in axis direction is not critical.

b) Spatial filter

A spatial filter of $200\ \mu\text{m}$ spherical aperture (Figure 5.10) is used for collecting the scattered light and, also, for reducing the errors from the trajectory ambiguity. It can be replaced with a smaller aperture in order to further reduce the errors.

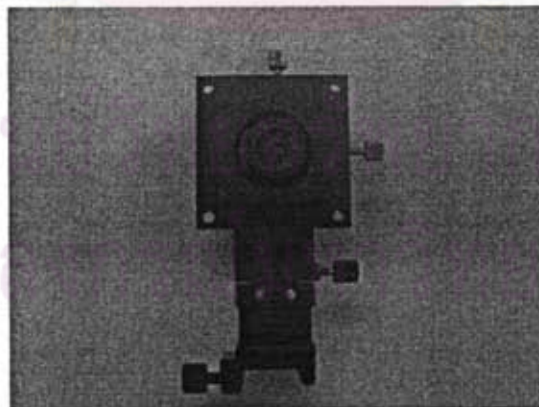


Figure 5.10 A $200\ \mu\text{m}$ spherical aperture special filter.

For the ideal LDA system

The purpose of the spatial filter is to limit the region of the measurement volume from where signals are received for the reduction of the trajectory ambiguity. Table 5.5 describes the set-up procedures for the success of this adjustment.

Table 5.5 The set-up procedures for adjusting the spatial filter.

Adjustment:

- 1) Setting the spatial filter on the optical rail at the position where the incident beam from the previous lens crosses.
- 2) Investigating a good position of the spatial filter with three axes of translation. It must be confirm that the scattered light left from this device has two divergent light beams with their maximum intensity as shown in Figure G.

It should be noted that while the special filter is being adjusted, the room should be dark in order to clearly notice the crossing beams.

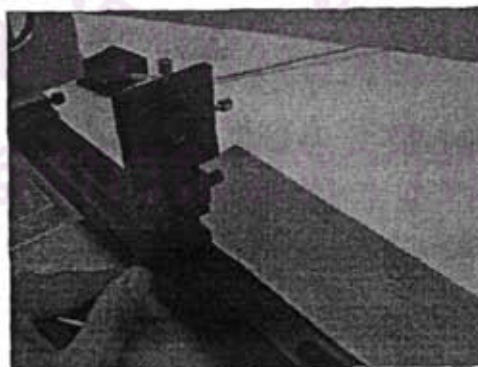


Figure G Spatial filter adjustment.

c) Symmetric-convex glass lens

A symmetric-convex lens (Figure 5.11) has an identical convex surface on both sides of the lens. A 100 mm focal length and 50 mm in diameter is chosen to receive the virtual imaging of real objects.

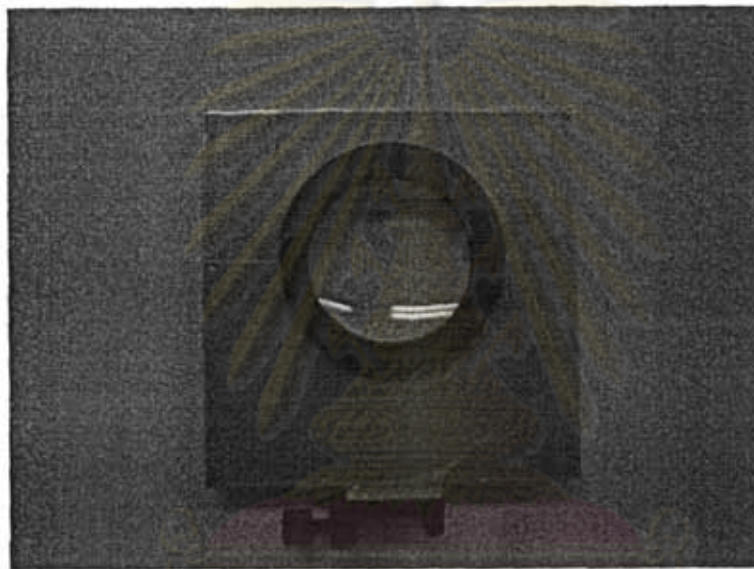


Figure 5.11 A symmetric-convex lens with 100 mm focal length and 50 mm in diameter.

ศูนย์วิทยทรัพยากร
จุฬาลงกรณ์มหาวิทยาลัย

For the ideal LDA system

The symmetric-convex glass lens is positioned at its focal length to collect the scattered light. Table 5.6 describes the set-up procedures for the success of this adjustment.

Table 5.6 The set-up procedures for adjusting the symmetric-convex glass lens.

Adjustment:

- 1) Setting this lens at the position of its focal length on the optical rail.
- 2) Making certain that it is located in a good position. It is can be done by using a graph paper to investigate that the leaving beams are perfectly parallel as shown in Figure H.

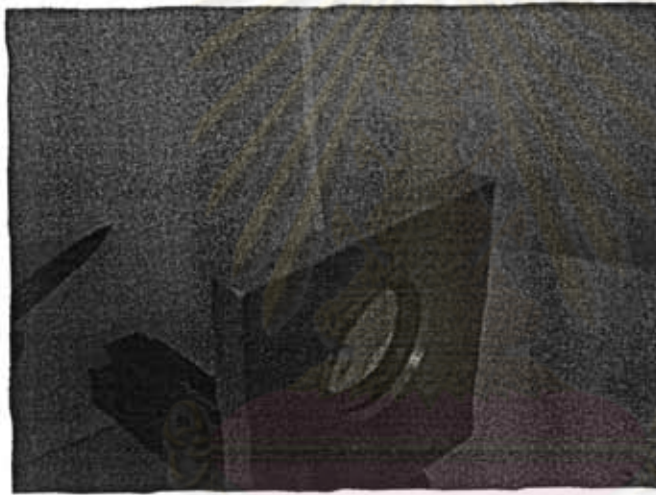


Figure H Symmetric-convex glass lens adjustment.

ศูนย์วิทยุทรัพยากร
จุฬาลงกรณ์มหาวิทยาลัย

d) Plano-convex glass lens

A plano-convex glass lens with the focal length of 40 mm and a diameter of 10 mm (Figure 5.12) is used to focus the scattered light into an optic fiber.

For the ideal LDA system

The position of the plano-convex glass lens is not critical, but the optical axis must be perfectly adjusted.

Table 5.7 describes the set-up procedures for the success of this adjustment.

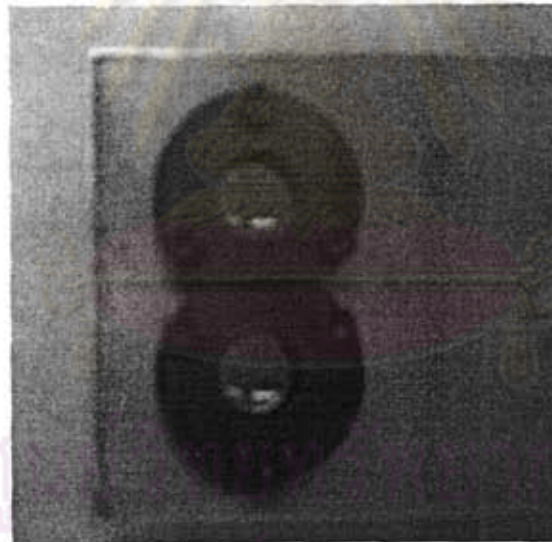


Figure 5.12 Two plano-convex glass lens with 40 mm focal length and 10 mm in diameter.

Table 5.7 The set-up procedures for adjusting the plano-convex glass lens.

Adjustment:

- 1) Setting this lens on the optical rail to focus the scattered light into an optic fiber. However, its position in axis direction is not critical as shown in Figure I.

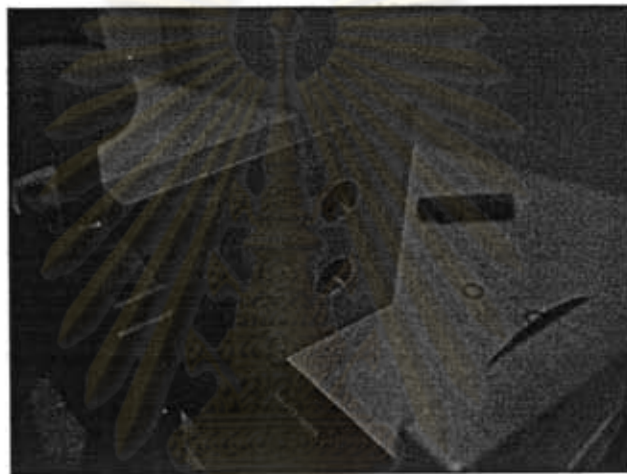


Figure I *Plano-convex glass lens adjustment.*

e) Photomultiplier or Photodetector

Finally, the light scattering is carried along the optic fiber to a photomultiplier (PM) tube (Figure 5.13) which contains with the 9 stage photo-cathode multialkali to detect the scattering signal and convert light into an electric signal.

Photomultiplier tubes are light detectors that are useful in low intensity applications. Due to high internal gain PM tubes are very sensitive detectors in

speed and linearity of response. Therefore, it should be careful when operating a high-level power supply.

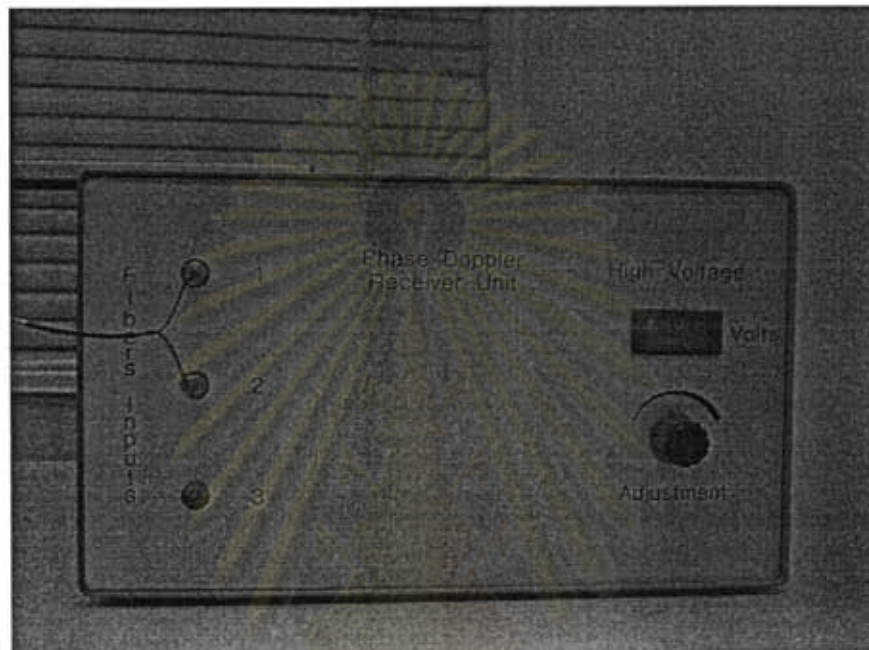


Figure 5.13 A Photomultiplier box.

It is important that all the optical components must be in a good alignment. The oscilloscope is required to notice the online signal burst by splitting the scattering signal from the PM and then routing to an oscilloscope.

5.2 PDA System Components

By using an extended receiving optical system from the LDA system with two photodetectors it is possible to obtain the PDA system for measuring particle size and velocity simultaneously. Thus, the only general difference between the LDA and PDA system is that the LDA system consists of only one photodetector while the PDA system consists of more than one photodetector (A typical PDA system uses three photodetectors [1]) to find out the Doppler difference. An optical configuration of a two detector PDA-system used in this work is shown in Figure 5.14.

The PDA receiver is well-positioned at the off-axis angle (e.g. 30°). It consists of a collection lens (300 mm focal length plano-convex glass lens) which produces a parallel beam of scattered light. This parallel light beam passes through a mask which defines the elevation angle of the two photodetectors. Two rectangular slits in the mask (Figure 5.15) allow the light to pass through to the photodetectors. The slits are located parallel to the vertical plane at the elevation angle of 3.34° .

It is recommended that the distance between two slits of the mask should be varied in order to obtain other elevation angles which has caused the different upper limits of the particle size. This is illustrated in Table 5.8 for three different masks (1, 2 and 3) and for a relative refractive index of 1.33, for which laser wavelength, the intersection angle and the off-axis angle were chosen of 632.8 nm, 4.85° and 30° , respectively

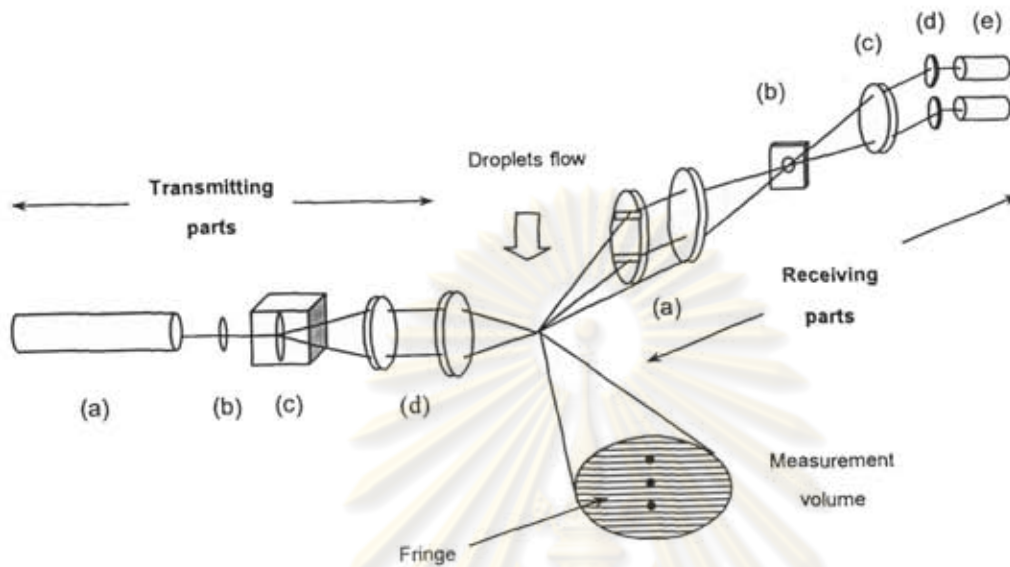


Figure 5.14 Optical configuration of a two detectors PDA system:

Transmitting parts: (a) Helium Neon laser;

(b) Laser focusing lens;

(c) Circular concentric diffraction array;

(d) Two plano-convex glass lenses;

Receiving parts: (a) Two plano-convex glass lenses;

(b) Spatial filter;

(c) Symmetric-convex glass lens;

(d) Two plano-convex glass lenses;

(e) Two photomultipliers.

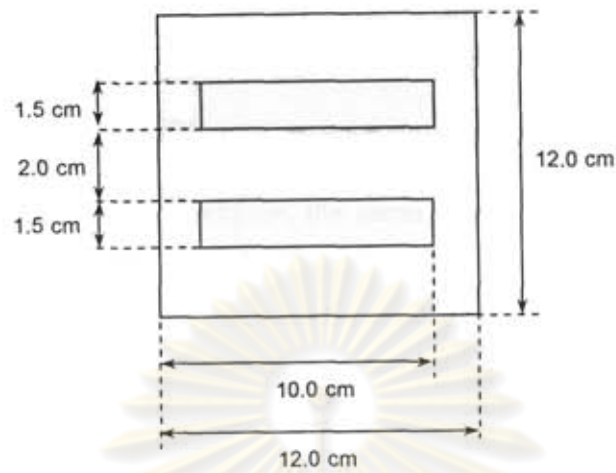


Figure 5.15 Two rectangular slits mask.

Table 5.8 The maximum measurable size of the PDA system for the different masks.

Masks	Distance between two slits (mm)	The elevation angle	D_{\max} (μm)
1	35	3.34	85
2	55	5.23	54
3	65	6.18	45

Note that the minimum size is limited by the law of geometrical optics. Which is applicable under the lower size range more than 4λ . Where λ is the laser wavelength. (the commonly accepted lower limit of about 5-10 μm [15]).

The light is then focused on a spatial filter by using the same lens (300 mm focal length plano-convex glass lens). Finally, the scattered light beyond the spatial filter is focused onto the two photodetectors using a 100 mm focal length and 50 mm in diameter symmetric-convex glass lens and; in addition, the same lens in LDV system (40 mm focal length and 10 mm in diameter plano-convex glass lens).

The Doppler frequency is a measurement of the particle velocity while the particle size is determined by a time lag or phase shift between both photodetectors and the optical properties of the scattering particle. Light scattering computations yield the exact relationship between the phase difference and the particle diameter. The complete set-up of a PDA instrument used in this work is shown in Figure 5.16.



ศูนย์วิทยทรัพยากร
จุฬาลงกรณ์มหาวิทยาลัย

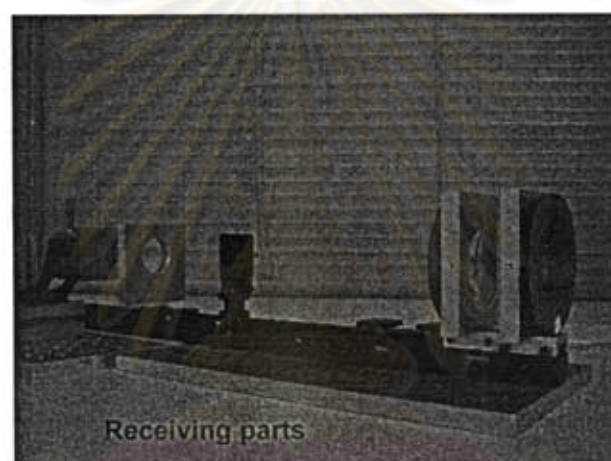


Figure 5.16 *The complete set-up of a PDA instrument.*

5.3 Signals and Signal Processing

The electronic signal given out by the photomultiplier contains the period of silence (i.e., there is no particle in the measurement volume) randomly interspersed with bursts of signal (i.e., a particle passes through the measurement volume). Figure 5.17 shows an idealized signal burst. The overall shape of the burst is a consequence of the fact that the laser beams producing the measurement volume will, inevitably, be stronger at their center than at their edges. As the particle passes through the edge of the measurement volume, where the fringes are weakly illuminated, the signal fluctuations are also weak. As the particle passes through the measurement volume center the signal fluctuations become larger and then decay again. As a consequence the signal can be split into two parts: a low frequency part called the *pedestal* (Figure 5.17 (b)) and a high frequency part that actually contains the *Doppler* signal (Figure 5.17(c)).

5.3.1 Signal Capture

To obtain the maximum information and accuracy from PDA experiments consideration must be given to the electronic equipment necessary to transform the raw signals from the detector into velocity and size information.

Signals from the PM tube are captured by the CompuScope 85G Data Acquisition Card. This is an autocorrelation processor that is interfaced to the PC computer.

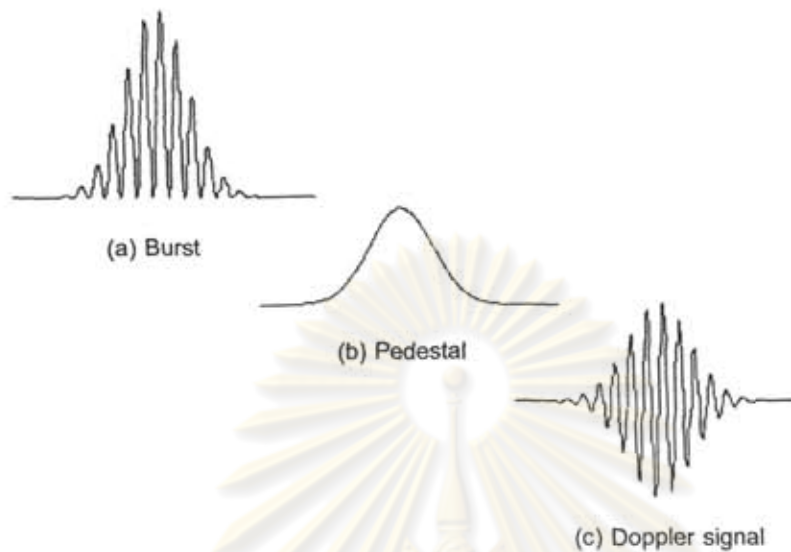


Figure 5.17 Anatomy of a typical LDA/PDA signal burst generated when a particle passes through the measurement volume.

CompuScope 85G Data Acquisition Card is the world's fastest PCI bus based waveform digitizer. It is capable of performing analog to digital conversion at rates as fast as 5 GS/s with 8 bit vertical resolution. The benefits of using a CompuScope 85G instead of a traditional digital oscilloscope are

- a) the sampling rates are faster than the traditional digital oscilloscope;
- b) it can be fitted inside a PC so an extra rack or bench space is unnecessary; and,
- c) it is easier to program.

Typical signal frequencies are in the order of Megahertz so the CompuScope 58G is more than adequate for an accurate and reliable signal reconstruction.

5.3.2 Signal Processing

The PDA software for data processing is necessary to control the PDA system with CompuScope 85G Data Acquisition Card from the PC computer and to collect the measurement data.

The software platform includes four parts as follows:

1) Configuration Setting Window

The configuration setting window represents the optical parameters and the measured particles properties. The optical parameter inputs correspond to the experimental set-up such as the focal length of the transmitting and receiving lenses, the intersection angle, the off-axis angle, the elevation angle and the wavelength of the laser. The software will then return the information about the measurement volume of the PDA system. The window which contains the optical parameters are grouped into 6 main parts (Figure 5.18) as follows:

ศูนย์วิจัยทรัพยากร
จุฬาลงกรณ์มหาวิทยาลัย

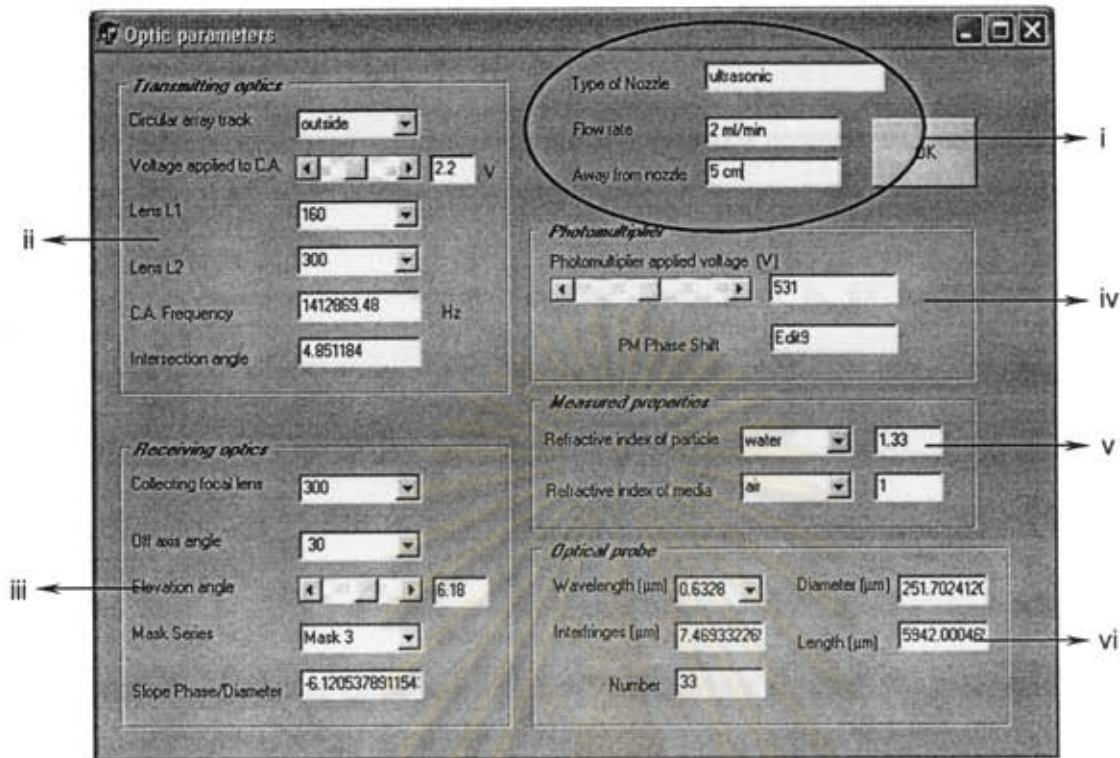


Figure 5.18 The experimental set-up program interface:

- i) Spray information, ii) Transmitting optics group box, iii) Receiving optics group box,
 iv) Photomultiplier group box, v) Measured properties group box,
 vi) Optical probe group box.

i) Nozzle information

In this part the information concerning the nozzle and the condition for operating the nozzle such as type of nozzle, liquid flow rate and the distance of the nozzle from the measurement volume can be filled. It has no effect on the data computing.

ii) Transmitting optics

The transmitting optics group box contains options for setting as follows:

- The circular array track is for setting the tracks corresponding to the adjustment of the circular concentric diffraction array. This option is set to inside, central and outside for track 1, track 2 and track 3, respectively. (default: track 3 or outside)

- The voltage applied to C.A. is for setting the power supply voltage in order to turn the circular concentric diffraction array. Changing the power supply voltage from 0 to 5 Volt will change the speed of the motor. (default: 0 Volt.)

- Lens L1 and L2 is for setting the focal length of the focusing lenses in the transmitting parts. (default: Lens L1 is set to 160 and Lens L2 is set to 300 mm.)

- C.A. frequency option represents the frequency of the fringe when the circular concentric diffraction array was turned. The user will compute it previously. The computation of the fringe frequency is described in Appendix B.

- Intersection angle option represents the intersection angle of the light beams for producing the measurement volume. It will be computed by the software. The computation of the intersection angle is described in Appendix C.

iii) Receiving optics

The receiving optics group box contains options for setting as follows:

- Collecting focal length option is for setting the focal length of the collecting lens in the receiving parts. (default: 300 mm.)
- Off-axis angle option is for setting the off-axis angle or the position of the receiving parts. (default: 30°)
- Elevation angle option is for setting the elevation angle which is defined by the mask series. The computation of the elevation angle is described in Appendix D.
- Mask series represent the mask which is used for allowing the light to pass through to the photodetectors. The series of masks are indicated by the distance between two rectangular slits in the mask. (default: Mask 1)
- Slope/phase diameter option represents the slope of the phase shift and diameter of the particle plot. It will be computed by the software. The computation of the relationship of the slope/phase diameter is described in Appendix E.

iii) Photomultiplier

The photomultiplier group box contains options for setting the power supply voltage to the photomultiplier. In this function, it should be more than 500 volts and goes up to 800 volts. It is advice that the low power supply voltage should be

applied while operating at the high intensity scattering light. On the other hand, the high power should be applied while operating at the low intensity scattering light in order to reduce the noise frequency.

iv) Measured properties

The measured properties group box contains options for setting the refractive index of the particle and the refractive index of the media. For example, in case that the measured particle is water and the media is air, the refractive index of the particle is 1.33 and the refractive index of the media is 1.0, respectively.

iv) Optical probe

The optical probe group box contains only an option for setting the wavelength of the laser beam. The other four values are automatically computed by the software according to the adjusted parameters.

- *Diameter* represents the beam waist size at the measurement volume. In this function, the beam waist is about 251.70 μm .

- *Interfringe* represents the fringe spacing in micrometers at the measurement volume which corresponds to the track of the circular concentric diffraction array.

- *Length* represents the length in micrometer of the measurement volume.

- *Number* represents the number of the fringes in the measurement volume which corresponds to the track of the circular concentric diffraction array.

2) Data Acquisition Window

The data acquisition window or scope window represents the signal processor shown in Figure 5.19. A number of parameters are adjusted to obtain an appropriated signal burst as follows:

i) Acquisition mode

The acquisition mode setting defines whether the CompuScope card should be operated in single or dual channel mode.

- In single channel mode, only channel A is available for input (Figure 5.20 (a)). Consequently, only the velocity of sample droplets can be measured.

- In dual channel mode, both channels A and B on CompuScope card are available for input (Figure 5.20 (b)). In this case the velocity and the size of sample droplets can be measured simultaneously.

Note that channels A and B represent the signal captured from photomultiplier 1 and 2, respectively.

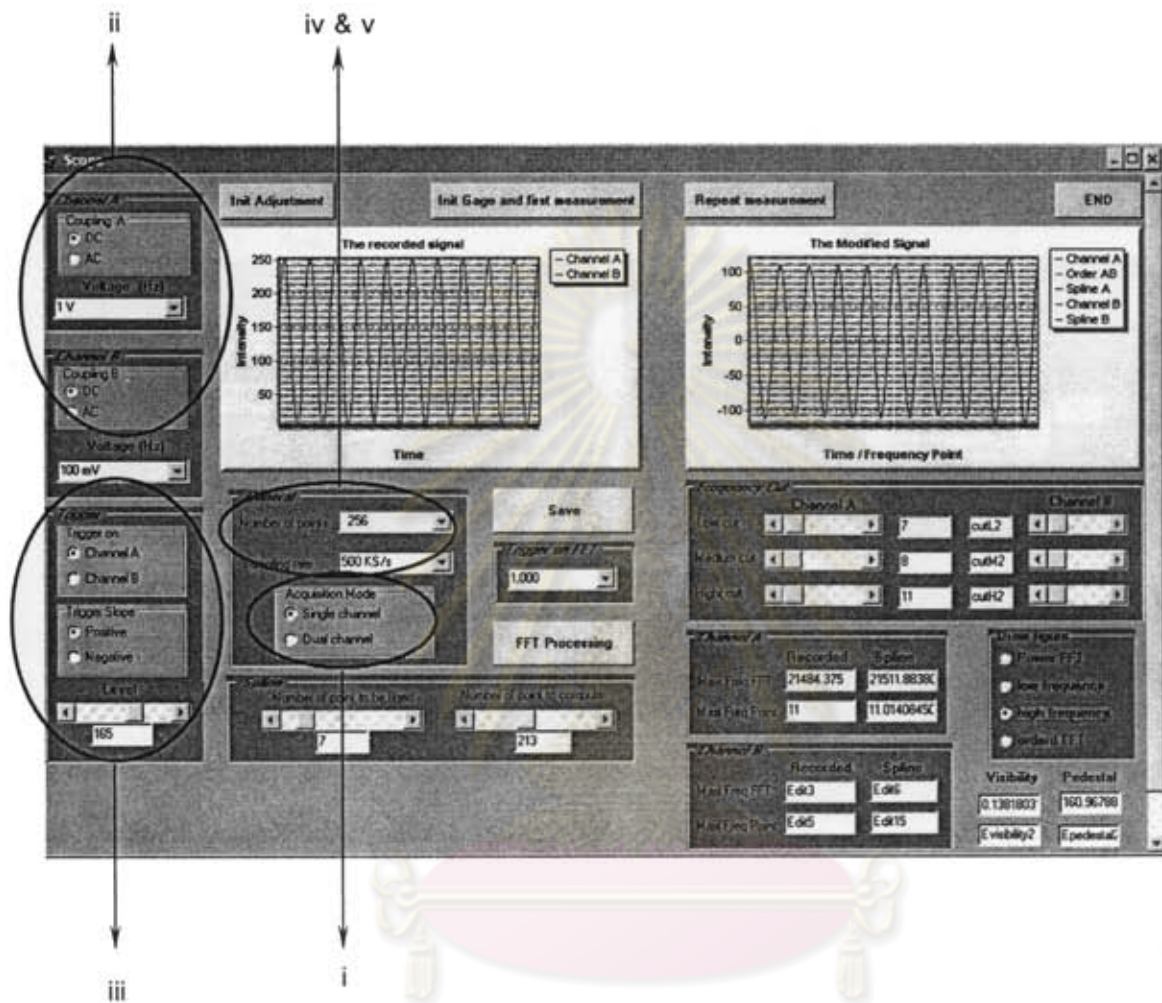


Figure 5.19 Data acquisition program interface:

i) Acquisition mode, ii) Input range, iii) Trigger setting,

iv) Sampling rate, v) Number of points.

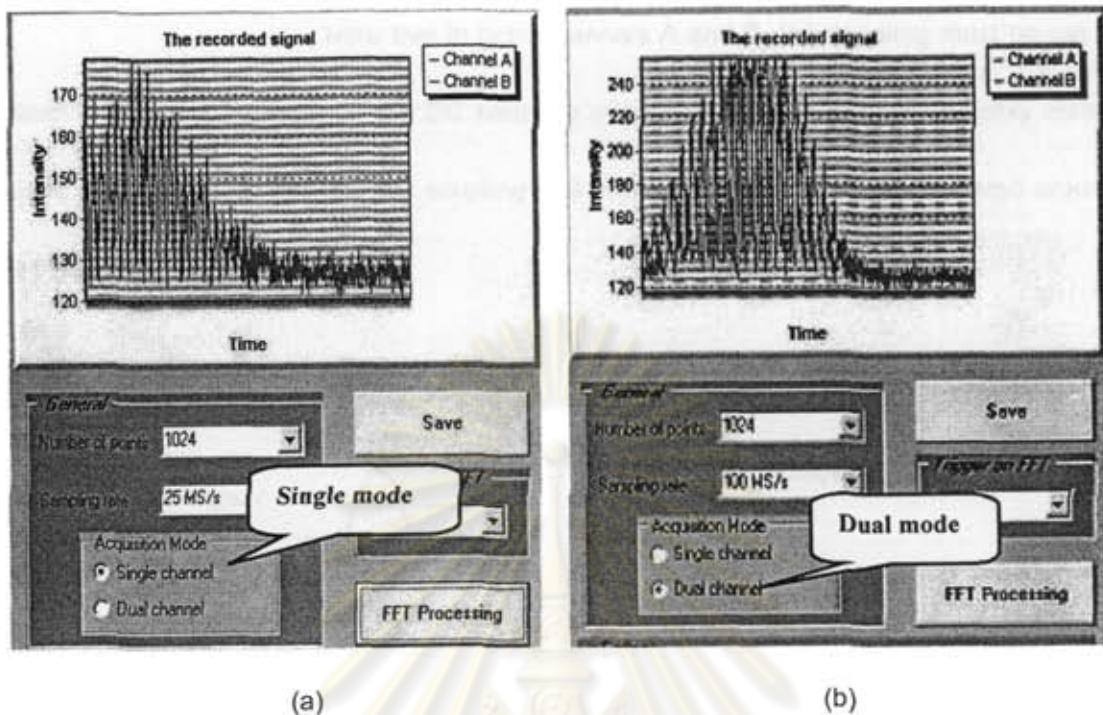


Figure 5.20 Scattering signals with (a) single channel mode and (b) dual channel mode.

ii) Input range

The input range is the range in Volts for the signal-capture (CompuScope) setting when acquiring data on channel A and/or B. If the input range is less than the maximum magnitude of an input signal the peaks of the signal will be cut off (Figure 5.21(a)). Obviously, it is preferable to obtain a good representation of the signal (no clipping signal) on the screen. The input range should be higher than the maximum magnitude of an input signal (Figure 5.21 (b)). Figure 5.22 also shows the captured signal with low input range.

Note that in both channels A and B, the coupling must be set at either in DC or AC mode. If the DC coupling was chosen, the signal will be only visible above its zero line; and, if the AC coupling was chosen, the signal will be centered around its zero line.

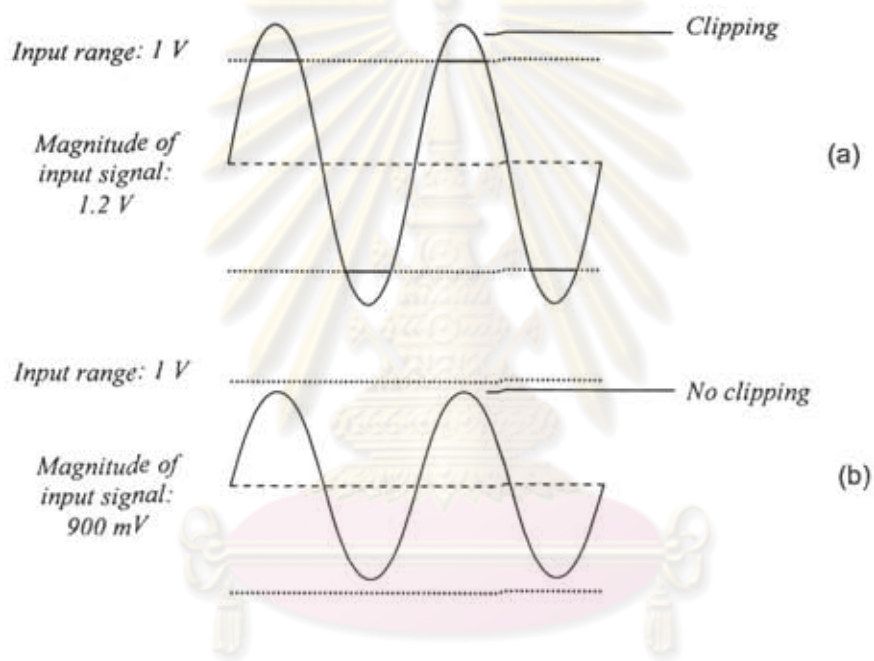


Figure 5.21 The effect of the input range:

(a) input range is less than the maximum magnitude of an input signal;

(b) an input signal is in the input range.

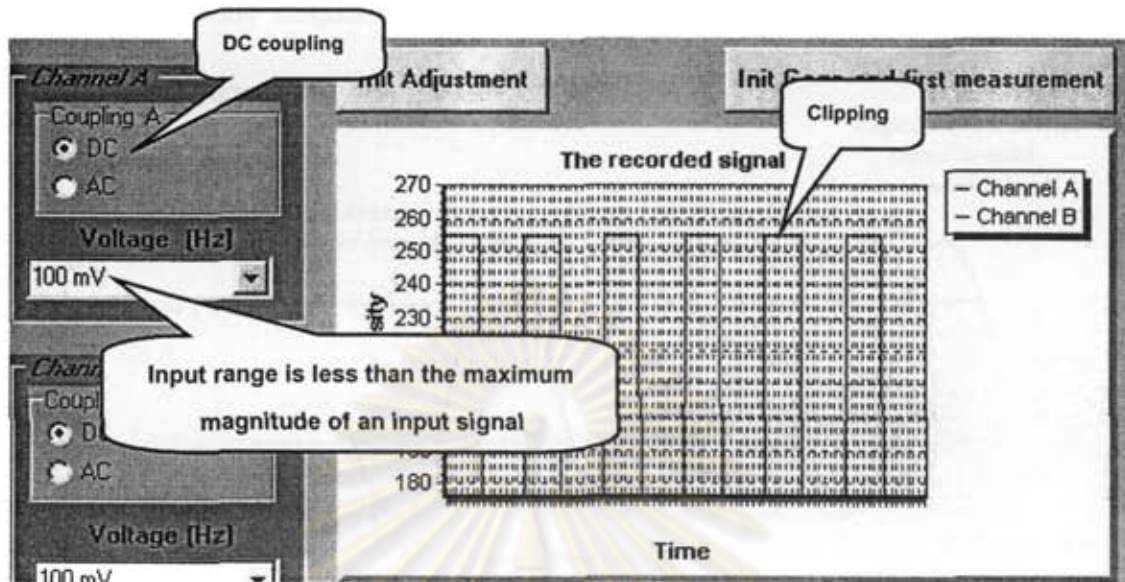


Figure 5.22 The effect of low input range in a signal.

iii) Trigger settings

The trigger settings contain options for changing the settings of individual channels such as trigger level and trigger slope. The trigger source can be selected from either channel A or channel B. The trigger event starts at the voltage of an input signal crossing the trigger level selected. For example, if the trigger level is set to +1 V, and the peak of signal is only at +900 mV a trigger event does not appear so that the recorded signal contains the period of silence or noise. But, if its peak is +1.1 V the trigger level will have been crossed, invoking a trigger event and subsequent data acquisition (Figure 5.23 and 5.24). In addition, the trigger slope also affects the detection of a trigger event by selecting at either positive or negative mode. The positive mode indicates a positive slope (i.e., the trigger appears on the rising edge of the signal (Figure 5.23 (a))).

The negative mode indicates a negative slope (i.e., the trigger appears on the signal's falling edge (Figure 5.23 (b))).

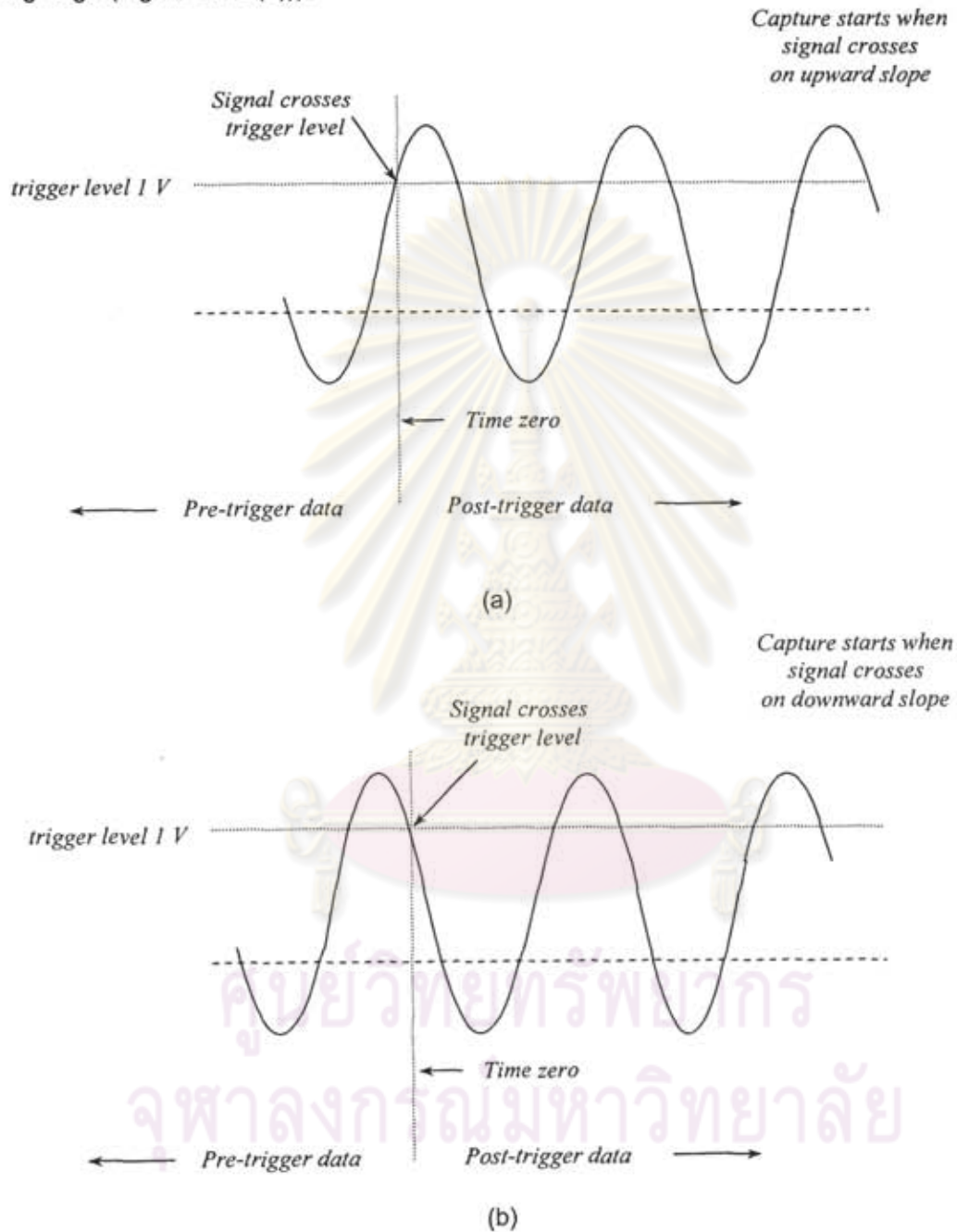


Figure 5.23 The effect of trigger level:

(a) Positive slop, (b) Negative slope.

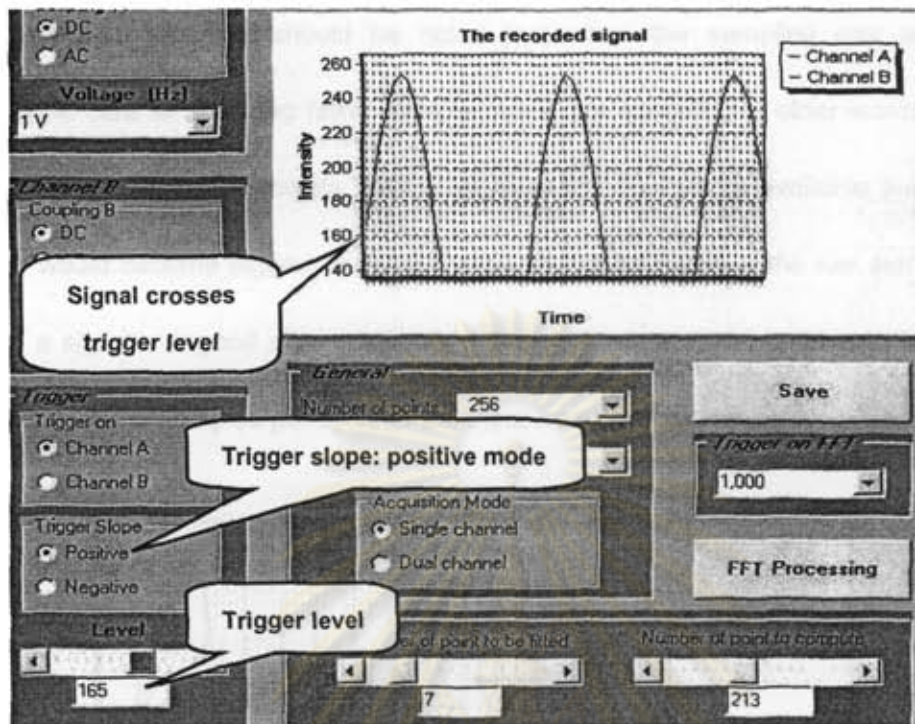


Figure 5.24 The effect of trigger level result in a signal.

Obviously, a good representation of the signal is those with the least noise as possible. The trigger level selected should not only be lower than the peak of the signal but also high enough to reduce the noise (low frequency signals).

iv) Sampling rate

The sampling rate defines how many sample points per second (S/s) should be acquired by the CompuScope card. It is advice to set the sampling rate to at least twice the input frequency. For example, if a 1 MHz signal is sampled, the sampling rate should be set at 2 Megasamples per second (MS/s), or higher.

It should be noted that when the sampling rate is low the CompuScope card is acquiring fewer sample points per second. In other words the time resolution of the signal decreases. However, with too few points available the resulting waveform would become jagged or not smooth. Figure 5.25 shows the low sampling rate results in a signal. A good representation of the signal is obviously obtained from taking the most number of samples per cycle of the input frequency on the screen as possible.

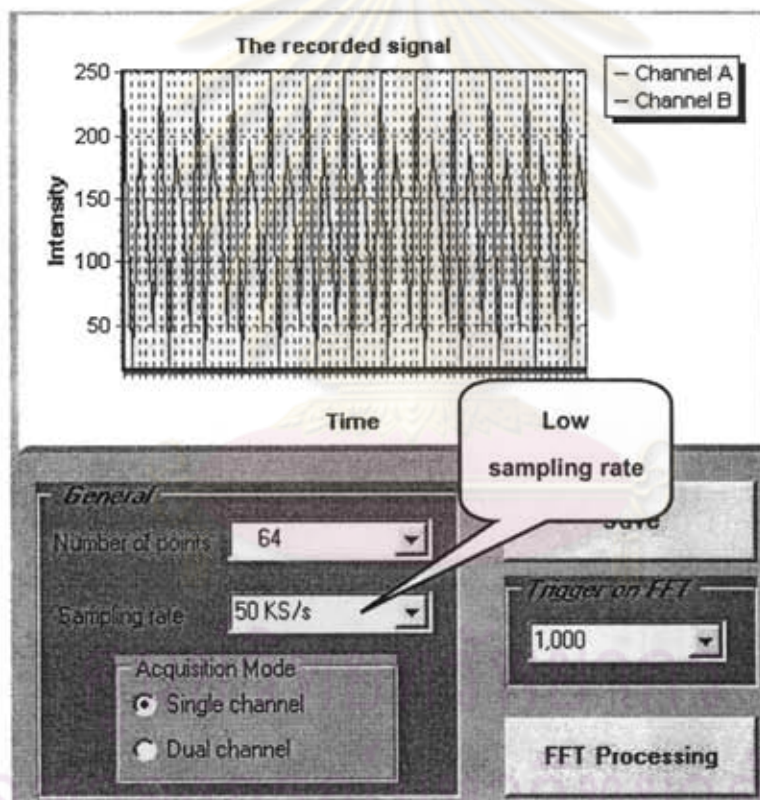


Figure 5.25 Low sampling rate result in a signal.

v) Number of points

The number of points represents the trigger depths (Figure 5.26) which are limited by the amount of memory on-board in CompuScope card. The maximum depth is 8192. This takes advantage of the deep memory of the CompuScope card buffers by allowing the hardware to stack captures in on-board memory, so that many small acquisitions can be computed in a very short amount of time. Data collected from each successive acquisition is stacked on top of the previous acquisition until the on-board buffer fills up.

For example, if a number of points of 1024 points are specified the first acquisition stores data in addresses between 0 and 1023; the next acquisition from 1024 to 2047; and so on until the buffer is full.

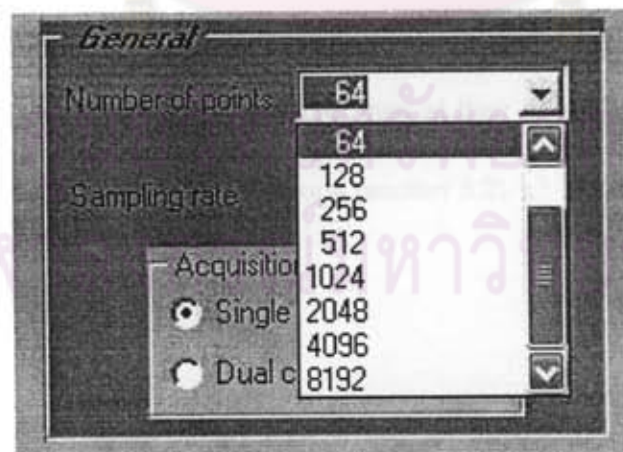


Figure 5.26 Example trigger depths.

It should be noted that the sampling rate and the number of points are related, so that both should be set in balance. The example below shows the relationship between the sampling rate and the number of points.

If the sampling rate is set at 1 KS/s, it defines that 1,000 points will be measured in one second. Therefore, if there are only 2 points it will be completed in 0.001 of a second (called the accuracy of the measurement). Similarly, if there are 8192 points the measurement will be completed in 8.192 seconds. Obviously, the higher the number of points will cause the longer time of measurement; so that if the sampling rate is low, the number of points should also be low in order to reduce the time of measurement. However, it must be sure that the sampling rate which is set is not lower than the input frequency.

Figure 5.27 shows the signal burst recorded from the particles crossing a measurement volume when all of those parameters are set properly. The overall shape of the burst is a consequence of the fact that the laser beams producing the measurement volume will inevitably be stronger at their center than at their edges. This case has been previously explained for an idealized signal burst (section 5.3).

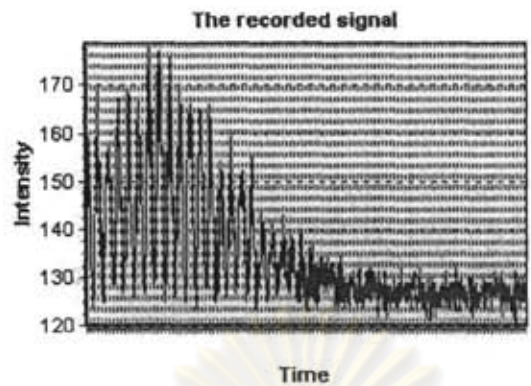


Figure 5.27 *The computable signal from particles crossing a measurement volume*

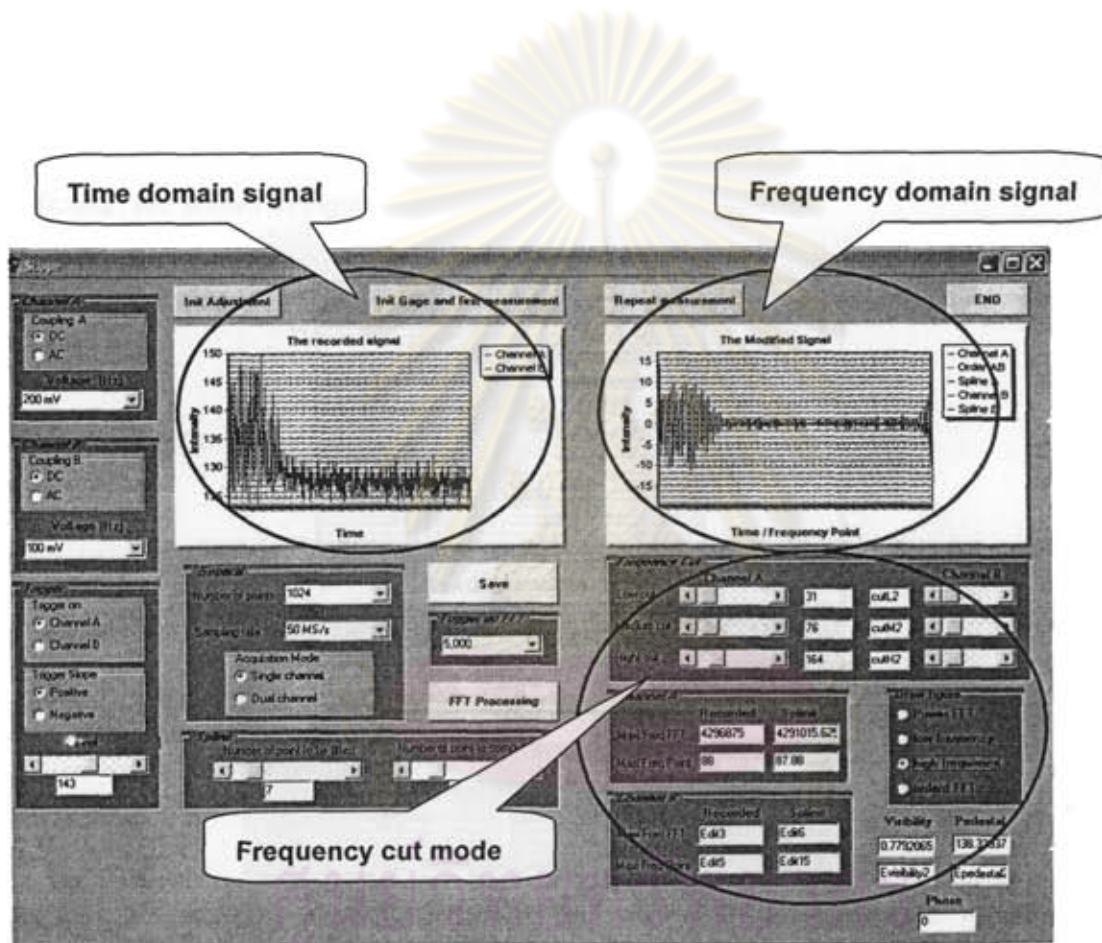
3) Data Processing Window

The data processing window is one part of the scope window which modifies the burst of signals by a Fast Fourier Transform (FFT) routine (Appendix A) and changes the acquired signal from the time domain to the frequency domain. Then the improvement of the signal quality is performed by using the frequency cut mode (Figure 5.28) which consists of a number of parameters as follows:

i) *the low cut filter* is used to remove high frequency part (Doppler) content in the signal. Consequently, the signal after modification will contain only the pedestal signal;

ii) *the medium cut filter* is used to ensure the good separation of pedestal and Doppler signal;

iii) *the high cut filter is used to remove the low frequency part (pedestal) content in the signal. Consequently, the signal after modification will contain only the Doppler signal.*



จุฬาลงกรณ์มหาวิทยาลัย
Figure 5.28 The data processing window.

All of parameters are adjusted by using the scrollbar buttons to select the position for cutting the signal in both channels A and B (Figure 5.29 (a)). The signal results can be displayed as either power FFT (the position of the signal that contains high frequency), low frequency (pedestal) or high frequency (Doppler) on the draw figure block diagram (Figure 5.29 (b)). To confirm the accuracy of the signal, the modified signal should be similar to the idealized Doppler and pedestal as possible. The signal examples after modification are shown in Figure 5.30.

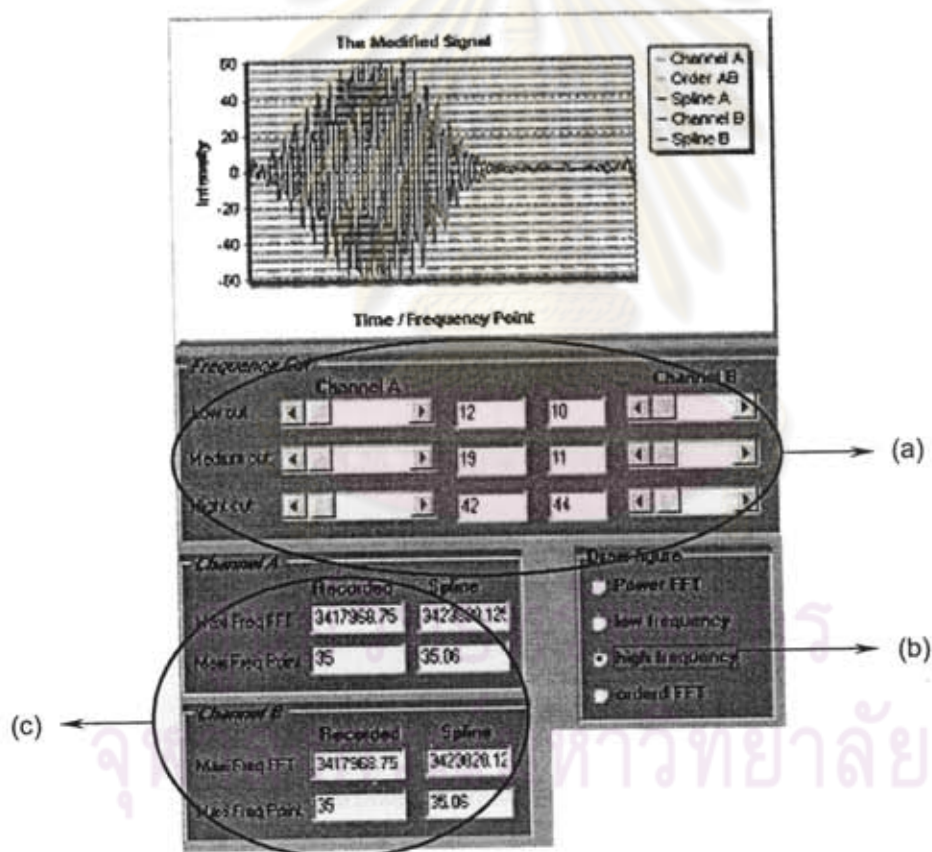


Figure 5.29 (a) Frequency cut mode; (b) Draw figure diagram;

(c) Information on modified signal.

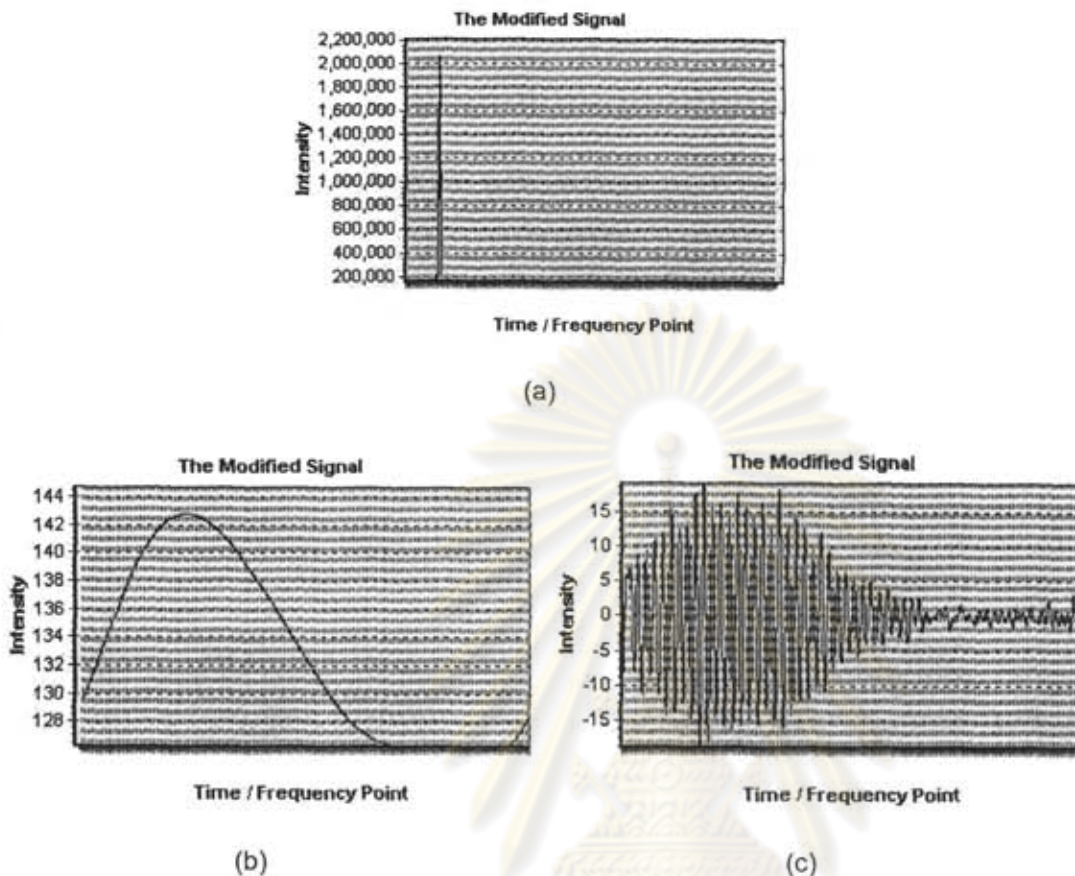


Figure 5.30 The signal processing.

(a) power FFT (b) pedestal signal (low frequency) (c) Doppler signal (high frequency).

In order to increase the accuracy when looking for the maximum position of power FFT, the spline interpolation must be used to fit the FFT. The number of points to be fitted along the curve and the number of points to compute must be set. For example, in Figure 5.31 the fitting has been realized by the selecting 7 points (the maximum and three points at its left and three at its right). Computing spline coefficients (a task which

is carried out by the procedure spline) and then computing the fit at 1000 points (a task which is carried out by the procedure spline). The information on the modified signal (Figure 5.29 (c)) is computed by the software when adjusting the parameters is completed. This information is:

- Max Freq FFT represents the maximum frequency of the signal;
- Max Freq Point represents the position of the maximum frequency.

Figure 5.32 shows the main components of a PDA instrument and an overview of the signal processing system.

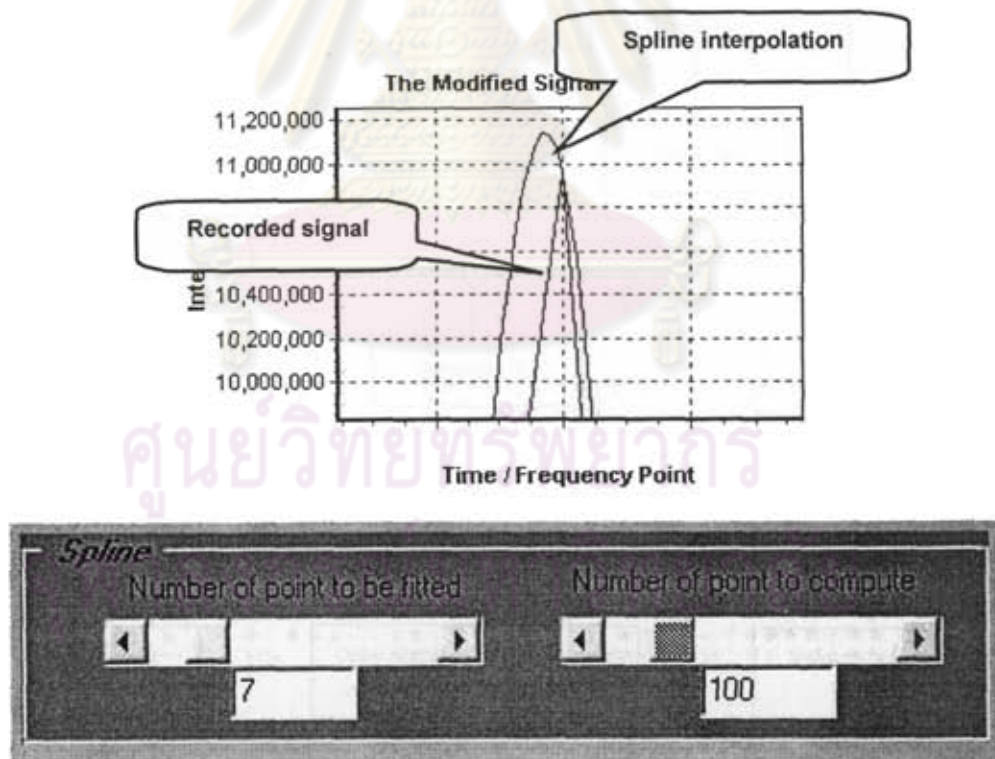


Figure 5.31 The spline interpolation.

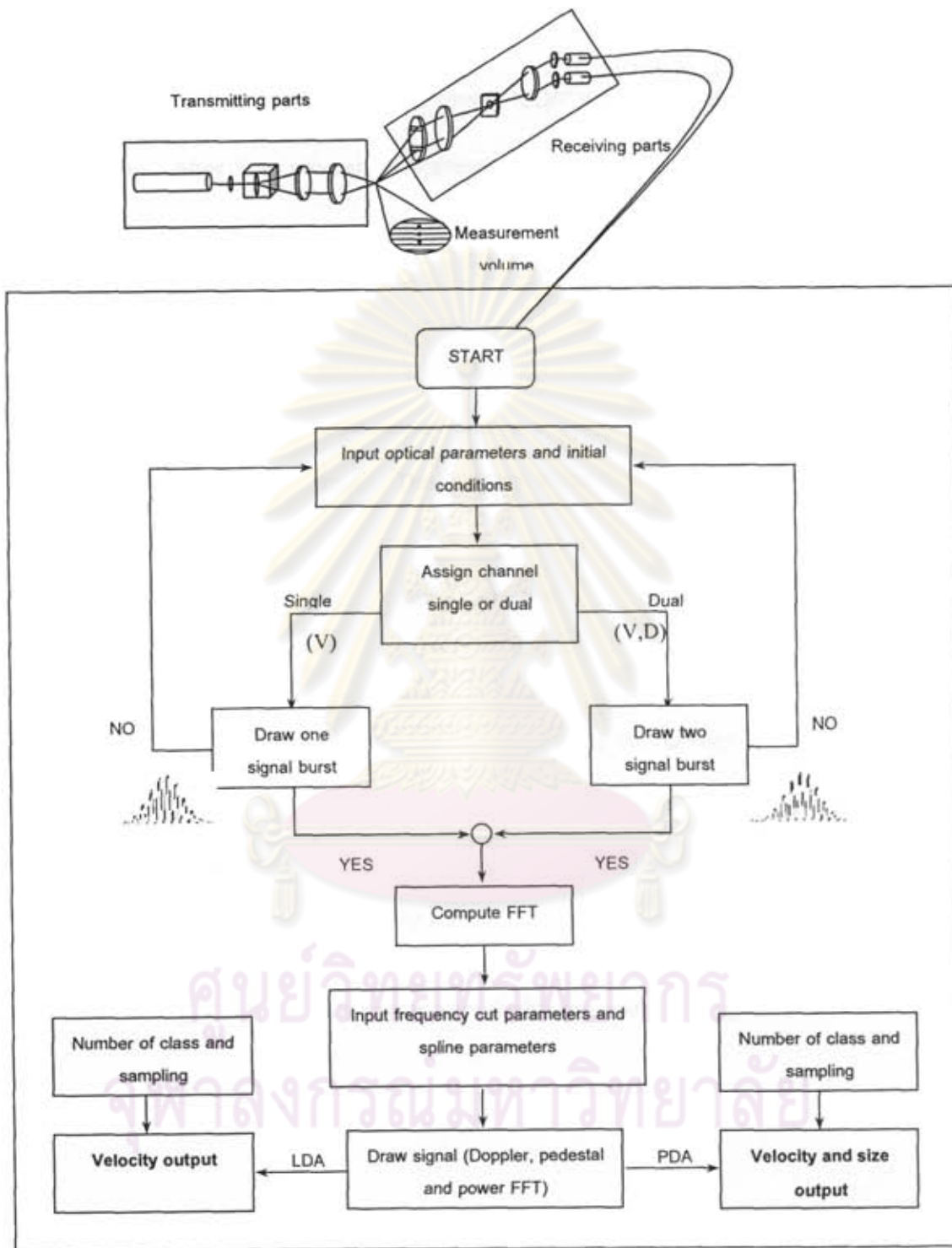


Figure 5.32 Flow diagram of developed PDA system.

5.3.3 Display of Results

The other windows on the screen "LDA" and "PDA" display the results of a measurement. After the program completely collects data, a resulted histogram is presented.

1) LDA result window

When the acquisition mode setting chosen is a single channel mode, only channel A is available for input. The present window displays a histogram of the computation results of a velocity measurement and also shows the measurement characteristics such as the mean, mean deviation, standard deviation, skewness and flatness. A number of parameters are adjusted as follow:

- the number of points represents the number of sampling counted particles;
- the number of class represents the range of the data selected to draw a histogram.

Figure 5.33 shows how the result should be after taking a measurement.

2) LDA/PDA result window

When the acquisition mode setting chosen is dual channel mode, both channels A and B on your CompuScope card are available for input. The present window displays a histogram of the computation results of a velocity and size measurement. It also

shows the measurement characteristics such as the mean, mean deviation, standard deviation, skewness and flatness. A number of parameters are adjusted as follows:

- the number of points represents the number of sampling counted particles;
- the number of class represents the range of the data selected to draw a histogram.

Figure 5.34 shows how the result should be after taking a measurement.

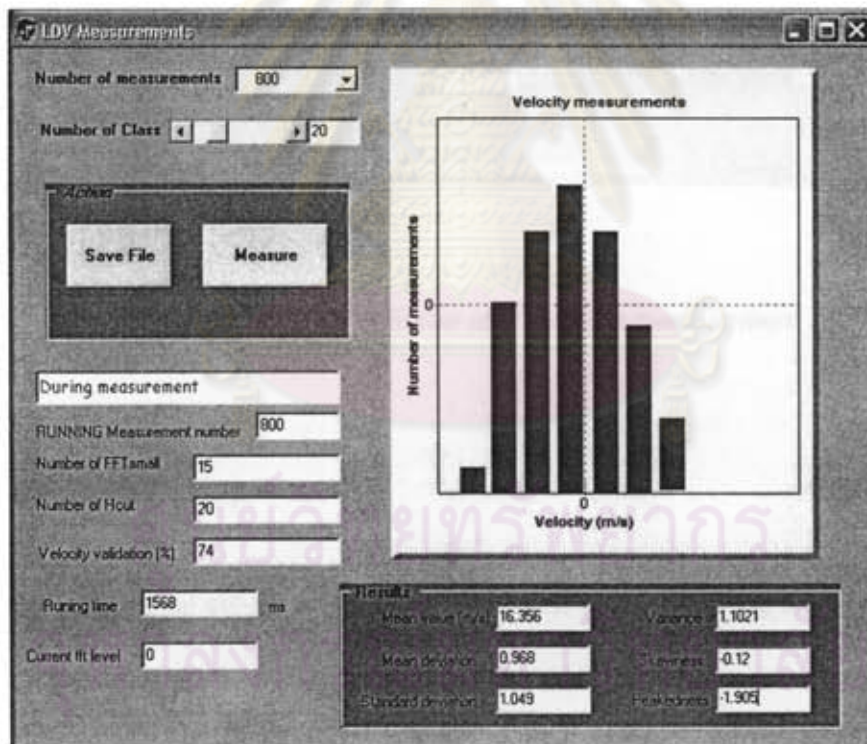


Figure 5.33 LDA window after taking a measurement.

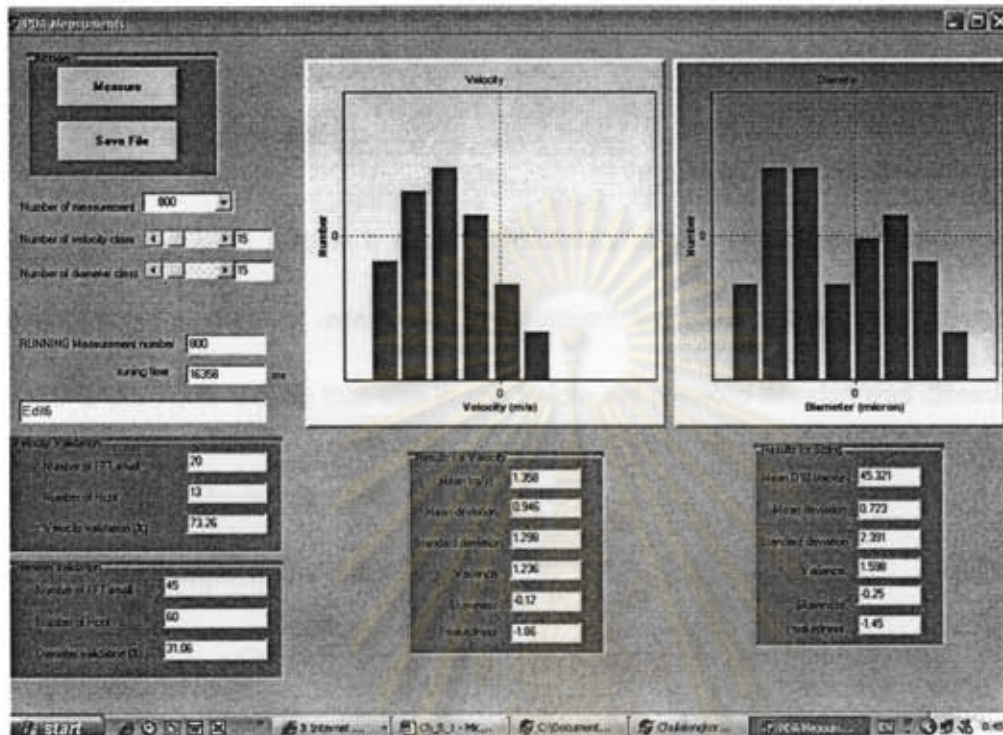


Figure 5.34 LDA/PDA window after taking a measurement .

5.4 Experimental Set-Up

The experimental set-up in this work consists of the transmitting and receiving parts described in the previous section. All components are mounted on an optical rail. Data evaluation is performed with the PDA software which was developed to compute the measurement information.

The following contexts present the default settings for the first session and the general experimental procedures for conducting the experiments:

5.4.1 Default Settings

In order to display a signal immediately upon startup the software assumes certain defaults on the first operation. Subsequent sessions will set the CompuScope hardware to the same setting that was in use before the previous session was closed.

The defaults for the first session are:

- CompuScope card setting

Capture mode: Continuous

Channel mode: Dual

Sample rate: Maximum

- Trigger setting

Trigger: Set to channel 1

Trigger level: 0 mV

Slope: Positive

Trigger depth: 4096 samples

- Channel setting

Identification: Channel A of the CompuScope is channel 1

Channel B of the CompuScope is channel 2

Colors: Channel 1 sets to red. Channel 2 sets to green

Input range: All channel set to ± 1 V

5.4.2 General Experimental Procedures

After all of PDA components have been aligned successfully, the general procedures to conduct the experiment are as follows:

- 1) Turn on the laser.
- 2) Once the laser is turned on, be cautious that the laser light can be harmful to the eyes. Under no circumstances, look directly into the laser beams or their reflections, nor put your head in a position where it might inadvertently do this. Two red beams should be visible emerging from the circular concentric diffraction array and passing through the focusing lens.
- 3) Select a track of the circular concentric diffraction array which is proper for each droplet size and change the proper mask as well. Note that, in order to carry out the experiment immediately the track of the circular concentric diffraction array is set on track 3 and vertical plane.
- 4) Turn on the motor to turn the circular disk and adjust the voltage to create the driving frequency.

- 5) Run the atomizing nozzle. Investigate the position where the beams pass through the droplets for adjusting the nozzle in the center position of the measurement volume (Figure 5.33).
- 6) Turn on the PM and adjust the applied the voltage.
- 7) Turn on the oscilloscope. The image of Doppler bursts should appear on the oscilloscope screen.
- 8) Start-up the PDA software and input the experimental parameters. Next enter into the scope window to select the acquisition mode and to set the input range at 100 mV. Be certain that the coupling setting is set to DC. Vary the sampling rate and number of point slowly until the bursts appear by clicking the 'Init Adjustment and Init Gage' and 'First measurement' buttons, respectively, to see the burst signals. This is the raw signal.
- 9) After obtaining the burst signals vary the trigger level on FFT and the spline mode to modify the signal. Click the FFT processing button to see the modified signal and then select the range of the frequency cut-off. Here the user can see the power FFT, pedestal signal and Doppler signal by selecting the draw figure on a radio button.
- 10) Continue the LDA window or the LDA/PDA window to conduct the next experiment.

It is noted that before opening the scope window the user must first completely input the experimental parameters in the configuration setting window. If any parameters are changed while the scope window is open the 'Init Adjustment and Init Gage' and the 'First measurement' buttons must be relicked to inform the CompuScope card for the newly input data.

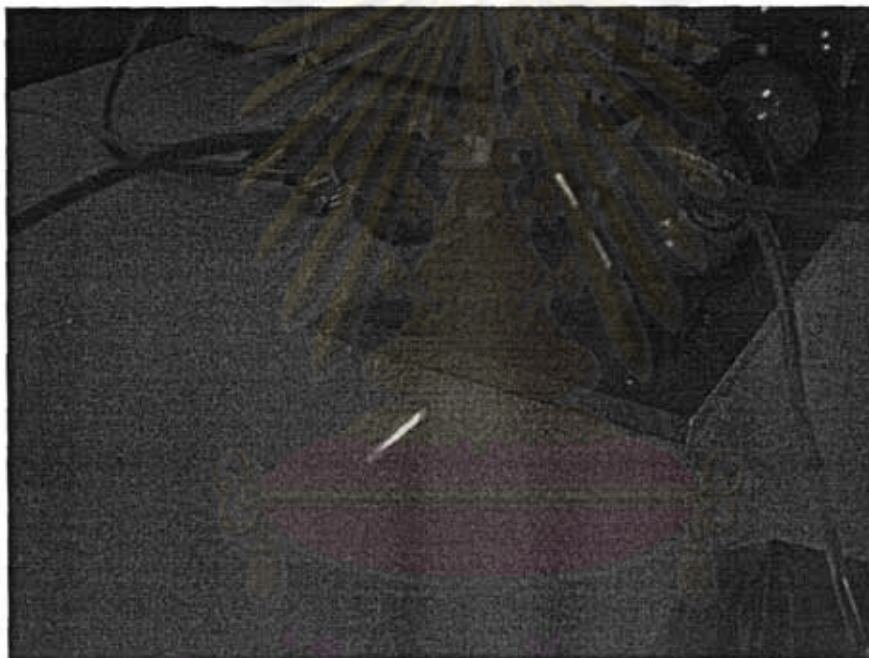


Figure 5.35 *The image of the spray nozzle indicating the measuring position.*

CHAPTER 6

RESULTS AND DISCUSSION

In order to investigate the PDA system developed in this work, a spectrum of experiments has been performed intentionally to ensure its reliability and accuracy. These experiments were organized as follows: i) first, the signal reliability experiments were conducted to confirm the response reliability obtained from the software developed in this work ii) secondly, the accuracy of the developed PDA instrument was examined by using standard glass spheres of precisely known size iii) thirdly, the instrument reliability experiments were conducted by taking the measurement results (velocity and diameter comparison) from the developed PDA instrument to compare with those of the commercial PDA instrument and finally, iv) the sources of discrepancies in the experiments were discussed.

6.1 Experiments for Verifying Reliability of Signal Processing System

6.1.1 Verification with the Signal Generator

Signal generator (Tektronix AFG310, Figure 6.1) was used to verify the signal obtained from the developed system with a frequency ranging from 10 kHz up to 100 kHz. A typical example of signal at 10 kHz is shown in Figure 6.2. Figure 6.3 illustrates the comparison of generated signal and the input signal employed in this verification. It could

be clearly seen that the generated signal is almost perfectly identical to the input one. This could be implied that the developed system could be reliably used for the signal processing.



Figure 6.1 Tektronix AFG310 signal generator.

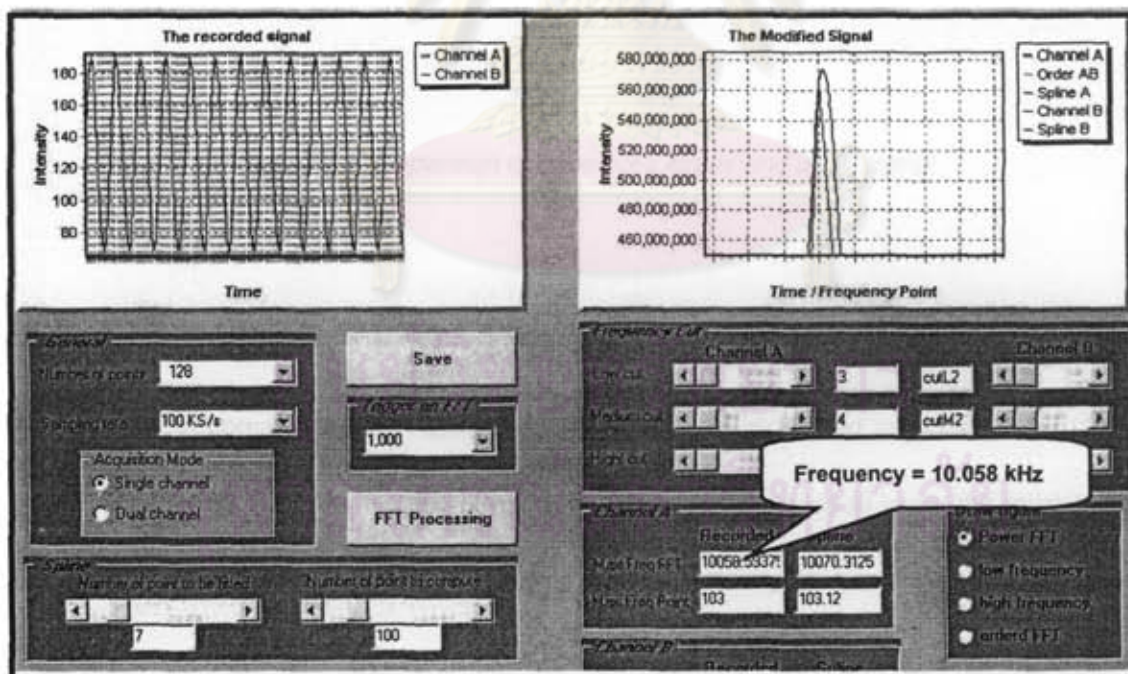


Figure 6.2 A typical example of signal at 10 kHz.

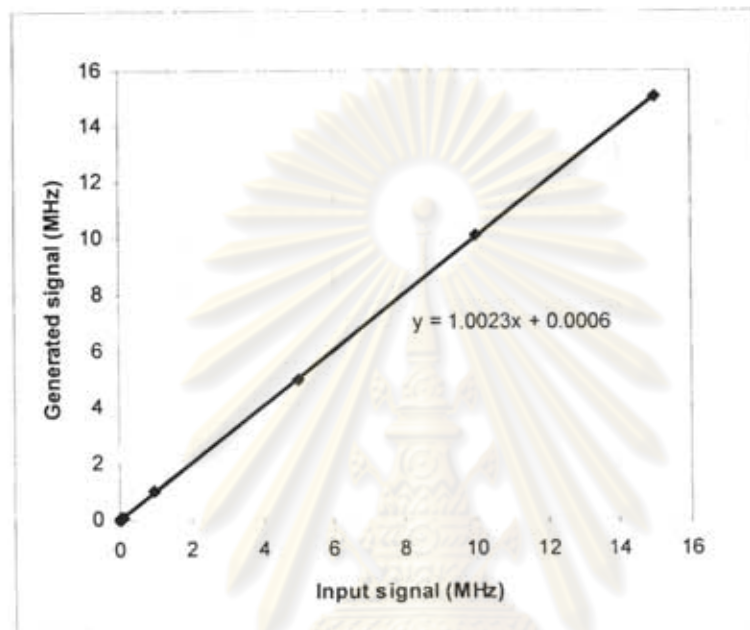


Figure 6.3 Comparison of generated signal and input signal.

6.1.2 Verification by Comparison with Commercial PDA System

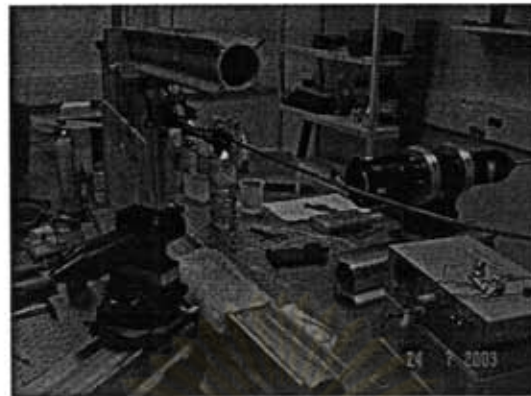
A commercial PDA system equipped with an air-cooled argon ion laser (2000 mW at wavelength 488 nm, Dantec Ltd., Figure 6.4) was employed to verify the reliability of the developed software. Within the examination, the velocity of droplets generated by an ultrasonic nozzle (Figure 6.5) was measured by using the same hardware but different softwares. The conditions of verification were as follows:

- Spraying frequency: 46 kHz

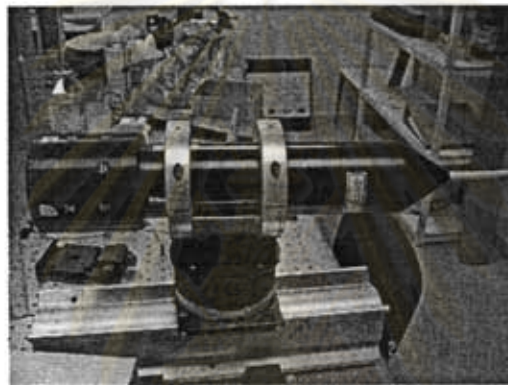
- Applied fluid: water at 18° C (France)
- Flow rate: 16, 33 and 66 mm³/sec
- Distance: 50 mm away from the nozzle tip

The mean and the standard deviation of the droplet velocity measured by the commercial and developed softwares are shown in Table 6.1. The dependence of the mean velocity and feeding rate of water is shown in Figure 6.6 while the distribution of the droplet velocity with the different water flow rate is shown in Figure 6.7. With the different water flow rate (16, 33, 66 mm³/sec), a fair agreement between the mean droplet velocities measured by the commercial software and the developed software could be obtained. The relative differences of the mean and standard deviation of droplet velocities measured by both softwares are less than 10% and 25%, respectively. Moreover, the increase in the droplet velocity with the increasing of water flow rate exhibits a good agreement with theoretical prediction.

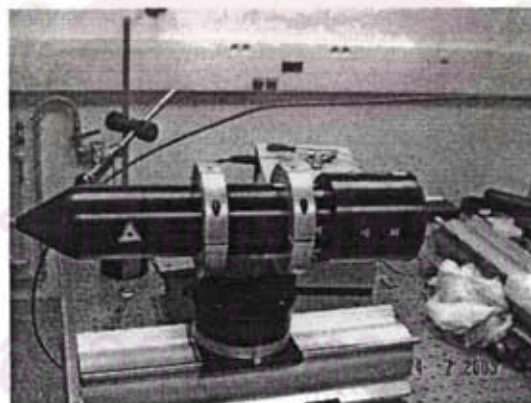
ศูนย์วิทยทรัพยากร
จุฬาลงกรณ์มหาวิทยาลัย



(a)



(b)



(c)

Figure 6.4 (a) *The Commercial PDA instrument (Dante Ltd.),*
(b) *The transmitting part,*
(c) *The receiving part.*

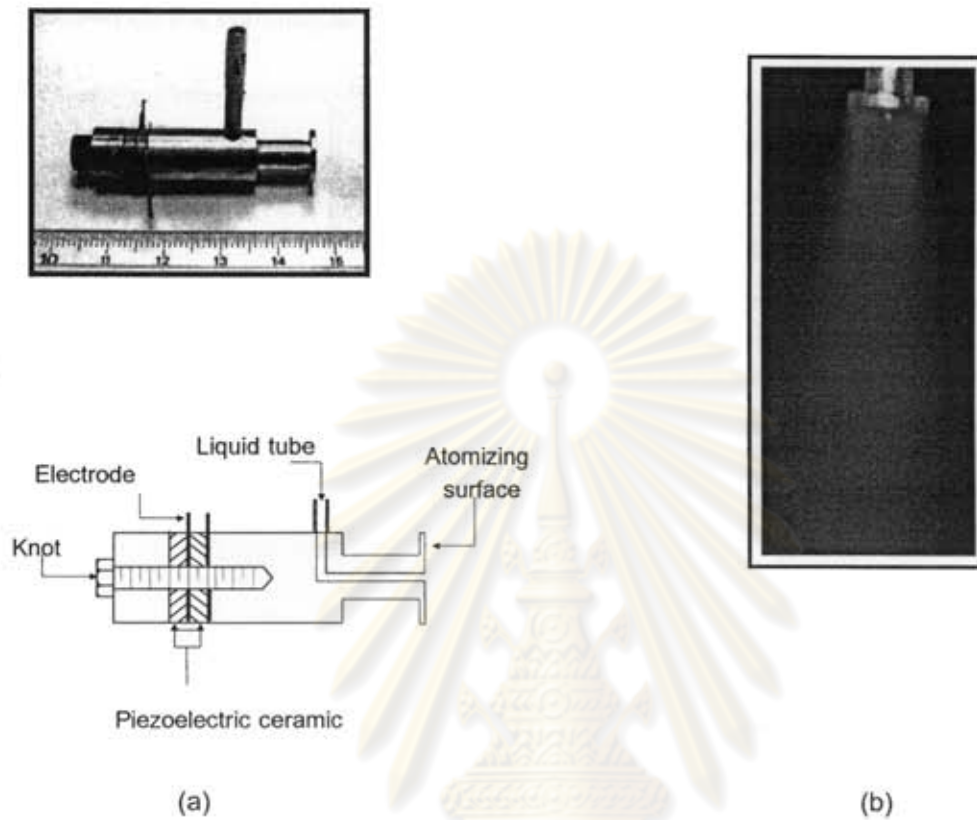


Figure 6.5 (a) Schematic of an ultrasonic nozzle (b) Image of spray profile.

ศูนย์วิทยทรัพยากร
จุฬาลงกรณ์มหาวิทยาลัย

Table 6.1 The experimental results of mean and standard deviation of the droplet velocity measured by the commercial and the developed softwares.

Water flow rate (mm ³ /sec)	Droplet Velocity (m/s)	
	Commercial software	Developed software
16	0.98 ± 0.10	1.05 ± 0.34
33	1.13 ± 0.10	1.24 ± 0.21
66	1.29 ± 0.10	1.37 ± 0.39

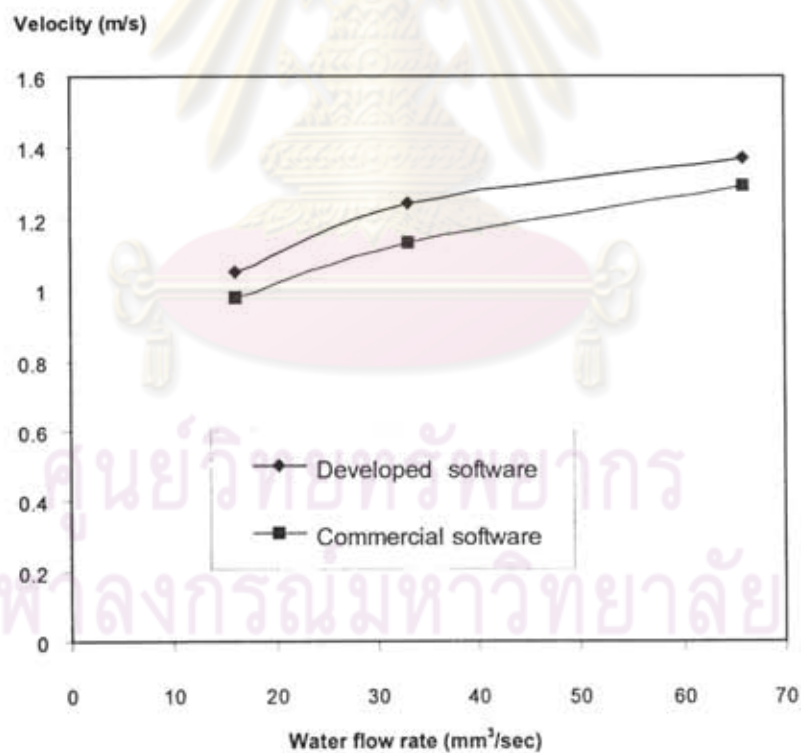


Figure 6.6 Comparison of mean droplet velocities obtained by the commercial and developed software.

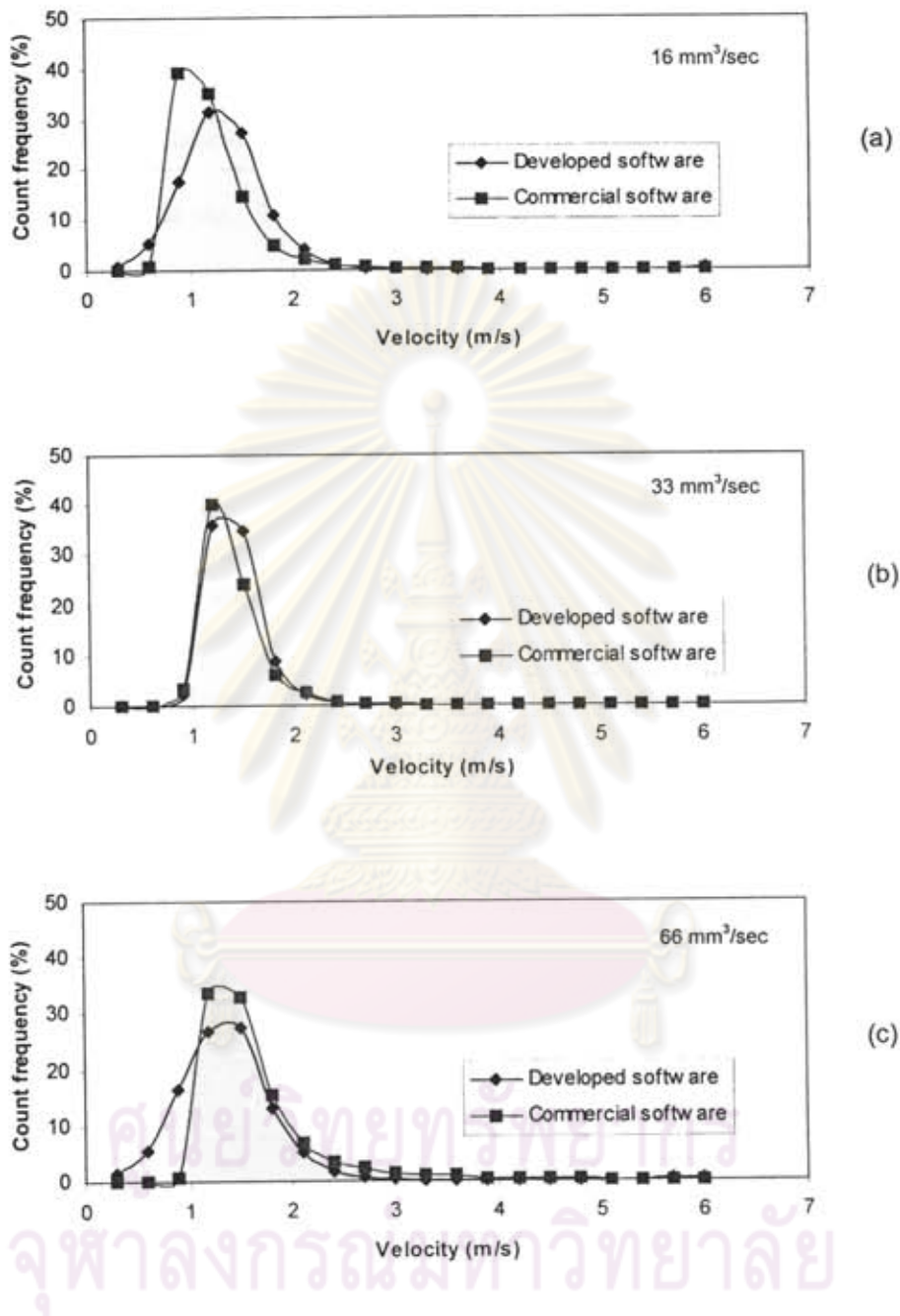


Figure 6.7 The comparison of the distribution of the droplet velocity obtained by the commercial and the developed software with the different water flow rate

(a) 16 mm³/sec (b) 33 mm³/sec (c) 66 mm³/sec.

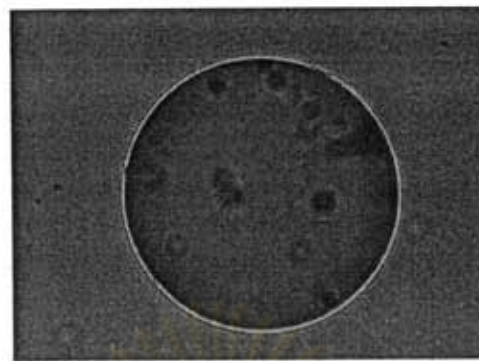
6.2 Verification of the Developed PDA System using Stationary Object

To confirm the accuracy of the developed PDA system, measurements of reference particle size were carried out. Transparent glass spheres with a refractive index 1.51 were employed as the reference particle. The glass sphere was attached to a thin pin mounted on the optical rail as shown in Figure 6.8. The diameter of transparent glass sphere was determined from microscopic images taken by a SLR camera (Panasonic, wv-CP2401G) and processed by an image processing program (Image Pro V.30). Such microscopic analysis was employed for verifying the measuring results of the developed PDA system.

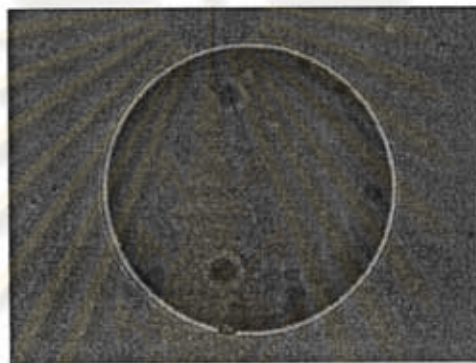


Figure 6.8 The photograph of the glass sphere attached to a thin pin at

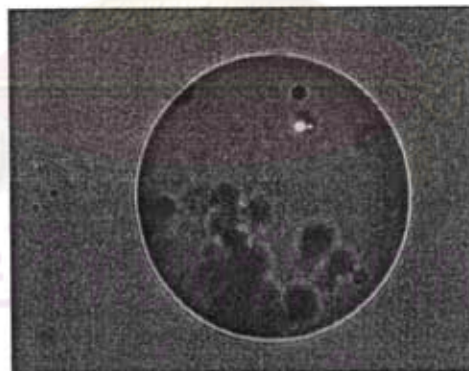
the measurement volume.



(a) 60 micron



(b) 62 micron



(c) 65 micron

Figure 6.9 Microscopic image of glass spheres of different size.

The measurement results shown in Tables 6.2, 6.3 and 6.4 are obtained from the investigation using the glass spheres of 60, 62 and 65 μm . The measurement exhibits the glass sphere diameters which are different from the microscopic results. It is possibly owing to the imperfect spherical shape of the glass spheres and some defects on their surfaces, which lead to the wider scattering signal. This discrepancy will be discussed in more detail in section 6.4. Figure 6.10 shows typical image of the recorded signal from the actual measurement.

Table 6.2 Diameter of glass sphere No. 1 measured with the developed PDA.

Circular concentric diffraction array	Voltage to turn the circular (V)	Particle diameter (micron)	
		Measurement	Reference
Track 1	2	74	60
	3	76	
	4	74	
Track 2	2	74	
	3	75	
	4	75	
Track 3	2	75	
	3	75	
	4	75	

Table 6.3 Diameter of glass sphere No. 2 measured with the developed PDA.

Circular concentric diffraction array	Voltage to turn the circular (V)	Particle diameter (micron)	
		Measurement	Reference
Track 1	2	78	62
	3	78	
	4	78	
Track 2	2	76	
	3	75	
	4	76	
Track 3	2	76	
	3	77	
	4	76	

ศูนย์วิทยทรัพยากร
จุฬาลงกรณ์มหาวิทยาลัย

Table 6.4 Diameter of glass sphere No. 3 measured with the developed PDA.

Circular concentric diffraction array	Voltage to turn the circular (V)	Particle diameter (micron)	
		Measurement	Reference
Track 1	2	79	65
	3	79	
	4	80	
Track 2	2	79	
	3	78	
	4	79	
Track 3	2	79	
	3	79	
	4	79	

ศูนย์วิทยทรัพยากร
จุฬาลงกรณ์มหาวิทยาลัย

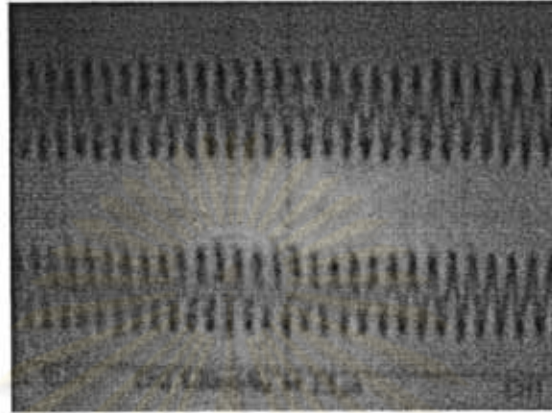


Figure 6.10 *The image of the recorded signal from the actual measurement volume.*



ศูนย์วิทยทรัพยากร
จุฬาลงกรณ์มหาวิทยาลัย

6.3 Verification of the Developed PDA System using Liquid Spray

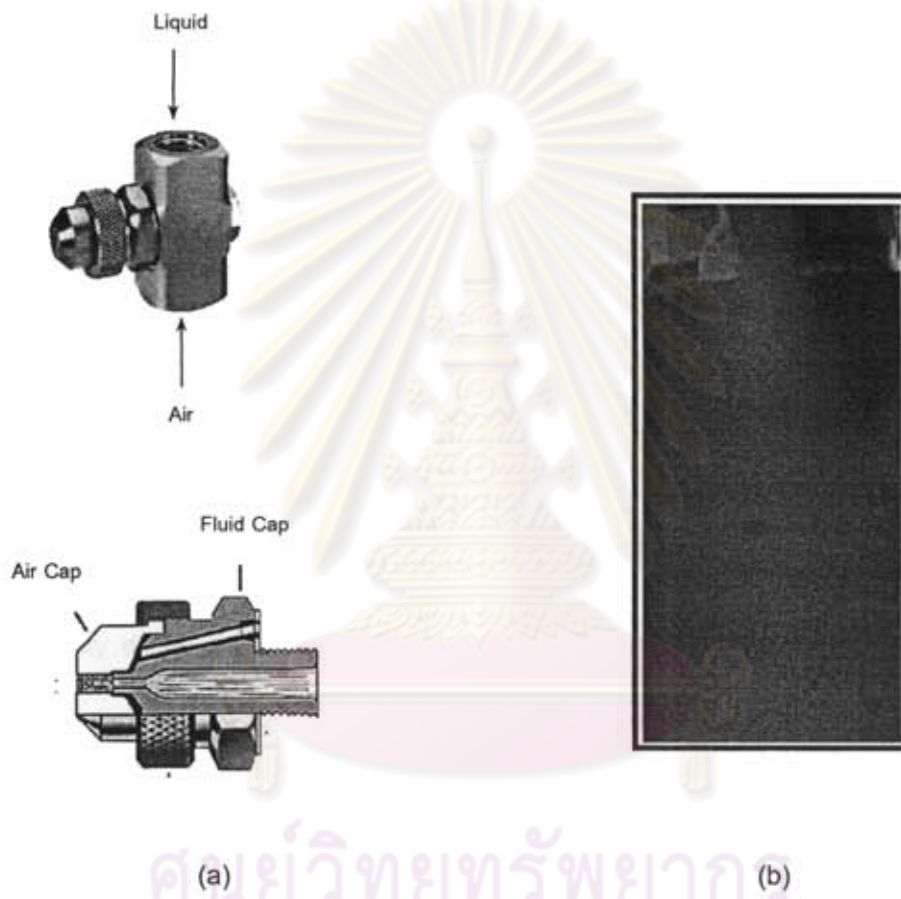
An experimental investigation of the reliability of the developed PDA instrument was conducted by comparison of the measurement results with those of the commercial PDA instrument (Dantec Ltd., Figure 6.4). Before presenting the investigating result of the two instruments, it is worth to compare the specification of the two instruments given in Table 6.5.

Table 6.5 The specification of the PDA system.

Parameters	Developed PDA instrument	Commercial PDA instrument
Laser wavelength (μm)	0.6328	0.488
Intersection angle** (deg.)		5.44
Track 1	1.99	
Track 2	2.85	
Track 3	4.85	
Fringe spacing** (μm)		5.42
Track 1	18.12	
Track 2	12.70	
Track 3	7.46	
Beam waist (μm)	251	140
Receiver focal length (mm)	300	400
Off-axis angle (deg.)	30	40
Elevation angle (deg.)	3.34	1.93
Detector using	2	4

Remark: ** The response of the developed PDA instrument will be illustrated using track 3

Water droplets were generated by a binary nozzle which was the Wide - Angle round spray model (Pawin Engineering Co., Ltd.) as shown in Figure 6.11.



ศูนย์วิทยทรัพยากร
 จุฬาลงกรณ์มหาวิทยาลัย
 Figure 6.11 (a) Schematic of a binary nozzle, (b) Image of spray.

6.3.1 Velocity Verification

The experimental comparison of the droplet velocity measured by the developed PDA instrument and the commercial PDA instrument was conducted under the following conditions:

- Atomizing air pressure: 0.05 and 0.10 N/mm²
- Applied fluid: water at 25° C (Thailand) and at 18° C (France)
- Flow rate: 250, 416 and 500 mm³/sec
- Distance: 50 mm away from the nozzle tip

The measurement results of the droplet mean velocity and their standard deviations obtained from the commercial and developed PDA instrument at three different water flow rates are shown in Table 6.6 and Figure 6.12. Meanwhile, the comparisons of the velocity distributions are shown in Figure 6.13 and 6.14 for the applied air pressure 0.05 and 0.10 N/mm², respectively. It could be seen that a fair agreement between the velocity distributions measured by using the commercial PDA instrument and the developed PDA instrument was verified. The velocity distributions exhibit their modes at almost the same value. Relative differences of the mean and standard deviation are less than 15%. The measurement result also shows that the velocity of the droplets increases with the increasing water flow rate, which is consistent with theoretical expectation.

Table 6.6 The experimental results of mean velocities and their standard deviations obtained by the commercial PDA and developed PDA instrument*.

Applied pressure (N/mm ²)	Water flow rate (mm ³ /sec)	Velocity (m/s)	
		Developed PDA instrument	Commercial PDA instrument
0.05	250	14.94 ± 0.4	11.48 ± 0.5
	416	18.73 ± 0.9	16.33 ± 0.7
	500	23.16 ± 0.6	20.14 ± 0.4
0.10**	500	39.80 ± 5.2	35.14 ± 2.5

Remark: * The experiments which conducted from the developed PDA instrument had been repeated three times.

** Because of the limitation of feeding pump, the experiments conducted here is limited to only a water flow rate of 500 mm³/sec for the case of applied air pressure 0.10 N/mm²

ศูนย์วิทยทรัพยากร
จุฬาลงกรณ์มหาวิทยาลัย

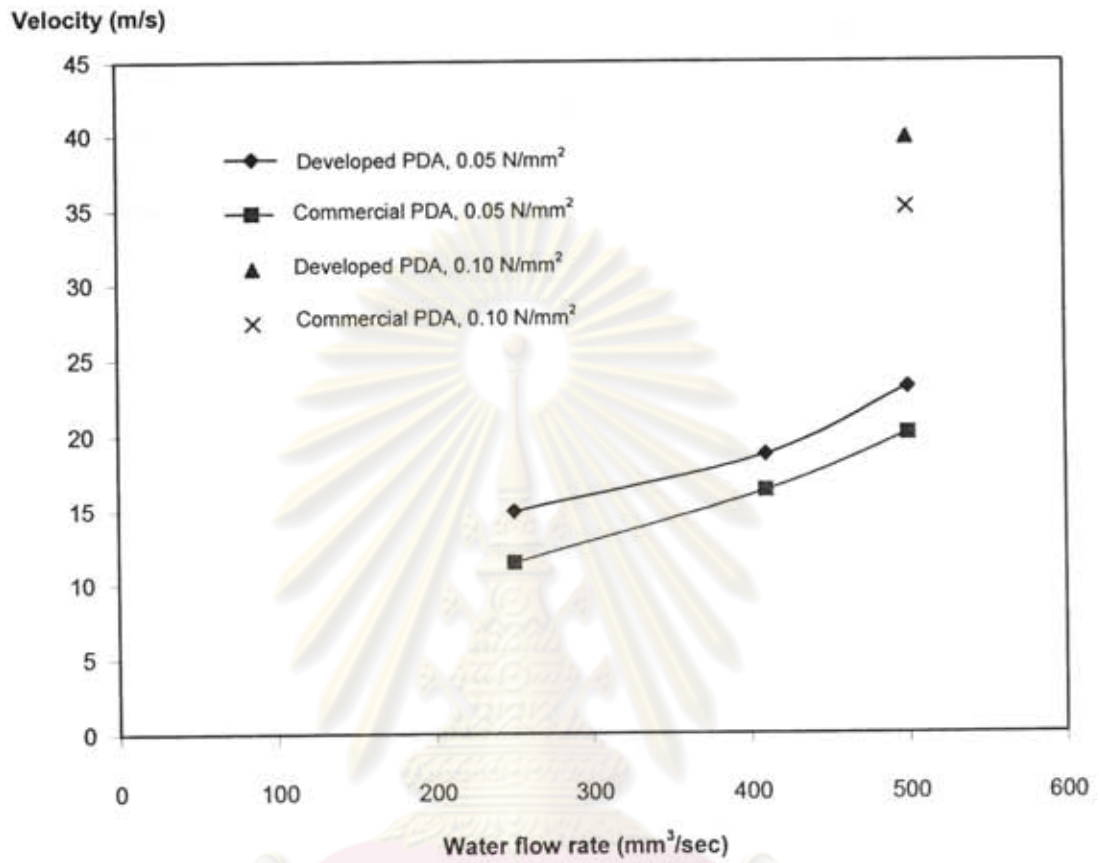
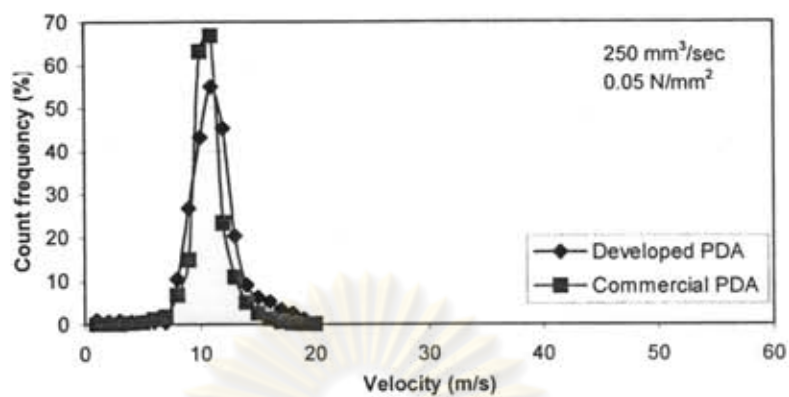
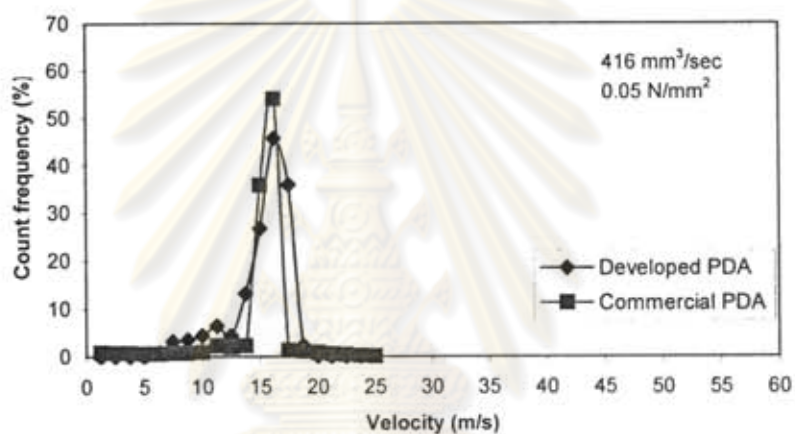


Figure 6.12 Comparison of mean velocity obtained by the developed PDA instrument and the commercial PDA instrument.

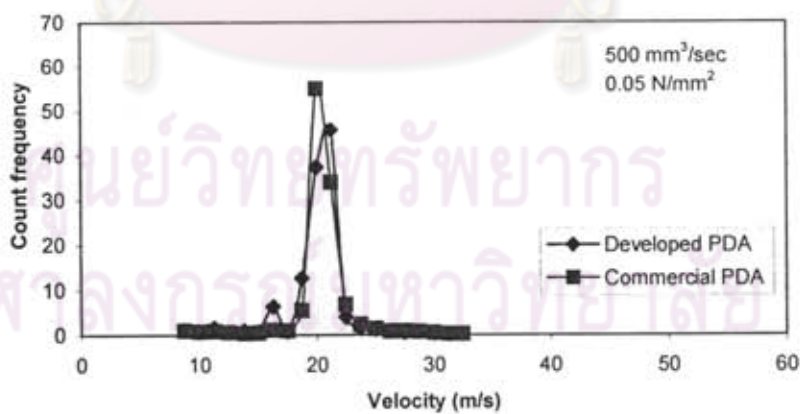
ศูนย์วิจัยทรัพยากร
จุฬาลงกรณ์มหาวิทยาลัย



(a)



(b)



(c)

Figure 6.13 The comparison of the velocity distributions obtained by the developed PDA instrument and the commercial one by using air pressure 0.05 N/mm² and water flow rate

(a) 250 mm³/sec (b) 416 mm³/sec (c) 500 mm³/sec.

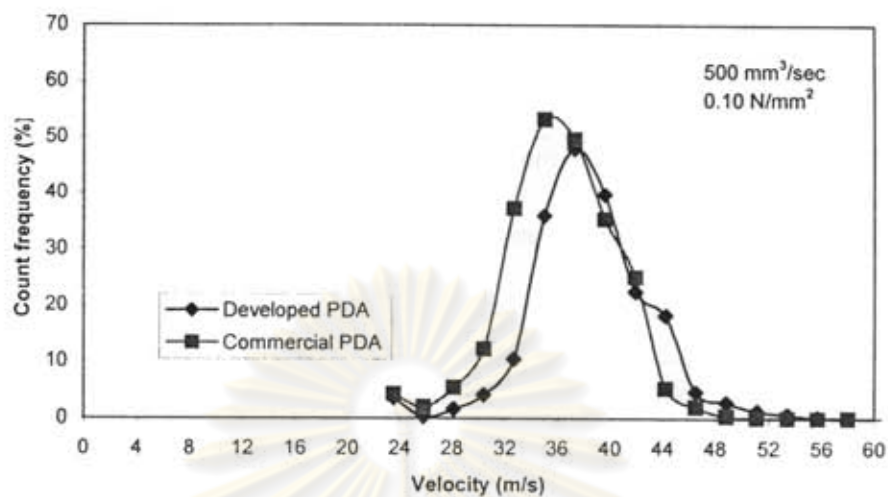


Figure 6.14 The comparison of the velocity distributions obtained by the developed PDA instrument and the commercial PDA instrument by using air pressure 0.10 N/mm^2 and water flow rate $500 \text{ mm}^3/\text{sec}$.

6.3.2 Diameter Verification

The experimental comparisons of the droplet size measured by the developed PDA instrument and the commercial PDA instrument were conducted under the following conditions:

- Atomizing air pressure: 0.05 and 0.10 N/mm^2
- Applied fluid: water at 25°C (Thailand) and at 18°C (France)
- Flow rate: 250 , 416 and $500 \text{ mm}^3/\text{sec}$
- Distance: 50 mm away from the nozzle tip

The results of the mean diameter of the droplets and their standard deviations obtained by the commercial and developed PDA instrument are shown in Table

6.7 and in Figure 6.15. The comparisons of the droplet size distributions are illustrated in Figure 6.16 and 6.17 for the applied air pressure 0.05 and 0.10 N/mm², respectively. The results indicate that there is a reasonable agreement between the droplet size distribution measured by using the commercial PDA instrument and the developed PDA instrument. Similar to the velocity measurement, droplet size distributions obtained from both instruments exhibit the modes at acceptably close value. The relative differences of the droplet mean diameter and their standard deviation are less than 25 and 30 %, respectively.

Table 6.7 The experimental results of mean diameter and their standard deviations obtained by the commercial PDA and developed PDA instrument*.

Applied pressure (N/ mm ²)	Water flow rate (mm ³ /sec)	Particle diameter (μ m)	
		Developed PDA instrument	Commercial PDA instrument
0.05	250	54.28 ± 4.1	44.49 ± 2.6
	416	56.02 ± 4.6	46.64 ± 2.3
	500	50.53 ± 2.4	47.07 ± 2.5
0.10**	500	55.67 ± 5.3	45.11 ± 3.1

Remark: * The experiments which conducted from the developed PDA instrument had been repeated three times.

**Because of the water limitation of feeding pump, the experiments conducted here is limited to only water flow rate, 500 mm³/sec, for the case of applied air pressure 0.10 N/mm².

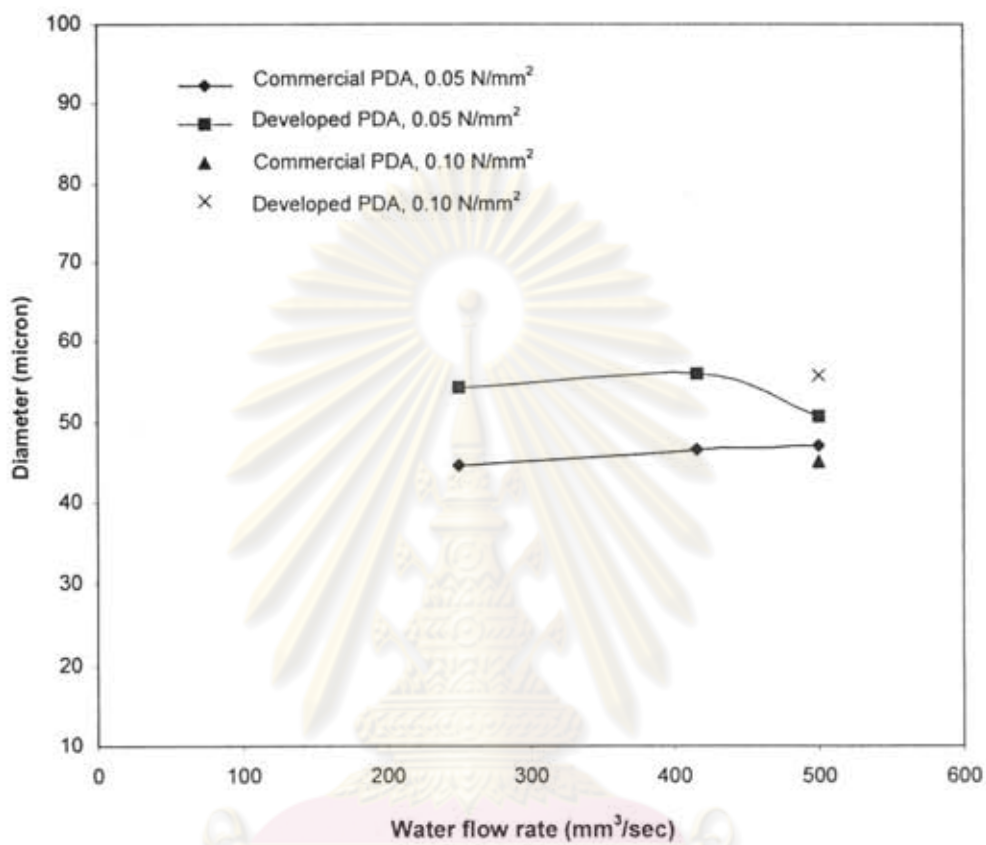


Figure 6.15 Comparison of mean diameter obtained by the PDA instrument under development and the commercial PDA instrument.

ศูนย์วิจัยทรัพยากร
จุฬาลงกรณ์มหาวิทยาลัย

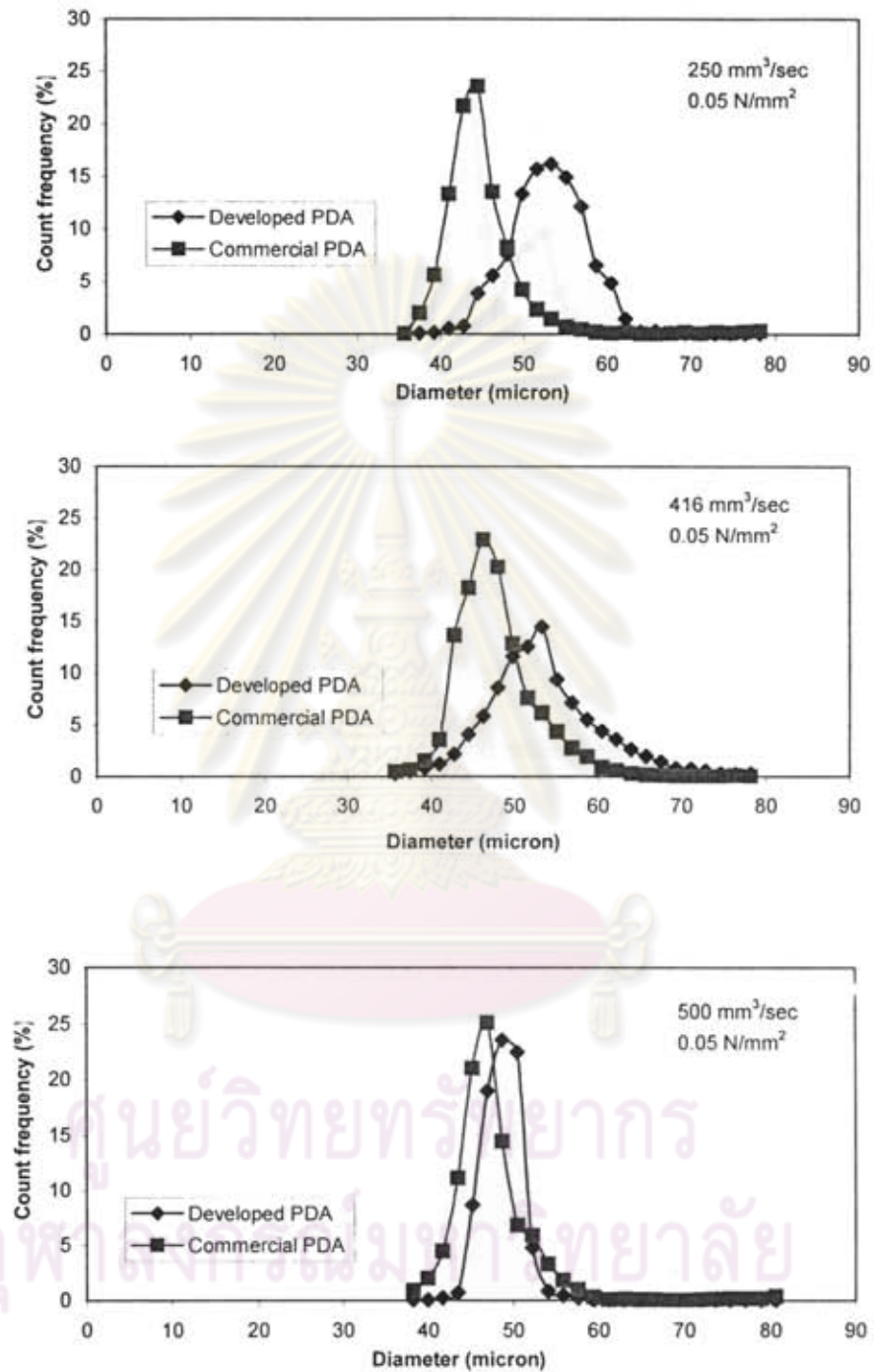


Figure 6.16 The comparison of the size distributions obtained by the developed PDA

instrument and the commercial PDA instrument by using air pressure 0.05 N/mm^2

and water flow rate (a) $250 \text{ mm}^3/\text{sec}$ (b) $416 \text{ mm}^3/\text{sec}$ (c) $500 \text{ mm}^3/\text{sec}$.

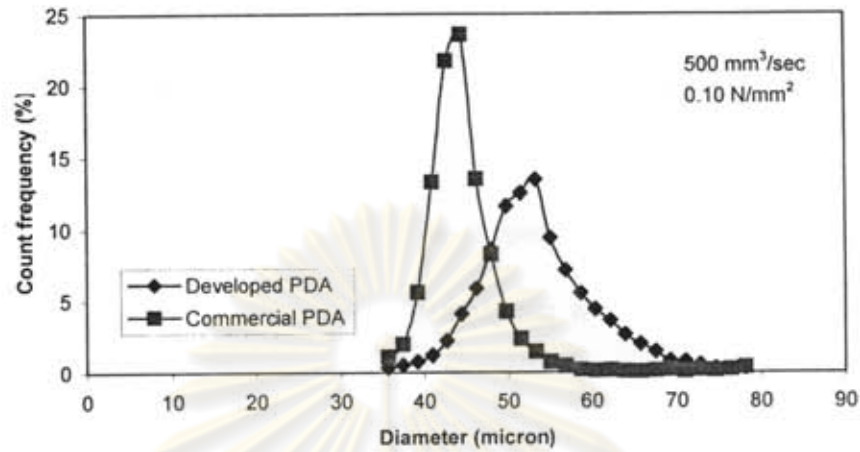


Figure 6.17 The comparison of the size distributions obtained by the developed PDA

instrument and the commercial PDA instrument

by using air pressure 0.10 N/mm^2 and water flow rate $500 \text{ mm}^3/\text{sec}$.

ศูนย์วิทยทรัพยากร
จุฬาลงกรณ์มหาวิทยาลัย

6.4 Sources of Discrepancies in the Experiments

Some possible sources of discrepancies in the instruments and in the comparison procedures can be specified as follows:

1) The loss of some of the smaller droplets due to the emitting light source. Whereas, the commercial PDA instrument equipped with a 2000 mW of Ar laser the developed PDA instrument has lower power emitting source of 17.0 mW of He-Ne laser. In 1994, DANTEC [2] studied the principle of scattering intensity measurement which indicated that the absolute intensity of the scattered light increases proportionally with the square of the particle size. However, for very small particle the scattering intensity is proportional to the fourth to sixth power of the droplet diameter. Consequently, the scattering light intensity obtained from the developed PDA in this work would result in the error of small droplet measurement.

2) The loss of some of the smaller droplets due to the large measurement volume, which can be indicated by the beam waist (the beam waist of the developed PDA instrument and the commercial one are 251 and 140 μm , respectively). It might be possible in these circumstances to count preferentially the larger droplets but ignore smaller droplets passing through the measurement volume if the measurement volume is too large.

Additionally, the large measurement volume is a possible source of uncertainty for detecting the fringes in parallel. The fringe spacing varies with the frequency of the Doppler burst. This will cause a larger standard deviation in the frequency estimation of

the peak. The effect of uncertainty for the fringes in parallel is illustrated in Figure 6.18. It

is indicated that the relative errors of the mean diameter is more than 40%.

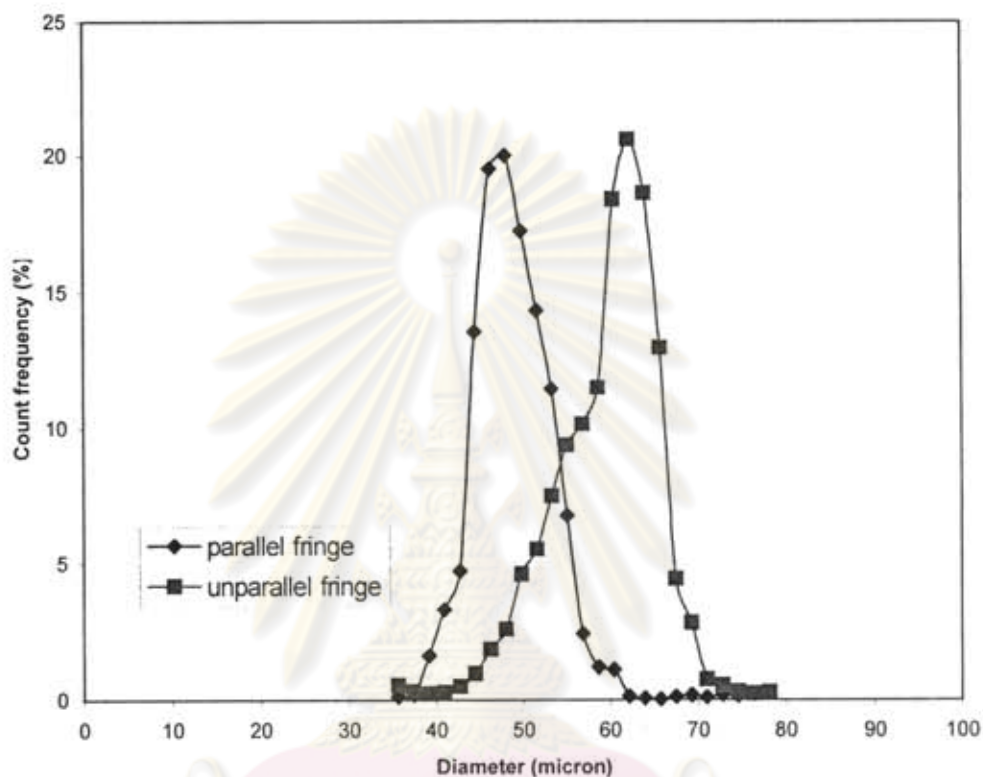


Figure 6.18 The comparison result of the diameter measurement for the unparallel fringe and the parallel fringe.

ศูนย์วิทยทรัพยากร
จุฬาลงกรณ์มหาวิทยาลัย

3) The measurable ranges obtained from both the developed PDA instrument and commercial PDA instruments are limited. With the used configuration, the developed PDA instrument limitation is in a range of 10 – 198 μm . However, using more detectors will

help extend the measurable range beyond these limits. The commercial PDA instrument has a broader range than the developed PDA instrument.

Figure 6.19 shows the diagram of the phase/diameter response which is calculated from the Geometrical optic theory [16] for each track of the circular concentric diffraction array. Such array will represent the upper size range of the developed PDA instrument. The values above zero in y-axis represent the phase/diameter relation for reflection mode. While the values under zero in y-axis represent the phase/diameter relation for 1st refraction mode. The response of the developed PDA instrument will be illustrated by using 1st refraction mode. Therefore, the upper size range of the developed PDA instrument can be summarized as follows:

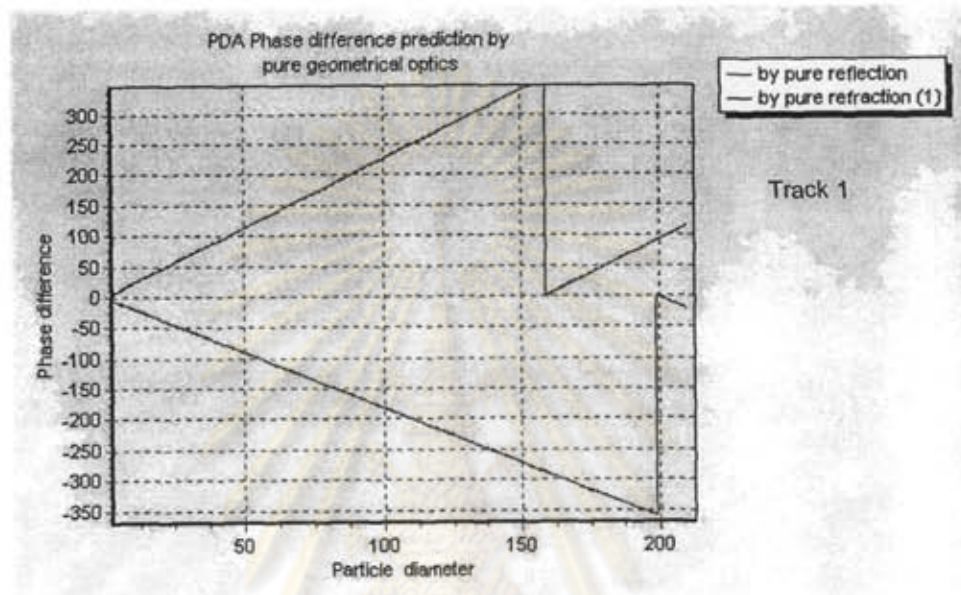
Track 1: fringe spacing 18.12 μm , the upper size range is 198 μm .

Track 2: fringe spacing 12.70 μm , the upper size range is 141 μm .

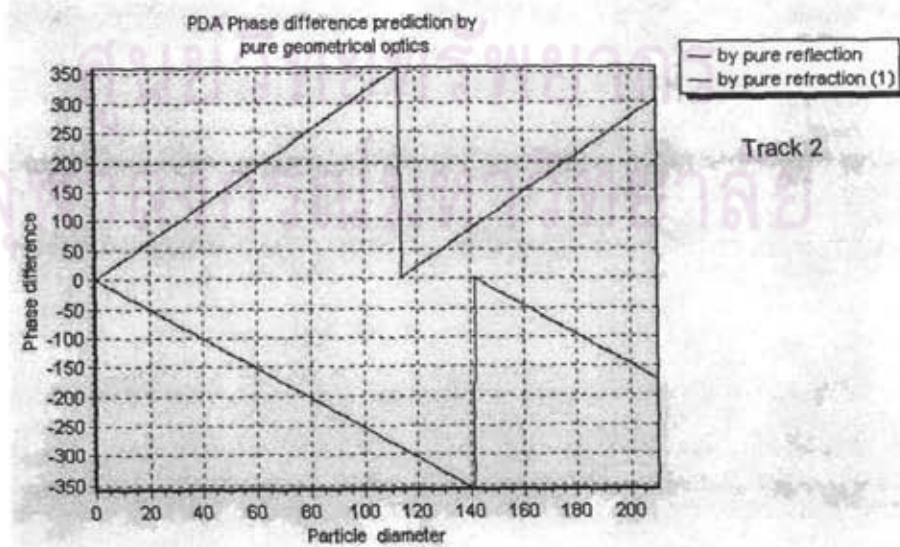
Track 3: fringe spacing 4.85 μm , the upper size range is 82 μm .

The tracks of the circular concentric diffraction array which affects the fringe spacing must be properly selected. In general, the size range of the measured particles must be smaller than the fringe spacing so that a completely modulated Doppler signal could be generated. As the particle becomes larger than the fringe spacing, the signal modulation is reduced and the scattering intensity received by the photodetector would become distorted. It should be noted that the minimum size is limited by the law of

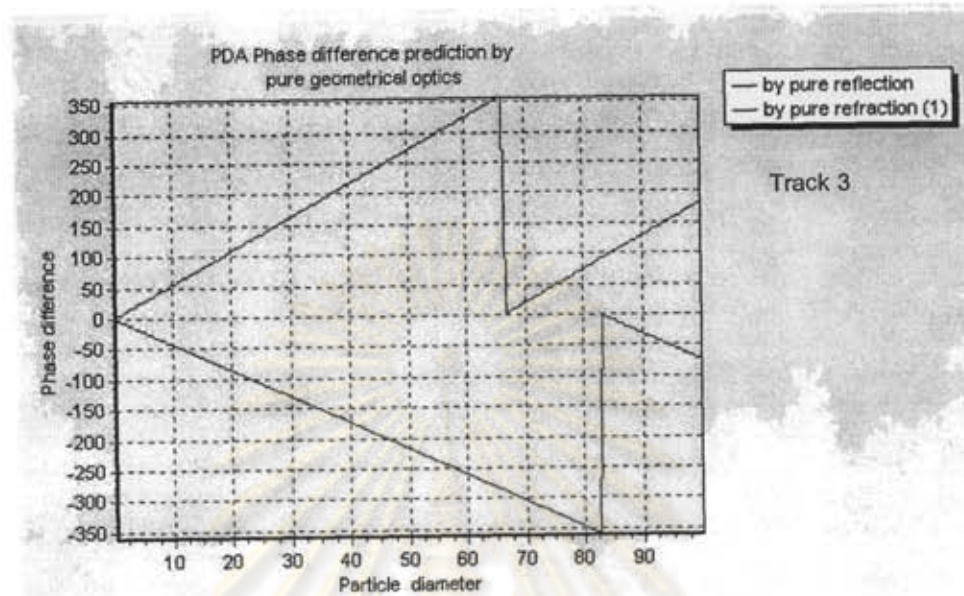
geometrical optics. This method is applicable under the size range lower than 4λ (λ is the laser wavelength). The commonly accepted lower limit is about $5\text{-}10\ \mu\text{m}$ [15].



(a)



(b)



(c)

Figure 6.19 The phase/diameter response for each track of

the circular concentric diffraction array: (a) track 1, (b) track 2 and (c) track 3.

Remark: The response of the developed PDA instrument was illustrated by using track 3.

4) Since the measurements conducted by the two instruments were not performed simultaneously, some variation in the spray atomization was inevitably present. Though the sampling locations of the developed PDA and the commercial PDA instruments were very close but still not identical.

CHAPTER 7

CONCLUSIONS AND RECOMMENDATIONS

7.1 Concluding Remarks

The aim of this research work is to develop a PDA instrument for measuring droplet velocities and their sizes. To ensure reliability and accuracy of the developed PDA instrument, comprehensive investigation was conducted. The following conclusions are made according to the experimental measurement using the developed PDA and the commercial PDA instruments.

- 1) The agreement in frequency measurement obtained from the signal generator of the developed software could verify the accuracy of the developed software and the signal recording.
- 2) The fair agreement in velocity measurement obtained by using the developed software with the commercial PDA instrument could also confirm the accuracy of the developed software. This difference is probably due to the signal processing when different methods of signal processing are employed. It is suggested that careful verification of the measuring instrument should be taken into account.

- 3) The verification result of the developed PDA instrument with the transparent glass sphere demonstrated insignificant difference compared with the results of microscopic analysis.
- 4) The velocity and size of water droplets which were measured by the developed PDA and the commercial PDA instruments could also exhibit fair agreement. This implies that there exist some sources of discrepancies in the experiments.

In addition, the particle size range of the PDA instrument developed in this work can be concluded in Table 7.1.

Table 7.1 The particle size range of the developed PDA instrument.

Circular concentric diffraction array	The upper limit of particle size range (micron)
Track 1	99
Track 2	98
Track 3	85

As for the lower limit of the particle size, it must be aware of the law of geometrical optics which could explain the light scattering behavior for very large particle, i.e., $D \gg 4\lambda$, where D is the particle diameter and λ is the wavelength of the light. The lower limit for the developed PDA instrument is about 2.53 micron. However, the

commonly accepted lower limit of the particle for the standard PDA instrument is about 5-10 micron [15].

Moreover, the developed PDA instrument can be constructed for only 1,200,000 baht of 10,000,000 baht for the commercial PDA instrument [2].

7.2 Recommendations

Two photodetectors were used in the experiment while four photodetectors are commonly employed in a commercial PDA system. Two photodetectors used in this developed PDA system result in the limitation of the measurable particle size range because the particle size can be determined from the phase difference between these two photodetectors. To extend the measurable particle size range by maintaining the measuring resolution three or more photodetectors are recommended. Additionally, more photodetectors might allow measuring reflective index, which could in turn be used to determine the composition of object measured by the PDA instrument.

Meanwhile, it should also be noted that the measurement size range of the instrument could also be extended by the other ways as follows:

- 1) changing the elevation angle;
- 2) changing the transmitting lens to obtain the other characteristic of the optical probe in diameter, the number of fringes and the fringe spacing.

Furthermore, it is recommended that future study should modify the software to compute the validation of the measurement in order to indicate the accuracy of the measurement results.



ศูนย์วิทยทรัพยากร
จุฬาลงกรณ์มหาวิทยาลัย

REFERENCES

- [1] David Lee Black, Mardson Queiroz McQuay, and Michel P. Bonin. "Laser-based techniques for particle size measurement", *Prog. Energy. Combust. Sci.*, 22, 267-306, 1996.
- [2] Clayton Crowe, Martin Sommerfeld, and Yutaka Tsuji. "Multiphase flows with droplets and particles." London: CRC Press, 1992.
- [3] L. E. Drain. "The Doppler technique." John Wiley & Sons, 1980.
- [4] P.A. Strakey and D.G. Talley. "Phase Doppler interferometry with probe-to-droplet size ratios less than unity, Part I: Trajectory errors", 11th Annual Conference on Liquid Atomization and Spray Systems, ILASS-Americas'98, Sacramento, CA, May 17-20, 1998.
- [5] Grant, G.R. and Orloff K.L. "Applied Optics", 12, 2913-6, 1973.
- [6] Orloff, K.L. and Logan, S.E. "Applied Optics", 12, 2477-81, 1973.
- [7] Brena de la Rosa, A., Sankar, S.V., Wang, G. and Bachalo, W.D. "Particle diagnostics and turbulence measurements in a confined isothermal liquid spray", *J. Eng. Gas Turb. Power*, 115, 499-506, 1993.
- [8] McDonell, V.G., Samuelsen, G.S., Wang, M.R., hong, C.H. and Lai, W.H. "Interlaboratory comparison of phase Doppler measurements in a research simplex atomizer spray", *J. Prop. Power*, 10, 402-409, 1994.
- [9] G.Wigley J. Heath, G. Pitcher and A. Whybrew. " Experimental analysis of the response of a PDA system to a partially atomized spray", *Part. Part.Syst. Charact.*, 1999.

- [10] Fabrice Onofri, Damien Blondel, Gerard Grehan, Gerard Gouesbet. "On the optical diagnosis and sizing of spherical coated and multilayered particle with phase Doppler anemometry", *Part. Part.Syst. Charact.*,1996.
- [11] H. Mignao, G. Grehan, G. Gouesbet, T. H. Xu, and C. Tropea. "Measurement of cylindrical particles with phase Doppler anemometry", *AppliedOptics.*, 35, 25, 1996.
- [12] N. Gauchet, T Girasole, K.F. Ren, G. Grehan and G. Gouesbet. "Application of generalized Lorenz-Mie theory for cylinders to cylindrical particle characterization by phase-Doppler anemometry", *Optical Diagnostics in Engineering.*, 2, 1997.
- [13] Lee G. Dodge, Deborah J. Rhodes, and Rolf D. Reitz. "Drop-size measurement techniques for spray: comparison of Malvern laser-diffraction and Aerometrics phase/Doppler", *Applied Optics.*, 26, 1987.
- [14] Nils Damaschke, Gerard Gouesbet, Gerard Grehan, Herve Mignon, and Cam Tropea. "Response of Phase Doppler Anemometer system to nonspherical droplets", *Applied Optics.*, 37, 1998.
- [15] Gerhard Gobel, Thomas Wriedt, and Klaus Bauckhage., "Micron and sub-micron aerosol sizing with a standard phase Doppler anemometer", *Aerosol Sci.*, 29, 1998.
- [16] Amir A. Naqwi, Franz Durst. "Light scattering applied to LDA and PDA measurements: Part1 Theory and numerical treatments", *Part. Part. Syst. Charact.*, 8, 1991.
- [17] Amir A. Naqwi, Franz Durst. "Light scattering applied to LDA and PDA measurements: Part 2 Computational results and their discussion", *Part. Part. Syst. Charact.*, 9, 1992.

- [18] Cameron Tropea, Tian-Hua Xu, Fabrice Onofri, Gerard Grehan, Per Haugen and Manfred Stieglmeier. "Dual-mode phase Doppler anemometer", *Part. Part. Syst. Charact.*, 13, 1996.
- [19] Dantec Ltd. "Dantec dynamics measurement technology", www.dantecdynamics.com.



ศูนย์วิทยทรัพยากร
จุฬาลงกรณ์มหาวิทยาลัย



APPENDICES

ศูนย์วิทยทรัพยากร
จุฬาลงกรณ์มหาวิทยาลัย

APPENDIX A

THE FAST FOURIER TRANSFORM (FFT)

A.1 Background

Today, the Fourier transform (FT) is used in many areas of Physics and other sciences, particularly as a way to analyze problems that arise in the processing of electronic signals, in optics and in solving differential equations.

The invention of the computer algorithm known as the Fast Fourier Transform (FFT) in the mid-1960s opened up the possibility of an even wider use of the FT in computational physics are frequently evaluated principally on their capacity to perform the FFT algorithm, and many special computers or add-on cards are available to perform the FFT algorithm at ultrahigh speed. The FFT algorithm is embedded in many modern technologies, from medical imaging system, through geophysical prospecting using seismology, to telephone networks and radio communication links.

A.2 Introduction to the Fourier Transform

A physical process can be described either in the time domain, by the values of some quantity h as a function of time t , e.g., $h(t)$, or else in the frequency domain, where the process is specified by giving its amplitude H (generally a complex number indicating phase also) as a function of frequency f , that is $H(f)$, with $-\infty < f < \infty$. For many

purposes it is useful to think of $h(t)$ and $H(f)$ as being two different representations of the same function. One goes back and forth between these two representations by means of the Fourier transform equations

$$H(f) = \int_{-\infty}^{\infty} h(t) e^{2\pi i f t} dt \quad (\text{A.1})$$

$$h(t) = \int_{-\infty}^{\infty} H(f) e^{2\pi i f t} df \quad (\text{A.2})$$

If t is measured in seconds, then f in equation (A.2) is in cycles per second, or Hertz (the unit of frequency). However, the equations work with other units too.

A.3 Sampling and the Sampling Theorem

Frequently, the function $h(t)$ is not measured or specified continuously, but rather is measured at fixed intervals of time, or sampled. If $h(t)$ is measured at the discrete times given by

$$t_k = k\Delta \quad k = \dots -3, -2, -1, 0, 1, 2, 3\dots \quad (\text{A.3})$$

where Δ is known as the sampling interval, then may write

$$h_k = h(t_k) \quad (\text{A.4})$$

and h_k is a discrete representation of $h(t)$.

The function $h(t)$ is said to be band limited if its Fourier transform $H(f) = 0$ for $|f| > f_c$, where f_c is a finite critical frequency. A function may be band limited because it

has been passed through a filter (e.g., an FM radio signal must be restricted by the station operators to the allowed band), or perhaps because it is generated by a process that has an upper limit to its frequency content (e.g., human speed)

The sampling theorem is very important, and states that a band-limited function $f(t)$ is completely specified by the sampled values $f(t_n)$, provided that the sampling interval is no longer than

$$\Delta = \frac{1}{2f_c} \quad (\text{A.5})$$

For a given sampling interval Δ , the frequency f_c is often known as the Nyquist frequency. The sampling theorem states that a band-limited function sampled at a rate higher than twice the Nyquist frequency may be completely reconstructed from these samples.

A.4 The Discrete Fourier Transform

Suppose that the function $h(t)$ has been sampled only at the discrete times t_k (either at the given times, or averaged over the corresponding time interval) given by

$$t_k = k\Delta \quad k = 0, 1, 2, \dots, N-1 \quad (\text{A.6})$$

where N is the number of samples. The Discrete Fourier Transform (DFT) is then defined as

$$H_n = H(f_n) = \Delta \sum_{k=0}^{N-1} h_k e^{2\pi i k n / N} \quad (\text{A.7})$$

where the frequencies f_n are given by

$$f_n = \frac{n}{N\Delta} \quad n = -\frac{N}{2}, -\frac{N}{2}+1, \dots, \frac{N}{2}-1, \frac{N}{2} \quad (\text{A.8})$$

This implies that the first frequency is $f_{-N/2} = -1/\Delta$, the central one is $f_0 = 0$ and the last is $f_{N/2} = 1/\Delta$. This corresponds to $N+1$ points, but the first and last are identical.

A.5 The Fast Fourier Transform (FFT)

The DFT requires the calculation of the sums

$$H_n = \sum_{k=0}^{N-1} W^{nk} h_k \quad (\text{A.9})$$

where $W = \exp(2\pi i/N)$. At first sight, this requires at least N^2 multiplications to generate all N of the coefficients H_n . But this is not the case. The summation may be broken into two parts, one over the even-numbered elements ($k=0, 2, 4, \dots$) and the other over the odd-numbered elements ($k=1, 3, 5, \dots$). In turn, each one of these parts can be broken into its even-numbered and odd-numbered parts, and the process can be continued until the summation has become divided into 1-point Fourier transforms. This repeated dissection of the series into even-and odd-numbered parts can be implemented in the computer by reversing the bit-pattern of the addresses of the data elements. After this is done, the required N values of H_n can be generated by making a sequence of 2, 4, 8, ... point summations. The total time for the operation scales not as N^2 but as $N \log N$, so that for

large transforms there is an enormous saving in time. This idea of bit reversal can be exploited in a very way which, along with the Danielson-Lanczos Lemma, makes FFTs practical as shown in Figure A.1.

As a consequence of the bit-reversal process, the application of the FFT to a vector of data in a computer leaves the resulting components of the transform in a rather mixed-up state.

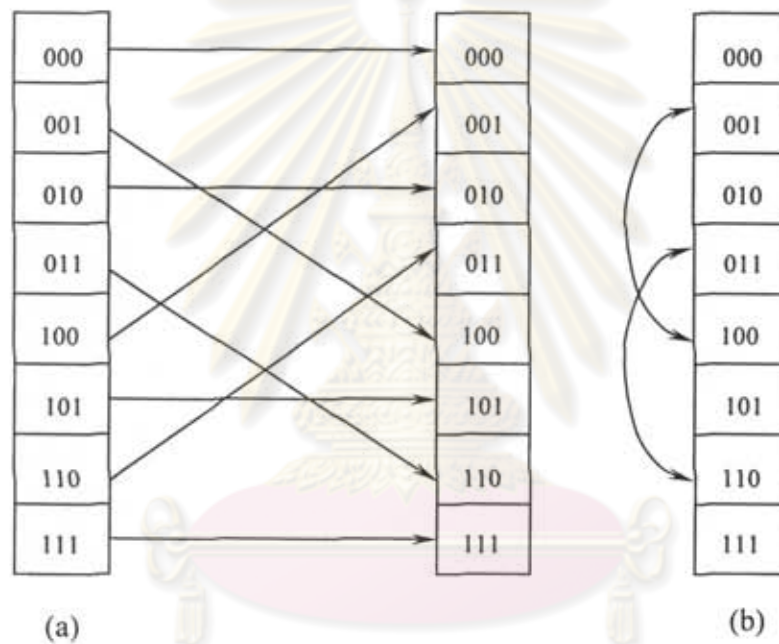


Figure A.1 Recordering an array (here of length 8) by bit reversal,

(a) between two arrays, versus (b) *in place*.

APPENDIX B

CALCULATION OF THE FRINGE FREQUENCY

As the circular concentric diffraction array turns, this causes the fringes in the measurement volume to move at a constant speed in the U or -U directions depending on the direction of the frequency shift or the direction of rotation of the circular concentric diffraction array. Therefore, the fringe frequency is related to the voltage of the motor adjusted to create the driving frequency as shown in Table B.1, B.2 and B.3 for track 1, track 2 and track 3, respectively.

Table B.1 The fringe frequency for track 1 of circular concentric diffraction array.

Voltage (V)	Fringe frequency (Hz)			
	1	2	3	Average
2.0	292,968.75	341,796.88	341,796.88	325,520.83
2.2	341,793.88	341,796.88	341,796.88	341,795.88
2.4	390,625.00	390,625.00	390,625.00	390,625.00
2.6	439,453.13	390,625.00	390,625.00	406,901.04
2.8	439,453.13	439,453.13	439,453.13	439,453.13
3.0	488,281.25	488,281.25	488,281.25	488,281.25
3.2	537,109.38	488,281.25	537,109.38	520,833.33
3.4	537,109.38	537,109.38	537,109.38	537,109.38
3.6	585,937.50	585,937.50	585,937.50	585,937.50
3.8	634,765.63	634,765.63	634,765.63	634,765.63
4.0	683,593.75	683,593.75	683,593.75	683,593.75
4.2	732,421.88	732,421.88	732,421.88	732,421.88
4.4	732,421.88	732,421.88	732,421.88	732,421.88
4.6	781,250.00	781,250.00	781,250.00	781,250.00
4.8	830,078.13	830,078.13	830,078.13	830,078.13
5.0	878,906.25	875,906.25	878,906.25	877,906.25

Table B.2 The fringe frequency for track 2 of circular concentric diffraction array.

Voltage (V)	Fringe frequency (Hz)			
	1	2	3	Average
2.0	537,109.38	585,937.50	585,937.50	569,661.46
2.2	634,765.63	683,593.75	683,593.75	667,317.71
2.4	732,421.88	732,421.88	732,421.88	732,421.88
2.6	830,078.13	830,078.13	830,078.13	830,078.13
2.8	927,734.38	927,734.38	927,734.38	927,734.38
3.0	976,562.50	976,562.50	976,562.50	976,562.50
3.2	1,025,390.63	1,074,218.75	1,074,218.75	1,057,942.71
3.4	1,123,046.88	1,123,046.88	1,123,046.88	1,123,046.88
3.6	1,220,703.13	1,220,703.13	1,220,703.13	1,220,703.13
3.8	1,318,359.38	1,318,359.38	1,318,359.38	1,318,359.38
4.0	1,367,187.50	1,416,015.63	1,367,187.50	1,383,463.54
4.2	1,464,843.75	1,464,843.75	1,464,843.75	1,464,843.75
4.4	1,562,500.00	1,562,500.00	1,513,671.88	1,546,223.96
4.6	1,660,156.25	1,611,328.13	1,611,328.13	1,627,604.17
4.8	1,757,812.50	1,708,984.38	1,757,812.50	1,741,536.46
5.0	1,806,640.63	1,806,640.63	1,806,640.63	1,806,640.63

ศูนย์วิทยทรัพยากร
จุฬาลงกรณ์มหาวิทยาลัย

Table B.3 The fringe frequency for track 3 of circular concentric diffraction array.

Voltage (V)	Fringe Frequency (HZ)			
	1	2	3	Average
2.0	1,269,531.25	1,269,531.25	1,220,703.13	1,253,255.21
2.2	1,367,187.28	1,318,359.38	1,367,187.50	1,350,911.39
2.4	1,464,843.75	1,513,671.88	1,513,671.88	1,497,395.83
2.6	1,708,984.38	1,708,984.38	1,708,984.38	1,708,984.38
2.8	1,855,468.75	1,855,468.75	1,806,640.63	1,839,192.71
3.0	2,001,953.13	2,001,953.13	2,001,953.13	2,001,953.13
3.2	2,246,093.75	2,148,437.50	2,197,265.63	2,197,265.63
3.4	2,392,578.13	2,343,750.00	2,343,750.00	2,360,026.04
3.6	2,539,062.50	2,587,890.63	2,587,890.63	2,571,614.58
3.8	2,734,375.00	2,734,375.00	2,734,375.00	2,734,375.00
4.0	2,929,687.50	2,880,859.38	2,880,859.38	2,897,135.42
4.2	3,076,171.88	3,076,171.88	3,027,343.75	3,059,895.83
4.4	3,271,484.38	3,173,828.13	3,222,656.25	3,222,656.25
4.6	3,417,968.75	3,417,968.75	3,369,140.63	3,401,692.71
4.8	3,515,625.00	3,515,625.00	3,515,625.00	3,515,625.00
5.0	3,662,109.38	3,710,937.50	3,662,109.38	3,678,385.42

ศูนย์วิทยทรัพยากร
จุฬาลงกรณ์มหาวิทยาลัย

The variation of the fringe frequency with the voltage to turn the circular concentric diffraction array in each track shows in Figure B.1.

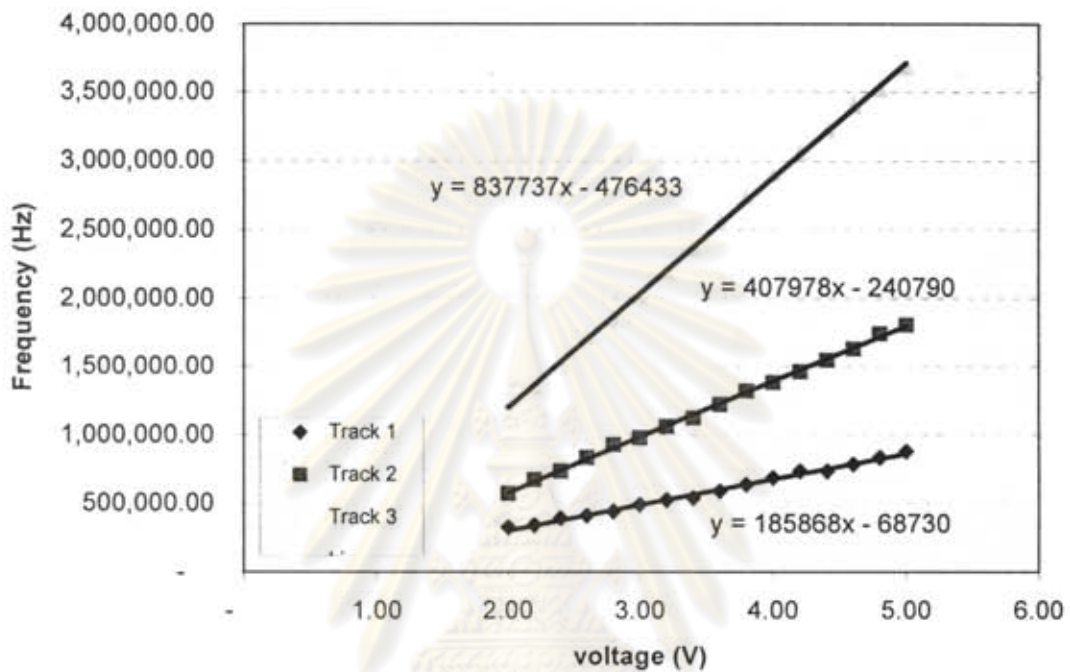


Figure B.1 The variation of the fringe frequency with the voltage to turn the circular concentric diffraction array.

ศูนย์วิทยทรัพยากร
จุฬาลงกรณ์มหาวิทยาลัย

APPENDIX C

CALCULATION OF THE INTERSECTION ANGLE

For three tracks of the circular concentric diffraction array the distance between the incident laser beam and the center of the circular array corresponding to each track of this device is changed. Therefore, the angle between the +1/-1 order called intersection angle (θ), is also changed.

To illustrate this Figure C.1 should be considered. The direction of the two beams left from the circular concentric diffraction array is diverted and crossed at the focusing point of the Plano-convex glass lens in order to conform a measurement volume.

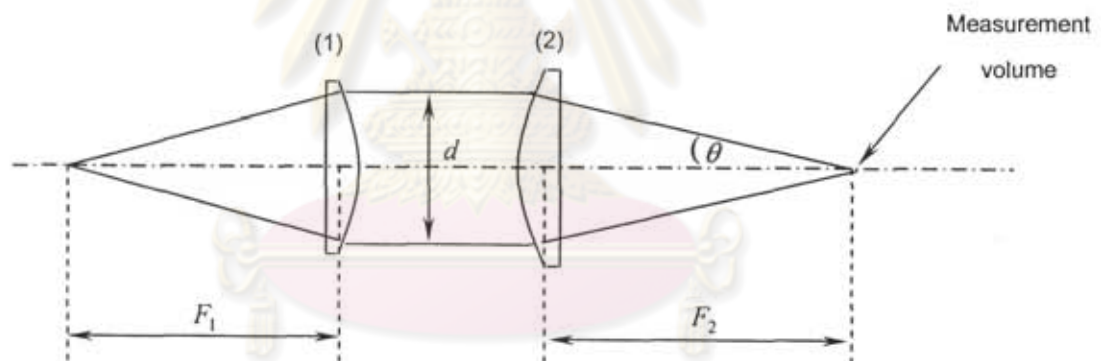


Figure C.1 Optical system geometry for calculation of the intersection angle:

- (1) A 150 mm focal length and 80 mm in diameter of Plano-convex glass lens;
- (2) A 300 mm focal length and 95 mm in diameter of Plano-convex glass lens.

Referring to Figure C.1

$$\tan\theta = \frac{d/2}{F_2} \quad (\text{C.1})$$

where θ is the intersection angle and d is the distance between two laser beams corresponding to each track of the circular concentric diffraction array. In this work the distances (d) measured are 10.5, 14.9 and 25.4 mm for track 1, 2 and 3, respectively; and F_2 is the focal length of the lens.

Which can be rearranged to show:

$$\theta = \tan^{-1}\left(\frac{d/2}{F_2}\right) \quad (\text{C.2})$$

For track 1 the intersection angle is:

$$\theta = \tan^{-1}\left(\frac{10.5/2}{300}\right) \quad (\text{C.3})$$

$$\theta = 1.00 \quad (\text{C.4})$$

Similarly, for track 2:

$$\theta = 1.42 \quad (\text{C.5})$$

And for track 3:

$$\theta = 2.42 \quad (\text{C.6})$$

ศูนย์วิทยทรัพยากร
จุฬาลงกรณ์มหาวิทยาลัย

APPENDIX D

CALCULATION OF THE ELEVATION ANGLE

The elevation angle (ψ) can be defined by a mask which allows the parallel light beam to pass through to the photodetectors as shown in Figure D.1.

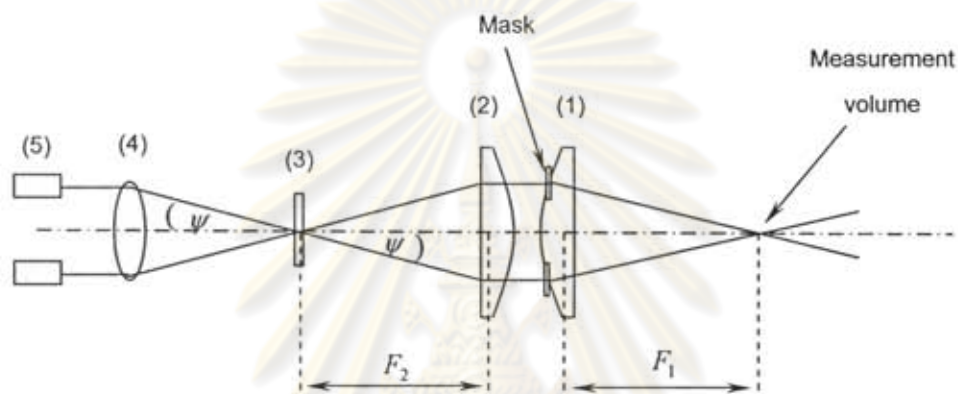


Figure D.1 Optical system geometry for calculation of the elevation angle:

- (1) A 300 mm focal length and 95 mm in diameter of Plano-convex glass lens with two slit mask; (2) A 300 mm focal length and 95 mm in diameter of Plano-convex glass lens; (3) A spatial filter; (4) A 100 mm focal length and 50 mm in diameter of symmetric-convex lens; (5) Photomultipliers.

Referring to Figure D.1

$$\tan \psi = \frac{d/2}{F_2} \quad (\text{D.1})$$

where ψ is the elevation angle, d is the distance between two laser beams corresponding to the mask and F_2 is the focal length of the lens.

Which can be rearranged to show:

$$\psi = \tan^{-1} \left(\frac{d/2}{F_2} \right) \quad (\text{D.2})$$

For example, if d is 35 mm then the elevation angle can be obtained as follows:

$$\psi = \tan^{-1} \left(\frac{35/2}{300} \right) \quad (\text{D.3})$$

$$\psi = 3.34 \quad (\text{D.4})$$

ศูนย์วิทยทรัพยากร
จุฬาลงกรณ์มหาวิทยาลัย

APPENDIX E

**CALCULATION OF THE PHASE-DIAMETER RELATIONS
(SLOPE/PHASE DIAMETER)**

The operational principle of PDA system to size particles can be explained by using the phase-diameter relations which is defined by the equation below:

$$\Delta\Phi = \frac{2\pi D n_m}{\lambda} \varphi \quad (\text{E.1})$$

The parameter φ depends on the scattering mode.

For reflection ($P = 0$)

$$\varphi = \sqrt{2} \left[\begin{array}{l} (1 + \sin \theta \sin \psi - \cos \theta \cos \varphi \cos \psi)^{1/2} \\ -(1 - \sin \theta \sin \psi - \cos \theta \cos \varphi \cos \psi)^{1/2} \end{array} \right] \quad (\text{E.2})$$

and for 1st order refraction ($P = 1$)

$$\varphi = 2 \left\{ \begin{array}{l} [1 + m^2 - \sqrt{2} m (1 + \sin \theta \sin \psi + \cos \theta \cos \varphi \cos \psi)^{1/2}]^{1/2} \\ - [1 + m^2 - \sqrt{2} m (1 - \sin \theta \sin \psi + \cos \theta \cos \varphi \cos \psi)^{1/2}]^{1/2} \end{array} \right\} \quad (\text{E.3})$$

where $\Delta\Phi$ is the phase difference of the scattered light, D is the particle diameter, λ is the wavelength of the light, θ is intersection angle, ϕ is scattering angles or off-axis angle,

ψ is the elevation angle of one photodetector and $m = n_d/n_m$ is the ratio of the refractive index of the particle (n_d) to that of the surrounding medium (n_m)

The following are the important parameters used in this work for calculating the phase-diameter relations:

- Light wavelength (nm)	632.8
- Intersection angle (degree)	
track 1	1.00
track 2	1.42
track 3	2.42
- Scattering angle (degree)	30
- Elevation angle (degree)	3.34
- Refractive index of water	1.33
- Refractive index of air	1.00

For 1st order refraction ($P=1$) and track 1 the parameter φ is

$$\varphi = 2 \left\{ \begin{array}{l} \left[1 + (1.33)^2 - (\sqrt{2})(1.33)(1 + \sin(1)\sin(3.34) + \cos(1)\cos(30)\cos(3.34))^{1/2} \right]^{1/2} \\ - \left[1 + (1.33)^2 - (\sqrt{2})(1.33)(1 - \sin(1)\sin(3.34) + \cos(1)\cos(30)\cos(3.34))^{1/2} \right]^{1/2} \end{array} \right\} \quad (\text{E.4})$$

By replacing equation (E.1) with equation (E.4) the phase-diameter relation can be obtained as follows:

$$\Delta\Phi = 1.78D \quad (\text{E.5})$$

Similarly, for track 2

$$\Delta\Phi = 1.85D \quad (\text{E.6})$$

And for track 3

$$\Delta\Phi = 1.64D \quad (\text{E.7})$$



ศูนย์วิทยทรัพยากร
จุฬาลงกรณ์มหาวิทยาลัย